Voxel-based additive manufacturing of biomimetic functionally graded materials

Alba Herranz de la Nava

Technische Universiteit Delft

VOXEL-BASED ADDITIVE MANUFACTURING OF BIOMIMETIC FUNCTIONALLY GRADED MATERIALS

by

Alba Herranz de la Nava

in partial fulfillment of the requirements for the degree of

Master of Science
in Biomedical Engineering

at the Delft University of Technology,

Student number:	4632109
Project duration:	January, 2018 – November, 2018
TU Delft supervisors:	dr. M. J. Mirzaali
	Prof. dr. A. A. Zadpoor
Thesis Comittee:	dr. M. J. Mirzaali
	Prof. dr. A. A. Zadpoor
	Prof. dr. ing. H. Vallery

TU Delft Delft University of Technology

ABSTRACT

Nature has evolved materials with outstanding mechanical properties, which attain high values of both strength and toughness. The key to their success lies in the combination of hard and soft constituents in a intricate pattern. The design of natural materials allows for the development of toughening mechanisms that increase the overall fracture energy of the sample while keeping the stiffness provided by the hard constituents, as it is demonstrated in the brick-and-mortar pattern of nacre. In addition, the development of graded material transitions avoids failure at material interfaces with a high mismatch in stiffness. This is crucial for the success of certain structures in the human body, such as the connections of ligaments and tendons to bone.

Due to their marvellous design and superior mechanical properties, natural materials are a source of inspiration for the development of biomimetic advanced materials. The advancement of multi-material additive manufacturing (AM) has eased the production of structures that combine materials with different properties. Voxel-based 3D printing is an innovative technique that allows for the strategic placement of voxels of different materials at a high resolution using PolyJet technology. Several studies have attempted to produce brick-and-mortar or graded patterns. However, the production of functionally graded structures by voxel-based additive manufacturing is still a novelty, and the effects of the graded pattern and material ratio have not been assessed. In addition, the performance of brick-and-mortar patterns and graded transitions in the same structure have not been evaluated.

In this project, several patterns for material graded transitions have been designed, produced by voxel-based AM and assessed by fracture mechanics and tensile tests. The effect of different material ratio distributions on the mechanical properties of the specimen have also been evaluated. Digital image correlation techniques provided insightful information about the strain distribution in certain patterns, and how they influence the fracture toughness of samples. A biomimetic model of a human knee was developed in order to compare the performance of sharp and graded interfaces in real-like scenarios. Furthermore, brick-and-mortar patterns with different designs, hierarchy levels and platelet aspect ratio have been created, and the patterns' single and combined effect with a gradient pattern have been assessed.

The results outlined that the function that determines the pattern for material change does not contribute significantly to an improvement of the mechanical properties, specially when the transition reaches points of pure material concentration. By contrast, when complementary material ratios are located at both sides of an interface, the fracture toughness of the samples is enhanced. Thus, it was demonstrated that the distribution of material ratio in a complementary manner but avoiding sites of pure hard material presents the most optimal boost of toughness in the specimens. The biomimetic human knee model proved the efficacy of graded material transitions over sharp material interfaces in withstanding higher tensile loads. Finally, the addition of graded transitions to brick-and-mortar patterns contributes to an increase of the fracture toughness of the samples, followed by a slight decrease of the overall stiffness. The increase of fracture energy is linked to the increased plasticity region in front of the crack tip that was revealed in DIC tests. Changing the placement of the crack tip and increasing the percentage of hard material that conforms the gradient could increase the overall stiffness as well.

ACKNOWLEDGEMENTS

After two wonderful years at the TU Delft, this master thesis represents the end of my period as a student. Since last January, I have been working on this project, from which I have truly learned. However, I have not gone through this graduation period alone, and I would like to thank everyone who has been involved in this project.

I would to express my great appreciation to my daily supervisor, Mohammad Mirzaali, for his great help in giving my project direction and for all his useful feedback and mentoring. I really enjoyed our meetings and appreciate the trust he put on me and his great advice.

I would like to thank my professor Amir Zadpoor for introducing me into this exciting field and providing me with the opportunity to work in this project, as well as for the useful input and scientific guidance.

I would like to thank Zjenja Doubrovski for the opportunity to use cutting-edge technology from the Applied Labs at the Industrial Design Faculty, for teaching me about voxel-based 3D printing and for his contribution to the creation of the samples and the biomimetic bone model.

A special thank to Tessa Essers, for assisting me with all the printing process and for her great help with the many complications I faced throughout it.

I would like to thank my fellow colleague students, Deepthi and Maike, for all the working moments we spent together and mutual help. I really enjoyed it.

I am specially grateful to my family, for their endless love and support in this adventure. I could not have reached all my goals without them.

A special thanks to Tim, for all his patience and support, for reading my drafts and listening to my presentations. For believing in me and always being there.

And last but not least, I am so grateful for all the amazing friends I have made, and all the adventures we have had together. For becoming my family away from home.

Alba Herranz de la Nava
Delft, November 2018

CONTENTS

List of Figures

List of Tables

NOMENCLATURE

Abbreviations

ACL	Anterior Cruciate Ligament
AM	Additive Manufacturing
DEJ	Dentin-Enamel Junction
DIC	Digital Image Correlation
LCL	Lateral Collateral Ligament
MCL	Medial Collateral Ligament
PCL	Posterior Cruciate Ligament
PLA	Polylactic Acid
UTS	Ultimate Tensile Strength

Symbols

ϵ	Strain
ϵ_f	Strain at Fracture
ϵ_{yy}	Strain Component yy direction
σ	Normal Stress
σ_f	Fracture Stress
E	Stiffness
U	Fracture Toughness

1

INTRODUCTION

Nature has successfully created materials with incredible mechanical properties. Through thousands of years of evolution, nature has adapted its structural features to the mechanical needs of each point within the structure [1, 2]. High values of both strength and toughness are accomplished in lightweight structures with intricate hierarchical designs [1]. The success of natural structural materials lies on three basic principles: their chemical composition, their hierarchical organization spanning from the nano- to the macro- scale and the fashion in which the assembly of the building blocks occurs [3]. The building blocks are universal and already available in nature. They can be organic, polymeric chains such as polysaccharides and proteins; or inorganic, mostly ceramic particles [4]. The organization of the building blocks into an elaborate hierarchical architecture and the strategic placement of different materials within the same structure makes the overall construction outperform the mechanical properties of the simple constituents on their own, as it can be observed in figure 1.1 [5, 6].

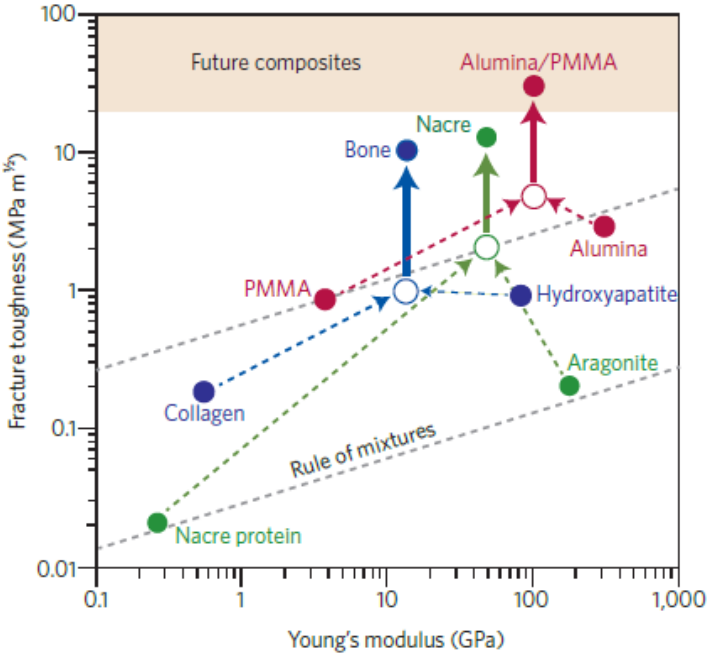

Figure 1.1: Comparison of the Young's modulus and fracture toughness of natural composites and their constituents. Adapted from [3].

The mechanical properties vary at different locations within the structure, for instance, reinforcing those places subjected to higher loads [5]. The designs often incorporate hard and soft components in a composite structure. The interfaces between those building blocks greatly influence the mechanical properties of the structures, and can serve as mechanisms to increase toughness [3, 7]. Other striking natural designs

avoid sharp interfaces by the use of functionally graded structures to link materials with a high disparity in mechanical properties [2]. For these reasons, nature certainly presents a good source of inspiration for the development of materials that outperform conventional materials in mechanical properties. Understanding the mechanisms behind stunning structures in nature is fundamental to mimic them. Manufacturing of advanced materials has been eased by the development of multi-material additive manufacturing (AM) and voxel-based 3D printing, allowing for a faster printing process, higher resolution of the prints and the increase of feasibility of design patterns [2, 7, 8].

1.1. CONFLICT BETWEEN STRENGTH AND TOUGHNESS

Structural materials should be both strong enough to withstand high loads and tough to allow some damage without failure. Strength refers to the resistance that a material presents to irrecoverable deformation. Toughness is the resistance to fracture, in the form of the amount of energy that is needed for a material to break or to expand a pre-existing crack [9, 10]. In synthetic materials, strength and toughness are usually mutually exclusive. This means that one property has to be chosen at the expense of the other, and the decision is made according to the final application and following safety rules [2, 5, 7]. Materials with a high strength are often brittle, not being able to dissipate energy when a crack appears. On the other hand, toughness can be enhanced by allowing some degree of plastic deformation, promoting ductility. The highest toughness possible within a material should be endowed by reaching both high strength and high ductility [9, 10]. This is possible in biological materials by the development of weak interfaces and toughening mechanisms [3].

1.1.1. IMPORTANCE OF INTERFACES

Interfaces have an important role in the mechanical properties of a material. Fracture resistance can be boosted in brittle materials by the development of weak interfaces, which prompt crack deflection and enable non-linear deformation [11, 12]. Moreover, the organization through different length scales activates energy dissipation by means of intrinsic and extrinsic toughening mechanisms [3, 9, 10]. Intrinsic toughening mechanisms try to increase plasticity, and act ahead the crack tip at sub-micro scales. Alternatively, extrinsic toughening mechanisms act behind the crack tip and try to prevent its further opening, working on the micro- scale [7, 9, 10].

Both high strength and toughness are found in nacre (Figure 1.2 a). It presents a characteristic brick- and -mortar structure. The bricks are made of stiff aragonite platelets, which are embedded in an organic matrix that acts like the mortar [11, 14]. The lower strength of the proteic mortar, compared to the ceramic platelets, triggers crack deflection in a guided manner through the interfaces [15]. In addition, the high ability to deform of the matrix increases ductility and energy dissipation, as well as contributing to strain hardening [16–18]. Moreover, the rough platelets surface and the mineral bridges in between them facilitate stress propagation. Thus, crack- bridging and platelet sliding, as well as the viscoplastic nature of the matrix contribute to the increase of toughness in nacre [3, 7, 19].

Bone is the main structural material in the human body, and presents both high hardness and stiffness. The two main types of interfaces in the structure: interfibrillar interfaces between the collagen fibril bundles, and cement lines between the osteons and interstitial bone [12]. These interfaces can easily deform, besides being weaker than the surrounding materials. Toughness is highly increased by the pullout of collagen fibrils that is required for crack propagation, which allow deformability and energy dissipation [20]. In addition, the cement lines accumulate a higher amount of microcracks, which are fundamental for crack twisting and crack deflection and bridging. Thus, the crack is directed through the path with higher amount of microcracks, augmenting plasticity and dissipating part of the crack driving energy [12, 13] (Figure 1.2 b).

1.2. FUNCTIONALLY GRADED STRUCTURES IN NATURE

The development of materials that present graded transitions in material properties is a smart strategy of biological materials to adapt to the mechanical needs of the structure. By the use of functionally graded structures, it is possible to avoid points of high stress concentration that rise from the contact between two materials with a high stiffness mismatch. These transitions can appear in a continuous or step-wise manner [2, 7]. In conventional synthetic materials, gradients rise mostly by oxidation, diffusion or clustering of par-

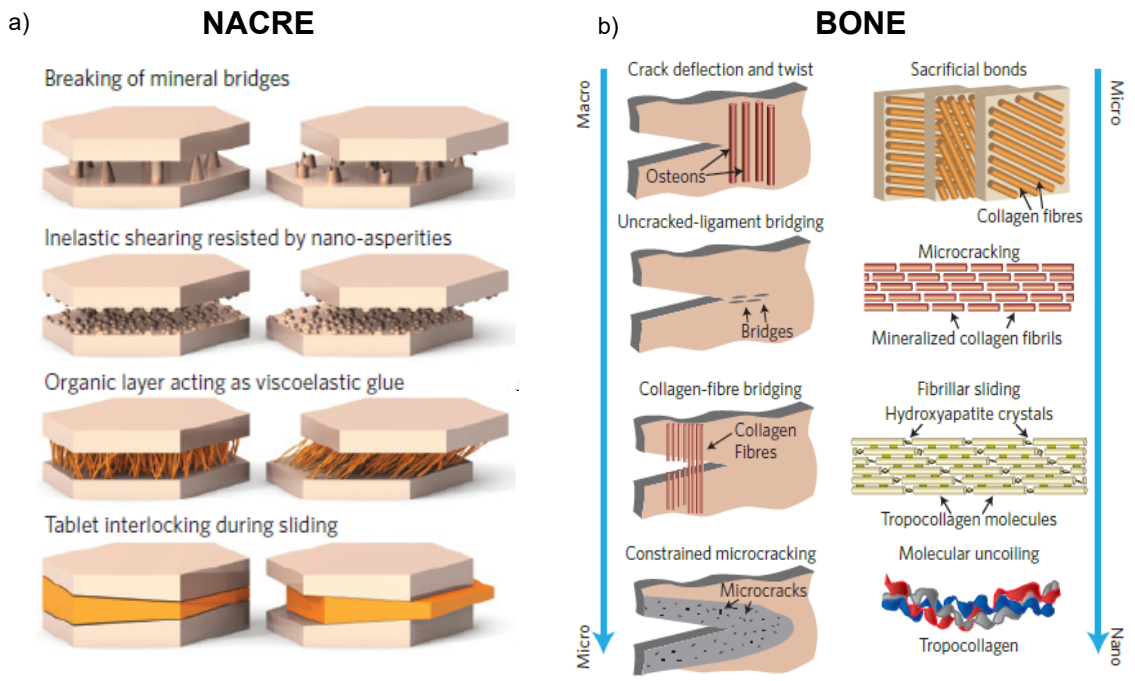

Figure 1.2: Illustration of the main toughening mechanisms in a) nacre and b) bone. Adapted from [3, 13].

ticles within the lattice or grain boundaries [21]. However, in natural materials these heterogeneities emerge from changes in the local chemical composition of the constituents or in the assembly of the building blocks [2]. Chemical gradients arise from changes in the constituents at molecular level, given by variations in the degree of mineral content [22, 23], allocation of inorganic ions [24] or in the degree of water content [25]. Structural gradients play with the multi-scale of the building blocks, and create intricate architectures by manipulating the underlying arrangement, distribution, size and orientation of the building blocks [26–32].

Similarly, nature uses graded transitions at the interface of materials with high mismatch in elastic modulus, in order to avoid failure due to localized high stress values [12]. This is highly important in structures that are subjected to cyclic loading, as found in the dentin-enamel junction in human teeth. The inner part of the teeth is formed by dentin, and it is composed by water, collagen and apatite [28]. The mineral content is arranged in dentinal tubules, conferring a high toughness to the material [33]. The dentin is covered by a thin layer of enamel, mainly composed of hydroxyapatite in the form of prisms. Besides the huge mismatch in elastic modulus - from $\approx$ 95 GPa in enamel to $\approx$ 20 GPa in dentin [34] - delamination and failure of the structure are avoided by the presence of a graded intermediate layer: the dentin-enamel junction (DEJ), which presents features from both materials [33, 34]. Any cracks that might originate in the brittle enamel fail to propagate further than the DEJ due to the increasing amount of organic fibers that appear closer to dentin, increasing the overall toughness of the DEJ by 10 times [35].

Graded interfaces are also used in the human body to link hard and soft tissues. This is exemplified in the tendon-bone enthesis, the graded interface where tendons and ligaments anchor to bone. The mismatch in elastic modulus in the region ranges from 0.4 GPa in tendon to 20 GPa in bone [36]. Four different regions can be distinguished in the interface. The first region corresponds to tendon, formed mostly by collagen type I and organized hierarchically from triple helices (4 nm in diameter), microfibrils, fibrils and fascicles (150-300 μm). The second zone is rich in collagen type II and III, which form a network thanks to the presence of aggrecan. Hydroxyapatite (HA) deposits appear embedded in collagen type II matrix in the third region, contributing to an increase of the stiffness. The fourth zone is bone, formed mainly by collagen type I and HA platelets [36–38]. In depth research about the tendon-bone interface has shown that the organization of collagen fibers has a direct influence on the stiffness, and that toughness is determined by the molecular

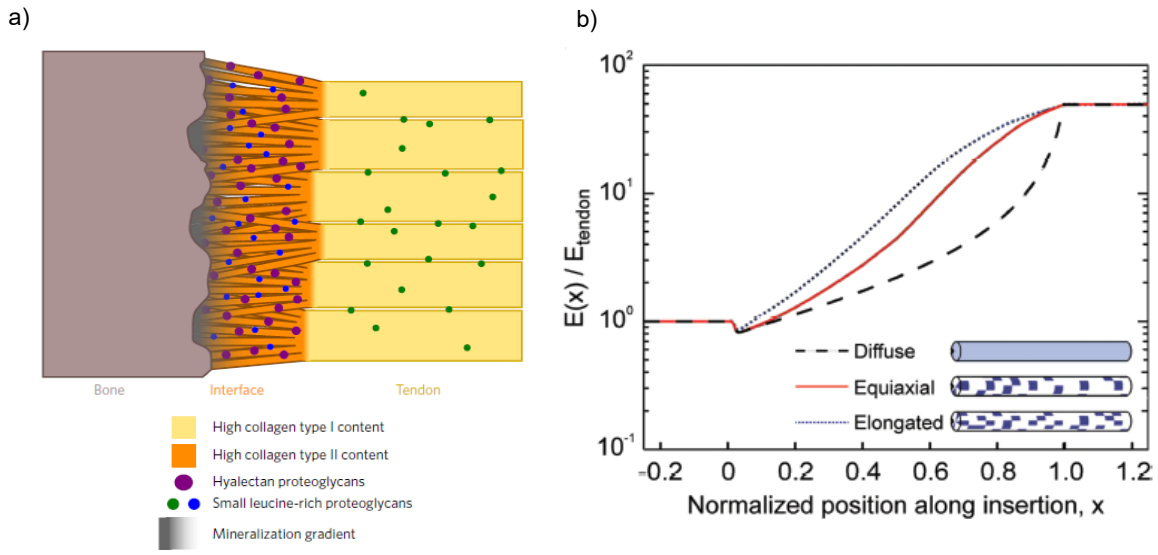

Figure 1.3: a) Schematics of the bone-tendon enthesis and b) Variation of the elastic modulus through the insertion. Adapted from [36, 38].

changes triggered by the rugged contact area with the bone [39, 40]. In tendons, collagen fibers are arranged parallel to each other, and aligned in the direction of the loading, but this organization is lost at the enthesis site, as it is illustrated in figure 1.3 a. When the bone surface is closer, collagen fibers begin to entangle into thinner fibers in a random manner, causing a drop in the elastic modulus with respect to that of tendon, but also increasing resilience by reducing stress concentrations [41, 42]. Moreover, the distribution of HA platelets has a direct response on the behaviour of the fibers.The mineral content increases closer to the bone side. There is a value of mineral content, known as percolation threshold, about which the scattering of collagen fibers is facilitated, increasing the contact area and influencing the stiffness [36]. The two contributions have an interesting result in the comprehensive stiffness of the interface. At first, there is a decrease in the elastic modulus caused by the entanglement of the collagen fibers, accompanied by an slight rise in stiffness due to the linear increase of the mineral platelets closer to bone, showing a non-linear graded transition comparable to a sigmoid-like function (figure 1.3 b) [1, 36].

This interface region owns its great success to its higher compliance compared to both tendon and bone, being able to experience high deformations, especially at the regions before the percolation is reached [41]. Unfortunately, after an injury there is no fully regeneration of the tissue [43]. After healing, scar tissue forms and it behaves as a sharp interface, not recovering the previous mechanical properties and not distributing stresses the way native tissue does, being a real problem for patients and showing the need to improve current recovery procedures [44].

1.3. MANUFACTURING OF BIOMIMETIC ADVANCED MATERIALS

Because of their amazing mechanical properties, there is currently a growing interest in manufacturing materials with improved performance inspired by nature. Manufacturing processes have been used for the mimicking of hierarchical and brick-and-mortar patterns, such as ice templating [45, 46], coextrusion [47], lamination [48–50], laser engraving [51] and foaming [52, 53]. Nonetheless, additive manufacturing has consolidated as an innovative and accurate method for the fabrication of complex designs. The development of multimaterial AM has allowed the production of structures that combine two or more materials, thus expanding the range of material properties within one print. Moreover, the advancement of voxel-based 3D printing enables a tight control over the location of the different materials and benefits from a very high resolution [54]. Voxel-based 3D printing controls the desired pattern at bitmap level, and it is made possible by using the PolyJet 3D printing technology. With this method, multiple molten polymeric drops are jetted through multiple nozzles arranged in line, thus printing layers in a wall-like manner. The printed polymers are cured by exposure to UV light after each layer is printed [55, 56]. This technology has been used to print brick-and-

mortar patterns [57–59], bone-like and biocalcite-like [57, 59], haversian [60], chess board [61] and designs that play with an interlocking topology [62–64]. All these examples showed an increase on the fracture toughness and elastic modulus larger than that of their constituent materials alone, linked to a larger blunting at the crack tip that hinders crack propagation [57, 59]. In addition, they demonstrated the voxel length[61] and the level of hierarchy [59] and the amount of hard material [63] influence the fracture behaviour.
In addition to the use of two or more materials for optimizing materials properties, additional control over the microstructure has been attained by magnetically assisted 3D printing. This procedure consists on adding magnetically coated platelets in the ink, and subjecting them to a low intensity magnetic field after printing to provide them with a certain orientation [7]. The printing equipment is custom-made. Kokkinis et al. used a tailored equipment that could use up to four inks and were mixed at different ratios before being extruded [65]. By combining a shaping ink with a texturing ink full of platelets and magnetically orienting the platelets before curing, they successfully produced samples with complex architectures and defined microstructure. Simmilary, Martin et al. explored the feasibility of 3D magnetic printing for producing structures inspired by osteons and nacre [66]. Their custom-made equipment used stereolithographic masks to provide orientation to the magnetically coated particles in the ink that is is located on a flat recipient, which select the groups of voxels that will present a certain orientation. After this process is accomplished, the ink is solidified by UV light and new uncured ink is brought in the platform.

The design of structures with a graded variation in stiffness is of great interest nowadays, given the applications they could have in diverse industries such as aerospace, automotive, healthcare and robotics. A functionally graded end-effector for a soft robot was developed by Kumar et al. using a Connex 500 equipment (Stratasys) [67]. The elastic modulus varies in 9 discrete steps over a range from 0.5 MPa to 1GPa. The result highlighted an increased strain delocalization, reduces stresses at the interface and provides appropriate anchoring for pneumatic mechanisms. The production of a continuous graded structure was aimed by Kokkinis et al. [68] using a two compartment extrusion platform containing two different inks with distinct properties. The inks are mixed right before being extruded, and a tight control over the mixing proportion of each ink at all times enables to produce prints whose Young's modulus values range in between those of the pure inks. The experimental models with this method demonstrated the decrease in the strain energy density as well as a higher control over crack propagation and confinement.

1.4. AIM OF THE PROJECT

The creation of synthetic advanced materials that combine mechanical properties from a wide range of materials is certainly a hot topic nowadays, and it is drawing much interest. The progress in current additive manufacturing techniques, and in particular of multi-material 3D printing techniques has increased the feasibility of producing structures that optimize the mechanical properties. The need to avoid failure at material interfaces with high mismatch in stiffness suggests the effectiveness of functionally graded transitions at the interfaces. As explained in the previous section, several research projects have been carried out in which gradients have been created by mixing inks with different properties upon solidification. In addition, further modifications have been introduced in the hierarchical structure and microstructure in order to increase the fracture strength of materials. Those research projects, however, did not create the designs by specifically indicating the location of the different materials withing the voxels that conform the pattern. Thus, there is no literature about the behavior of graded patterns created by voxel-based additive manufacturing and at such high resolution with polyjet technology. In addition, this technique has never been been used to incorporate hierarchy and gradients simultaneously.

This project aims to provide design guidelines for the production of graded structures that avoid failure at the interfaces, tune fracture mechanisms and outperform the mechanical properties of the single constituents alone. In addition, the combined effects of gradients with brick-and-mortar and hierarchical structures will be inspected. The main research questions that are assessed in this project are the following:

1.4.1. RESEARCH QUESTIONS

Question 1: How does the gradient pattern that determine material variation affect the fracture and tensile properties?

Approach: Several patterns determining material variation rate will be designed, printed and tested. Those will include vertically and horizontally graded transitions.

Question 2: How does the different material ratio distribution influence the mechanical properties of graded patterns?
Approach: Samples containing complementary ratios of material and correlative graded transitions at both sides of the interface will be designed and assessed.

Question 3: Would the functionally graded transitions outperform sharp material interfaces in a situation that mimics a real scenario?
Approach: A biomimetic model based on a human knee will be created. The knee ligaments made of functionally graded and non-graded soft material will be compared.

Question 4: How would be the effect of combining gradients with brick-and-mortar patterns? How do additional levels of hierarchy affect the mechanical behaviour?
Approach: Patterned designs combining brick-and-mortar and graded material variations will be designed, printed and evaluated. A second level of hierarchy within the structure will be added on both cases and its effects assessed.

1.4.2. STRUCTURE OF THE REPORT

After providing an introduction to the topic and explaining the aim of the project, the following chapter will consist on a description of the methodology of the experiments, the analysis of the results and a discussion about them. Finally, the main conclusions will be stated.

2

EXPERIMENTAL APPROACH

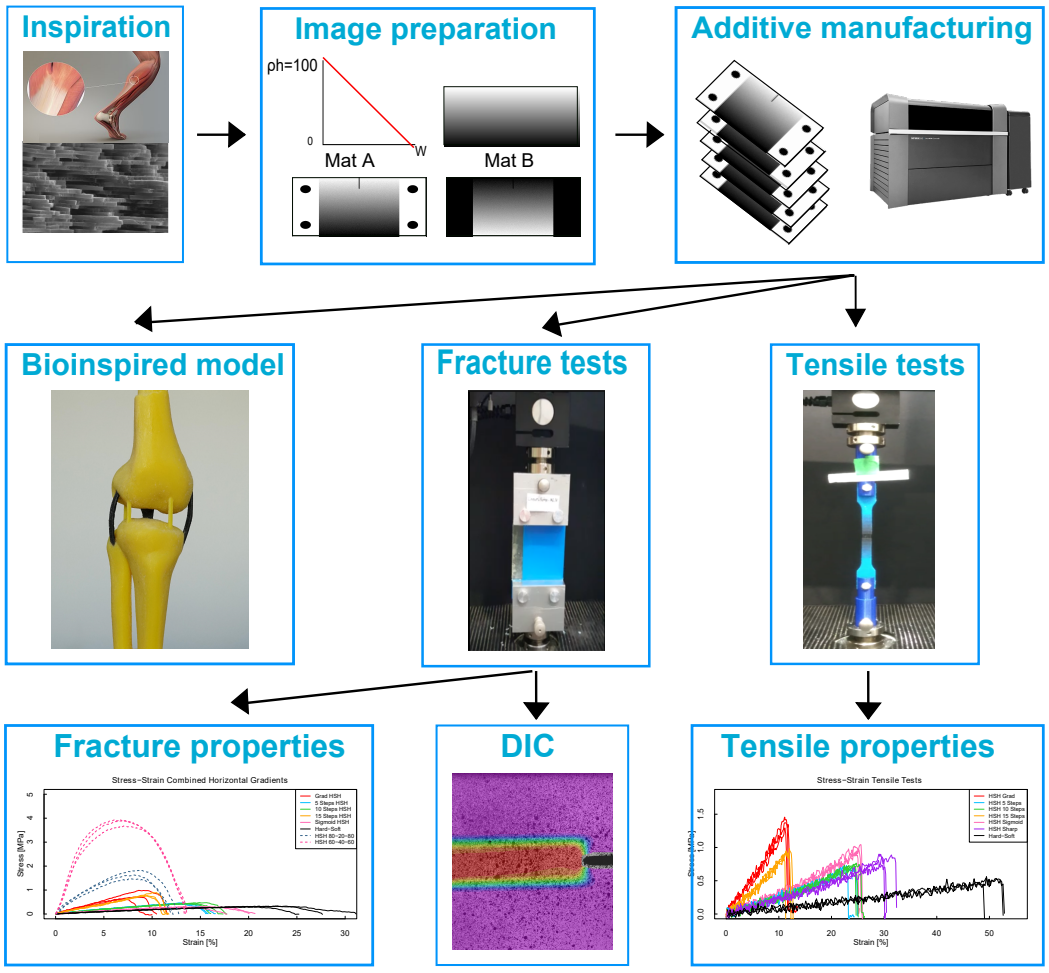

Figure 2.1: Schematics of the experimental procedure followed in this project.

In this chapter, the experimental methodology of the project will be explained. Figure 2.1 shows an overview of the experimental procedure of the project. Nature is a source of inspiration for the creation of materials with advanced properties. The samples are thoughtfully designed, by determining a function or pattern that describes material distribution. The samples are produced by additive manufacturing. A total of 41 patterns were considered, each of them printed in triplets, rendering a total of 123 specimens. The

different models of samples will undergo different types of tests: tensile and fracture tests. Digital image correlation (DIC) will be used in fracture tests to obtain more complete information about the distribution of strains. Finally, a bioinspired model will be used to check if the designed graded pattern outperforms sharp material connections.

2.1. VOXEL-BASED 3D PRINTING

Voxel-based 3D printing is a cutting-edge additive manufacturing method. Voxels refer to three dimensional pixels, a volume element on a grid in a 3D space. This technique allows for a higher precision in the deposition of two distinct materials. The exact position of a voxel with a certain material can be determined, in contrast to other 3D printing methods that use STL files [56]. Therefore, it is highly convenient for the creation of structures that possess intricate designs combining two different materials and achieving a high resolution.

Figure 2.2: Objet350 Connex3 printer from Stratasys (www.stratasys.com).

2.1.1. OBJET350 CONNEX3

The printing equipment is a Polyjet multi-material 3D printer. The printer is equipped with eight printing heads from which three pairs are able to print up to three different materials. The two left printing heads are used to print support material that will assist the printing process and provide extra stability. Each printing head contains multiple aligned nozzles that expel material drops. The material is provided in a liquid format in cartridges that are connected to the printing heads. The material droplets, containing monomers and photo initiators, are cured and solidify upon exposure to UV light. The UV exposure takes place in the printing tray right after each layer is printed, thus triggering direct solidification and enabling the continuous printing of successive layers, as well as promoting a good adhesion between voxels of different materials [69]. In order to not alter the material properties by the position on the printing tray or by overexposure to the UV light, the samples were built one at a time, and maintaining the same position and orientation. The resolution of the printer is 600 dpi in the X-axis, 300 dpi in the Y-axis and 847 dpi in the Z-axis. As a result, the native resolution of the printer renders a voxel whose size is 42x84x30 μm [56].

The materials that were employed in the samples belong to the Vero and Agilus material sets. The Vero family consists on rigid materials with a high tensile strength and limited elongation at break. By contrast, the Agilus family presents rubbery characteristics, with a high elongation at break and a low tensile strength [70]. After the samples were built, the support material was carefully removed and the specimens were cleaned with ethanol.

2.1.2. SAMPLE PREPARATION

Voxel-based additive manufacturing methods, in contrast to other additive manufacturing methods, do not make use of STL files. Instead, they use binary Bitmap files, in which the values of 0 and 1 are assigned to a different material each. The digital materials mode of the printer enables this option [56, 71].

First, a gray-scale image is generated using MATLAB. Gray-scale images possess pixels whose values range from 0 to 255. This image possesses the desired graded pattern, which follows a mathematical function that

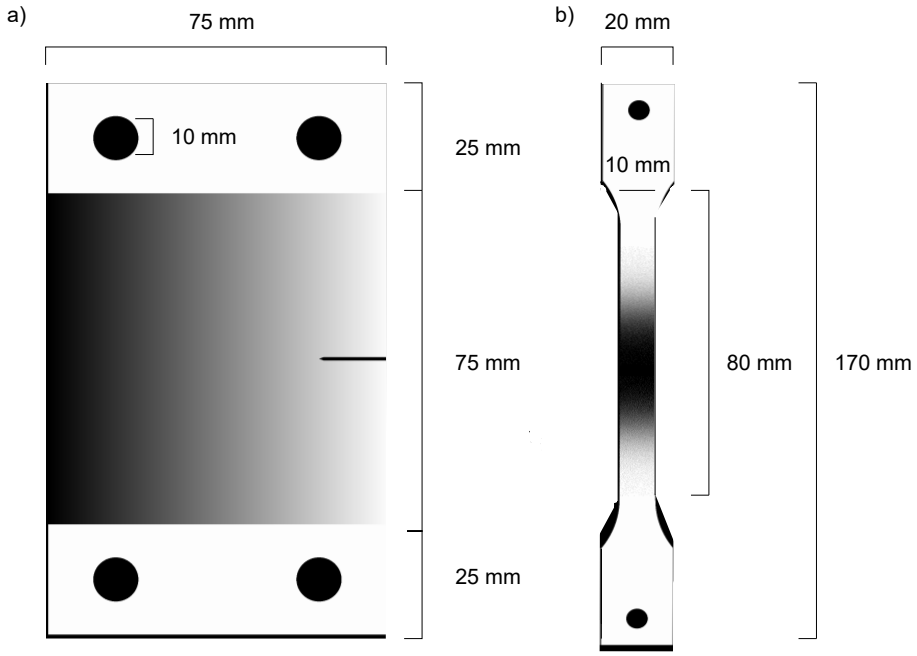

Figure 2.3: Dimensions of the samples for the fracture and tensile tests

.

determines material change. Two main orientations for the gradients were selected; a hard-soft vertical transition and a hard-soft-hard symmetric horizontal transition. The graded transitions also followed continuous or discrete (step-wise) material transitions. However, bitmap files can only have either 0 or 1 values. In order to adapt the graded gray-scaled patterns to suitable bitmap files that can be read by the printer, the images were subjected to halftoning methods [72]. These algorithms can create the illusion of a continuous tone, while they are made out of white and black dots. The algorithms check the different densities of printing material on each location, and based on that, the different materials are assigned within neighbouring voxels. For the samples, an error diffusion algorithm was applied to the initial image [73]. With this method, the material placed in a voxel influences the material arrangement of the surrounding voxels by the way the quantization errors are distributed. The error coefficients from the previous pixels are passed on to the new pixels that are processed, thus rendering a binary image whose black and white units are arranged in a semi-ordered manner.

Each layer to be printed corresponds to a different bitmap file. The bitmap files for each material are complementary to each other, meaning that the pixel location in which each material has to be deposited is indicated with a pixel value of 1. That same pixel presents a value of 0 for the other materials. Two different types of samples with different shapes were created, depending on the test they were aimed for:

- The samples aimed for the fracture tests presented a single-edge notch that was printed within the sample (Figure 2.3 a). The samples had a squared working area of 75x75 mm, and a thickness of 3 mm. The initial crack spanned 20% of the width of the sample, thus 15 mm, and was strategically placed at the weakest point of the pattern. In order to attach the samples to the grippers for the tests in the machine, two areas of hard material were printed in the upper and lower sites of the samples. Their width was equal to the width of the working area, and the length was 25 mm. This addition serves as an attachment for the grippers that will connect to the machine. In order to facilitate that, it includes two holes that connect to the pins for the attachment, whose diameter is 10 mm.

- The samples that were meant for the tensile tests follow the size specified by the international standard protocols ISO 527-1 for plastics and JIS K 7161. They consist on a strip of length 80 mm, width of 10

mm and thickness of 4 mm. The strip is included in a dogbone structure that eases the attachment to the gripping system, of 170 mm length and 20 mm width, as it is seen in Figure 2.3 b.

2.2. FRACTURE MECHANICS SAMPLES

The samples assessed for fracture mechanics correspond to rectangular samples with a single-edge notch on one side. The tests could not be carried out using the ASTM standards because the materials used did not meet the specifications of these procedures [74]. However, the experimental set-up and the size of the samples are similar to previous studies where tensile tests of single-edge notched samples were carried out [8, 57, 59, 60, 62, 75, 76]. The crack is placed at the weakest point of the structure, in order to facilitate crack propagation. The samples are attached to the machine by a custom-made gripping system made of aluminium, and fixed by aluminium pins. The equipment used was a Lloyd tensile test machine (LR5K). The load applied to break the samples was measured by a 5 kN load cell, which is a reasonable limit that exceeds the maximum load required to break the specimens. The displacement rate was set to 2mm/min and the pre-load to 1 N. The displacement rate was applied to the upper part of the specimens, while the lower part remained static. The loading was performed until the samples were completely fractured. The time, load, deflection from preload and extension were retrieved from the tests at a frequency of 20 Hz. From this data, the fracture properties were obtained using the software RStudio (RStudio, Inc., Boston, MA, 2015).

2.2.1. FRACTURE PROPERTIES

An overview of the fracture properties assessed is detailed in this section:

- Normal stress (σ): The normal stress (MPa) results from the ratio of applied load (F) over the area where it is subjected (A_0), which was determined as $A_0 = t * (w - a_0)$, where t is the thickness, w the width and a_0 the pre-formed crack length.
- Strain (ϵ): The strain refers to the relative displacement with respect to the initial length of the sample between the grippers (l= 75mm). It is indicated as a percentage (%) or as a dimensionless ratio.
- Stiffness (E): The stiffness, or elastic modulus (E) refers to the stiffest slope of the elastic part in the stress-strain curve. To obtain it, a regression algorithm was used, in which a moving box of width of 0.2% strain finds the stiffest slope possible in a small window.
- Fracture stress (σ_f): The fracture stress was defined as the maximum stress.
- Fracture toughness (U): The fracture toughness refers to the energy required in order to break the samples (MJ/m^3), and it is represented as the area below the stress-strain curve. The formula shows that a high fracture toughness is reached with the contributions of a high fracture stress and strain.

$$U = \int_0^{\epsilon_f} \sigma \, d\epsilon \tag{2.1}$$

- Strain at fracture (ϵ_f): It is defined as the strain value of the last recorded data, at the moment the total fracture of the sample takes place.

2.2.2. SAMPLE DESIGNS

The single-edge notched samples used to test the fracture properties of the different material distributions are divided into two different patterns: designs that explore different functions for graded transitions of materials and brick and mortar patterns to assess the effects of hierarchy, also in combination with gradients.

GRADIENTS

The graded patterns follow continuous and discrete transitions, and all of the patterns keep an overall hard volume fraction of 50%. Vertical gradients vary from hard material at the crack tip to soft material at the bottom part (Figure 2.4). The vertical gradients are inspired by the attachment of tendons to bone, mimicking a hard-soft transition. In the figures, white represents hard material and black corresponds to soft material. The manner in which the graded transition takes place is represented, and defined as the variation of hard

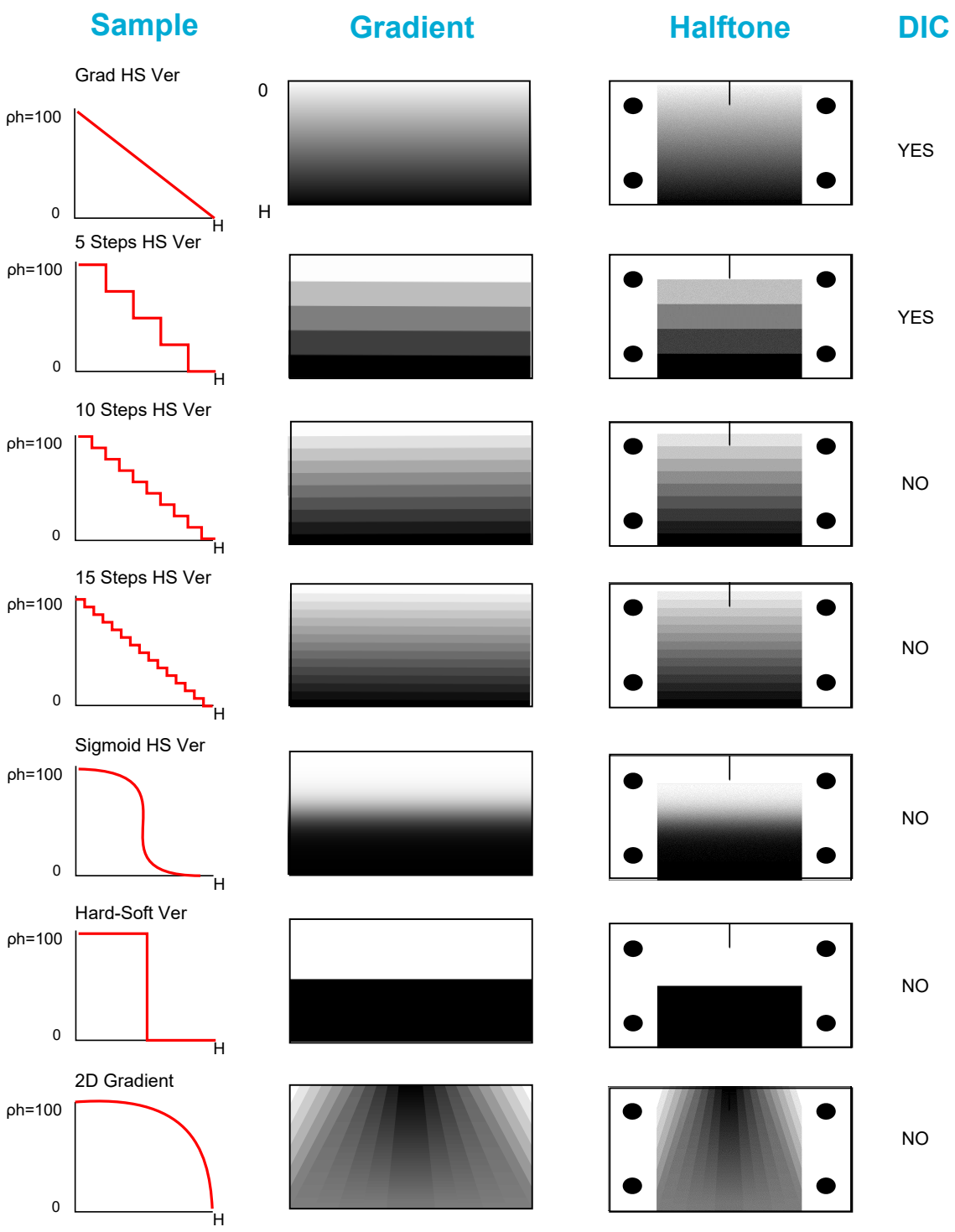

Figure 2.4: Overview of the different vertical gradients patterns, including the function for material change (left), the gray-scaled image (center), and the samples after being processed with the halftoning algorithms (right). The material change rate is given as the amount of hard material (ρ_h) through the height of the pattern (H), which is 75mm.

material density (ρ_h) through the height of the pattern (H). One design shows a two-dimensional gradient, in which the material is distributed in a radial manner, being completely soft at the crack tip and 50% hard at the lower part (Figure 2.4).

Figure 2.5 represents the horizontally graded patterns, where the hard material is situated on the edges, close to the grippers, and soft material is confined in the middle part, close to the notch. A specific design presents a two-dimensional gradient where a vertical and horizontal gradient are combined. On one half, the gradient goes from 0 to 50% hard material, whereas on the other half, the variation goes from 100 to 50% hard material. The material interface is located at both sides of the preformed crack.

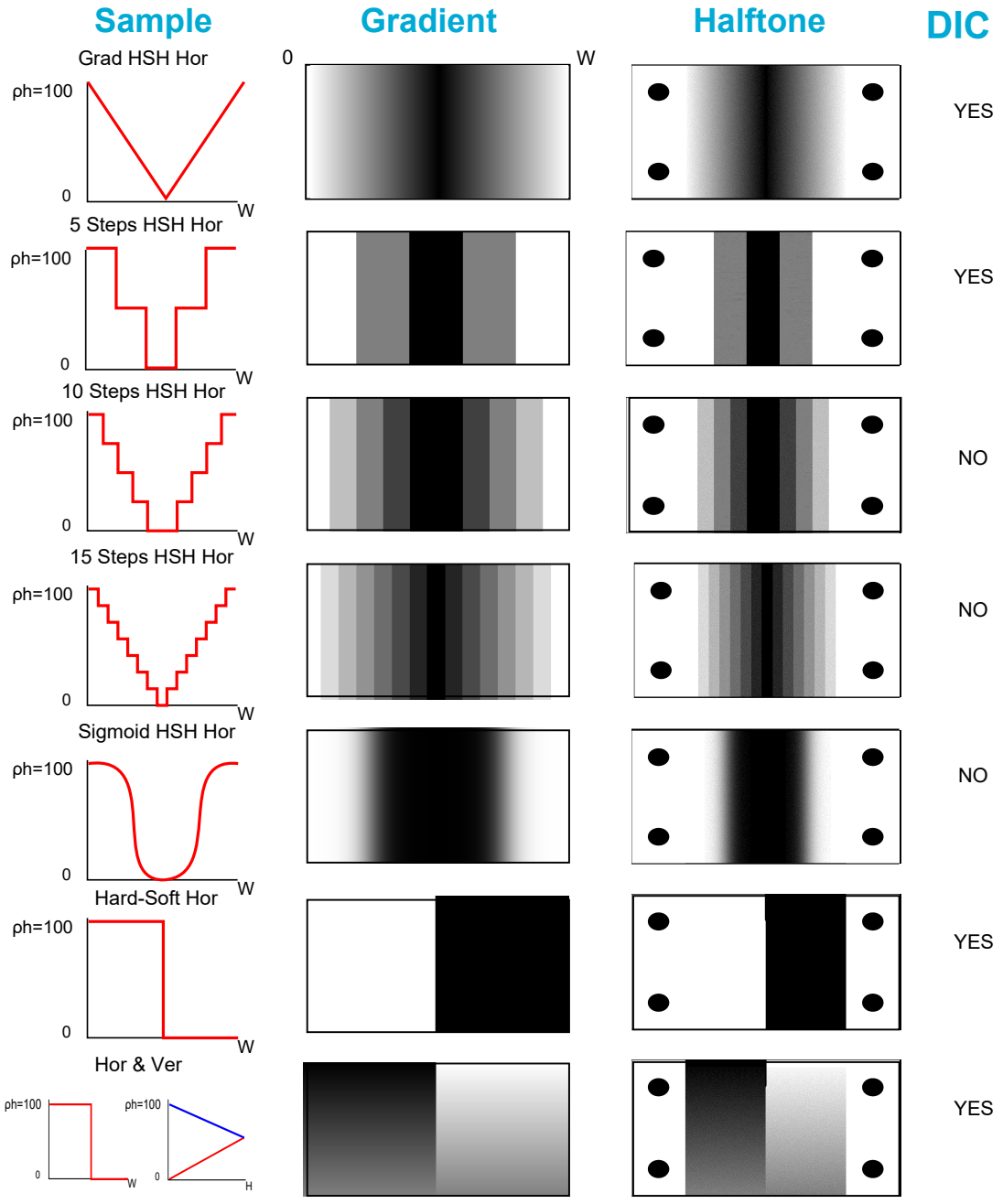

Figure 2.5: Summary of the horizontal gradients assessed. The material change rate is given as the amount of hard material (ρ_h) through the width of the pattern (W), which is 75mm.

Another batch of samples was created, where different horizontal gradients where assessed (Figure 2.6). In those samples, different percentages of hard and soft material where reached, but avoiding concentrations of pure hard or pure soft material. Thus, there were samples where the percentage of hard material ranges from 80-20-80% and 60-40-60%, or there is a complementary material interface between 20-80% and 40-60% of hard material. In order to avoid sharp interfaces between the grippers and the half with the higher amount

of soft material in the samples with 20-80% and 40-60% of hard material, a smoothening gradient was performed through the first 4 voxels, until the desired density was achieved. In all the samples, the overall hard to soft percentage was approximately 50%. A detailed review of all the patterns used and the relative ratio of hard and soft material is found in the Appendix A.1. All the samples were printed in triplets. For this batch of samples, the control groups were given by three samples of pure hard and soft material, and three samples with 50% hard material distributed amongst the voxels in a semi-random manner from a previous study [71].

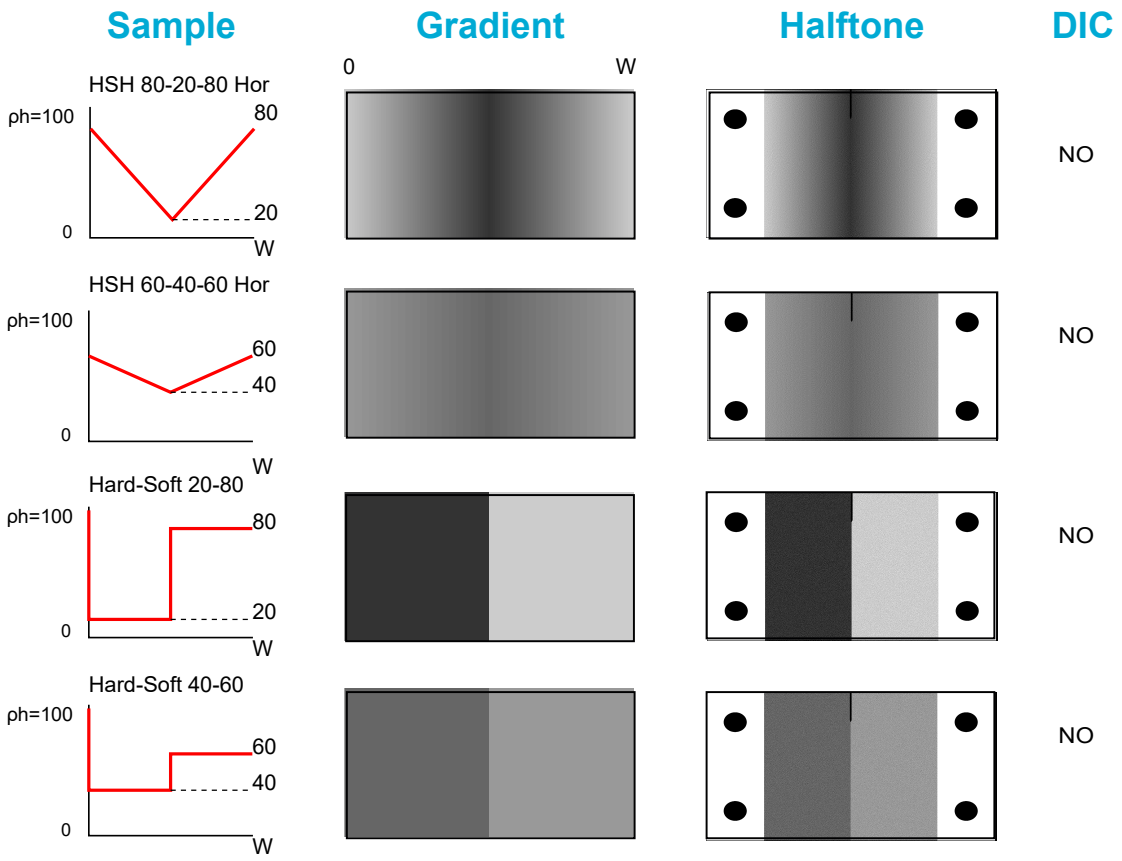

Figure 2.6: Summary of the horizontal gradients presenting different density ranges and complementary interfaces. The material change is defined by the density of hard material (ρ_h) through the width of the pattern (W), The samples hard-soft 20-80 and hard-soft 40-60 present a complementary amount of hard material at both sides of the interface. They experience a sharp drop in the density plot because the half of the sample with the highest amount of soft material is connected to the gripping part through a small gradient, in order to avoid stress concentrators and breakage.

HIERARCHY AND GRADIENTS

The effects of hierarchy on the fracture properties of a material were determined by the design of three different patterns inspired by the brick-and-mortar structure of nacre. Two patterns present a single level of hierarchy, containing unit cells whose aspect ratio is 2.5 and 5.6 respectively. A second level of hierarchy is introduced in another design, presenting an aspect ratio of 5.6 for the unit cell and ratio of 15 for the second level of hierarchy, representing a fibril 2.8.

Finally the single-level with ratio 5.6 sample and the two-level sample are combined with the horizontal gradient with 100-40-100% of hard material to inspect the modulated effects of hierarchy in combination with graded properties. A detailed overview of the relative material ratio for these samples is depicted in the Appendix A.1.

All the samples were printed in groups of three units. A summary of these samples is displayed in Figure 2.7. For these samples, the horizontal gradient with composition 100-40-100% hard material was used as control group. In addition, three more sample subsets were included as controls following different material distributions caused by different halftoning algorithms: Semi-Random, Random, and Ordered [71]. For each pattern,

two groups with overall 50 and 75% hard material were considered, thus, adding six extra samples.

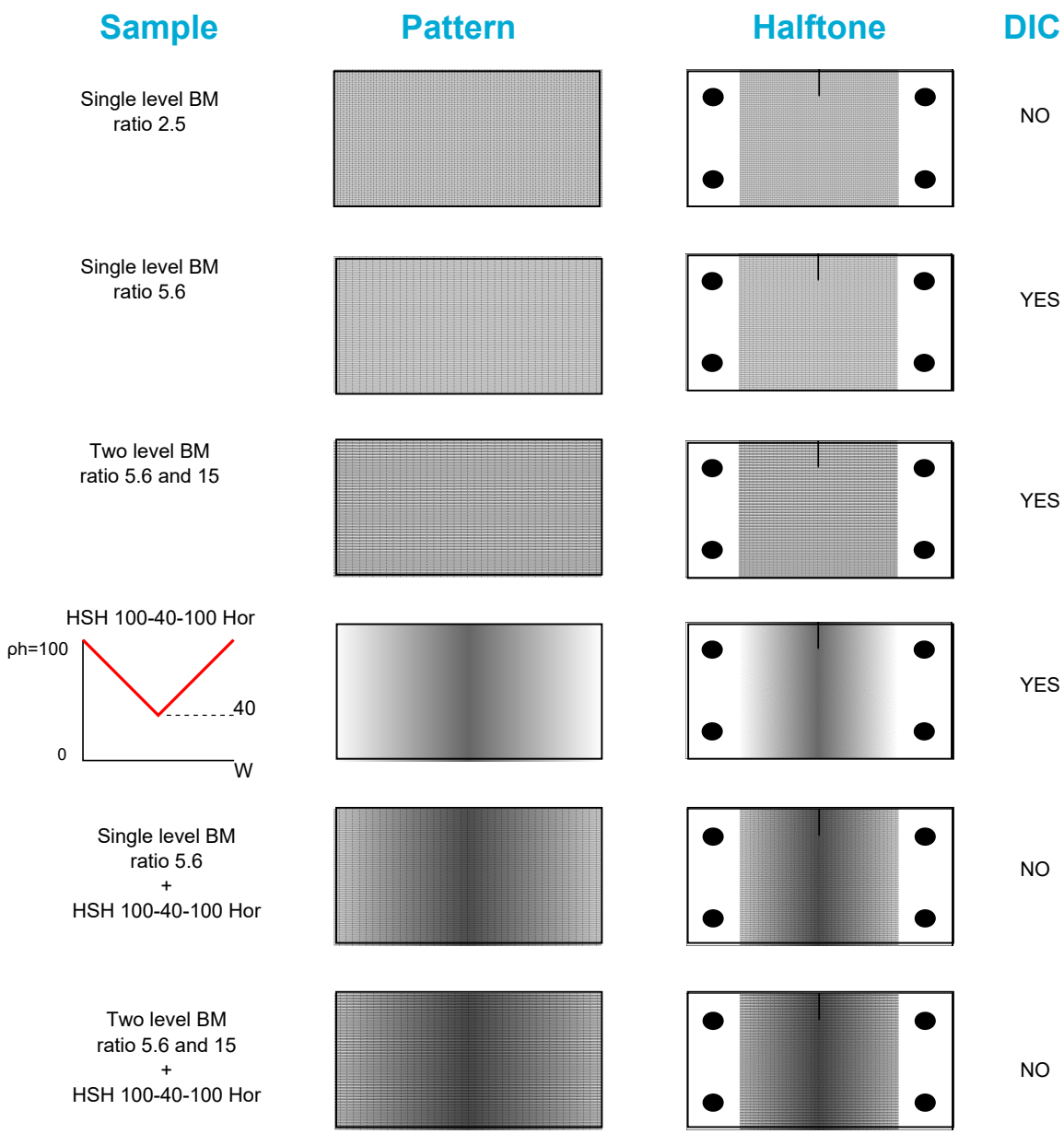

Figure 2.7: Summary of the brick-and-mortar patterns and their combination with a gradient of 100-40-100% hard material.

2.3. TENSILE TEST SAMPLES

The dogbone samples underwent tensile tests in the same LLOYD tensile test machine as the fracture mechanics samples. The gripping system was custom made for the samples, consisting of a cylindrical holder and pins to fix the samples. They were fabricated by a fused deposition modelling (FDM) 3D printer (Ultimaker 2+, Geldermalsen, The Netherlands) using fused polylactic acid (PLA) filaments (MakerPoint PLA 750 gr Natural). The pure hard samples were tested using aluminium grippers with identical dimensions. The measurements were taken with the 5 kN cell load from the previous tests. The dimensions of the samples allowed for the use of the same loading protocols as for the fracture tests. Therefore, the test set-up was maintained: 2 mm/min displacement rate and a pre-load of 1 N, recorded at a frequency of 20 Hz. From

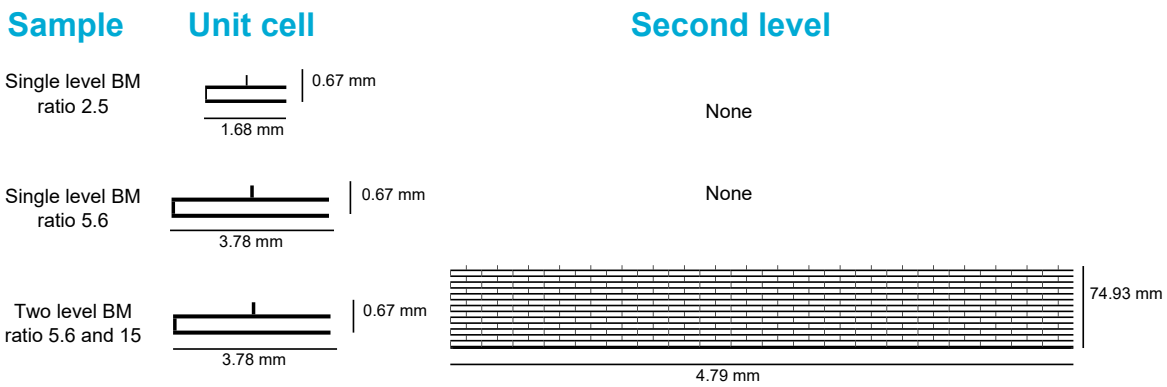

Figure 2.8: Overview of the unit cells and hierarchical levels of brick-and-mortar patterns.

the tests the force and displacement were obtained. The stress and strain were calculated, as well as the ultimate strength, elastic modulus, toughness and strain at fracture. These results were obtained and analyzed in RStudio (RStudio, Inc., Boston, MA, 2015).

2.3.1. TENSILE PROPERTIES

An overview of the tensile properties assessed is detailed below:

- Normal stress (σ): The normal stress, whose units are given in MPa, is a consequence of the applied load (F) over the cross-sectional area (A_t). The area is given as $A_t = t_t * w_t$, where t_t is the thickness and w_t is the width.
- Strain (ϵ): The strain is given as the relative displacement to the initial length of the sample ($L = 80mm$). It is expressed as a dimensionless ratio or percentage (%).
- Stiffness (E), or elastic modulus, is the stiffest slope of the elastic part in the stress-strain curve. The same regression algorithm was used to obtain it as in the fracture mechanics properties.
- Ultimate Strength (UTS), expressed in MPa, refers to the maximum stress in the stress-strain curve.
- Toughness, given as the energy required per volume for the sample to break, and expressed in MJ/m^3. It can be obtained from integrating the area under the stress-strain curve.
- Strain at Fracture (ϵ_f): It is the last recorded value of strain at the moment of total fracture of the sample.

2.3.2. SAMPLE DESIGNS

Different designs were selected for the assessment of the tensile properties of different gradients, as well as sharp interfaces. Each sample was printed in triplets and the patterns are shown in Figure 2.9. The control groups are given by pure hard and soft samples.

2.4. DIGITAL IMAGE CORRELATION

Digital image correlation (DIC) is an image analysis method which can determine the distributions of strain in 2D of an object under loading, by tracking the position of black speckles sprayed over a white painted sample. The DIC tensile tests were carried out on a Zwick Roell machine (Zwick GmbH & Co. KG) using a 20 kN load cell. In order to enhance the contrast with the black speckles, the samples were lighted with a Profilux LED while the tests were performed. Two high resolution cameras recorded the test and were connected to the computers. Before the tests, they had been calibrated to obtain the relative angle and position with respect to each other in all directions. During testing, a picture was taken every second until the complete fracture of the sample took place. The data retrieved from the displacement of the speckles was analyzed by the software Vic-3D (Vic-3D 8, Correlated Solutions, SC, USA), in order to obtain the stress and strain distributions. For

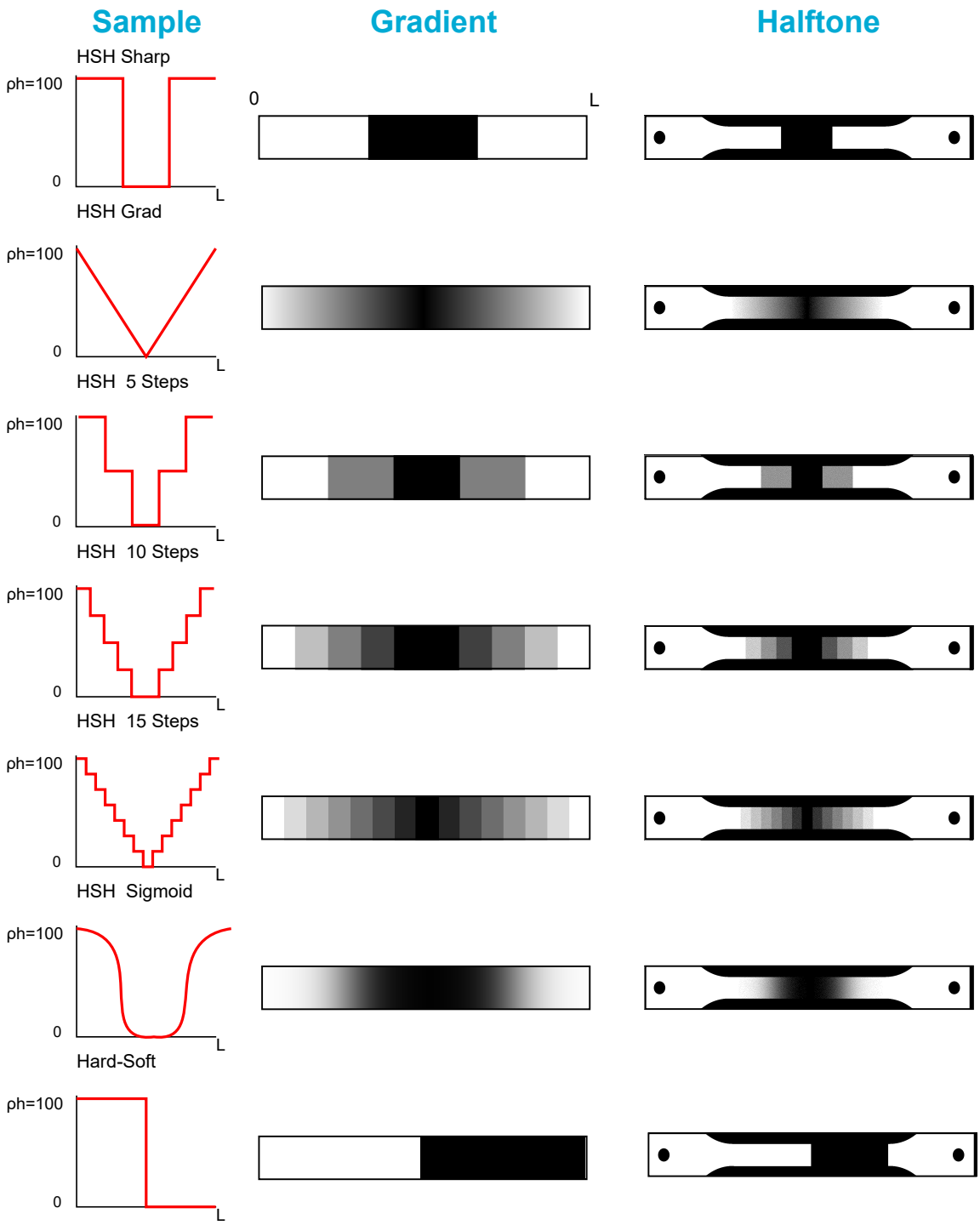

Figure 2.9: Summary of the patterns assessed for tensile properties. The graded patterns are symmetrical through the length of the tensile pattern (L), which is 80 mm. The graded pattern is defined as the density of hard material (ρ_h) along the length.

the calculations, it was determined a subset of 29 and a step size of 7.
The ϵ_{yy} strain component was obtained, which refers to the strain in the axis parallel to the applied force. It is defined in Eq 2.2, as the change in length l_f over the original length l.

Table 2.1: Samples selected for DIC testing

Samples selected for DIC

Gradients	Brick-and-Mortar & Gradients	Others
Single level Brick-and-Mortar ratio 5.6	Grad HS Ver	Hard-Soft Hor
Two level Brick-and-Mortar ratio 5.6 and 15	5 Steps HS Ver	Hor & Ver
HSH 100-40-100	Grad HSH Hor	
	5 Steps HSH Hor	

The samples selected for the DIC imaging are indicated in Table 2.1.

$$\epsilon_{yy} = \frac{l_f}{l} \tag{2.2}$$

2.5. BIOINSPIRED MODEL

A real application for the graded structures was determined by mimicking a model found in nature, as it is the human knee and its ligaments, as it can be see in Figure 2.10. An appropriate file of the model was searched in the open source database Thingiverse. The knee model was adapted from [77] and consisted on the femur, tibia and fibula. The lateral collateral (LCL), medial collateral (MCL), anterior cruciate (ACL) and posterior cruciate (PCL) ligaments were included in the model, and the patella bone was left out, as well as the lateral and medial meniscus. The total length of the bone models is 24 cm, and the lengths of each of the ligaments are: 3.5 cm for the MCL, 3cm for the LCL, and 1.5 and 2 cm for the ACL and PCL respectively.

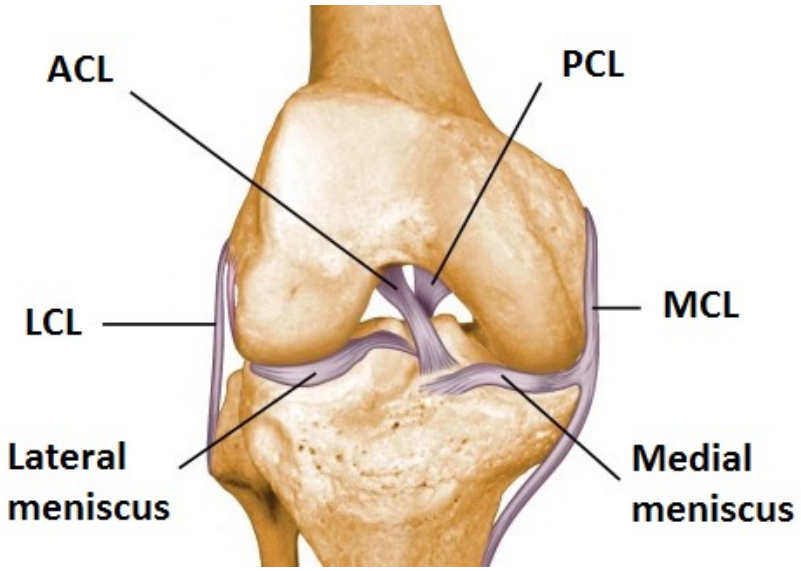

Figure 2.10: Schematics of the main ligaments in the human knee, depicting the lateral collateral ligament (LCL), medial collateral ligament (MCL), anterior cruciate ligament (ACL) and posterior cruciate ligament (PCL). In the 3D printed model, the lateral and medial meniscus are not included.

Two models were fabricated, with two different designs for the elliptical ligaments. The first one presented completely soft ligaments, meaning that there is an abrupt interface between hard and soft material at the attachment site. The other presents a linearly graded connection to the bone, which takes place over a small region of 1 mm length (Figure 2.11.)

The samples were printed with the Objet350 Connex3 3D printer, combining soft (Agilus) and hard (Vero) materials. The final 3D printed knee models for the graded ligaments are shown in Figure (2.12), and the models containing the non-graded ligaments are shown in Figure 2.13.

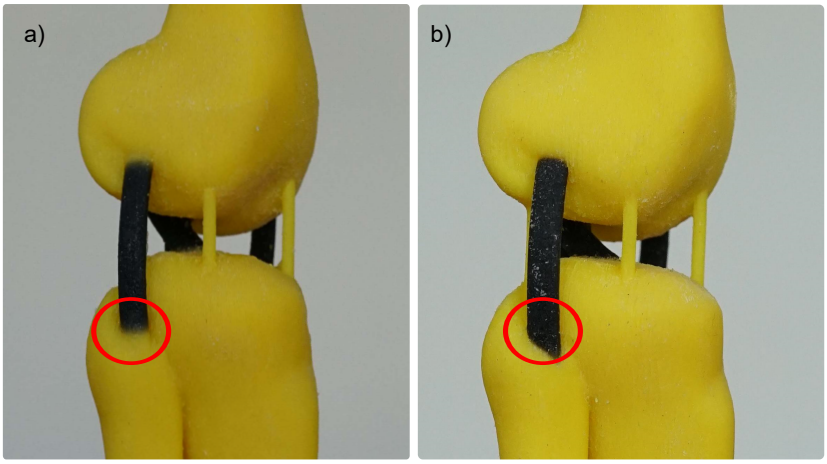

Figure 2.11: Detailed view of the connections of the soft rods to the stiff bone in the biomimetic knee model: a) Graded connection and b) Sharp interface.

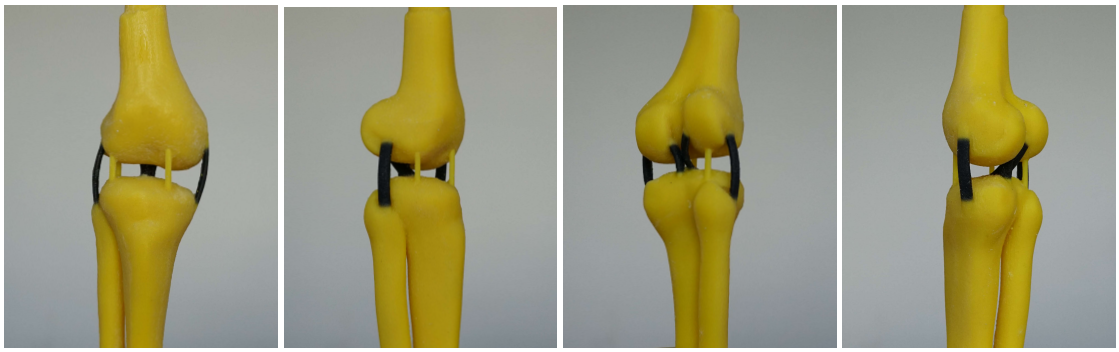

Figure 2.12: 3D printed models of the knee with functionally graded connections. The attachment of the soft rods is carried out in a graded manner through a short region. The images show the anterior (top left) and posterior (bottom left) views and the lateral perspectives (top and bottom right). The yellow sacrificial strips ease the cleaning process.

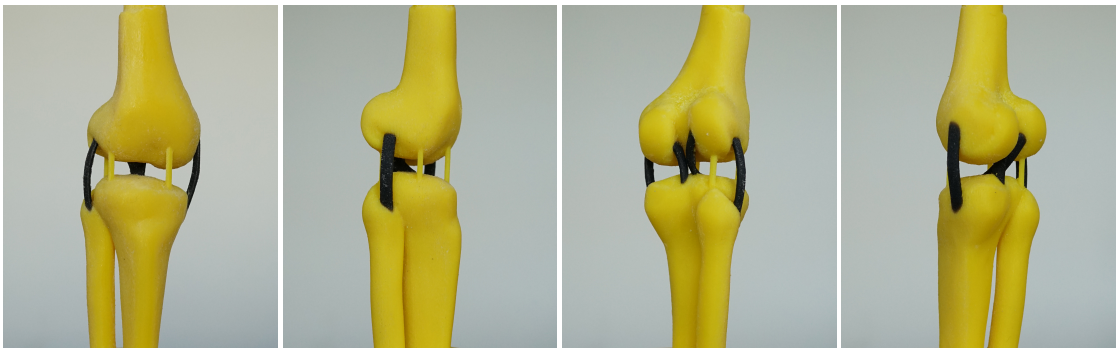

Figure 2.13: 3D printed models of the knee with non-graded connections to the soft ligaments. The attachment presents a sharp hard-soft interface. The images show the anterior (top left) and posterior (bottom left) views and the lateral perspectives (top and bottom right). The yellow sacrificial strips ease the cleaning process.

2.5.1. TENSILE TESTS

Tensile tests were performed on the bone models with graded and non-graded ligament connections. The test were performed in the Lloyd (LR5K) machine used in the former tests, following the same protocol as with the single-edge notched and dogbone samples, but using a cell load of 100N to avoid higher amount of noise in the measurements. The bone samples were directly attached to the machine. The samples had holes that fitted tightly the dimensions of the screws of the machine and the cell load, and they were secured with pins. The information regarding the load and deflection from preload was retrieved and analyzed.

3

RESULTS

3.1. FRACTURE MECHANICS OF GRADIENTS

The fracture mechanics of the samples with 50% amount of hard and soft material was obtained from the data retrieved from the tensile test machine, in which the load and deflection from preload were recorded. From there, stress and strain values were derived by taking into account the cross-sectional area of the samples and the initial length. Furthermore, fracture properties such as the fracture stress, fracture energy, Young's modulus and strain at fracture have been analyzed.

3.1.1. STRESS-STRAIN GRAPHS

The stress-strain plots of the samples with vertical gradients are shown in Figure 3.1, together with a sample with a sharp interface. The graded samples follow a common trend, reaching stress maximum values close to 5 MPa. By contrast the sample with the sharp interface reaches higher values of maximal stress. All of the samples exhibit a brittle fracture, characterized by presenting a small area under the stress-strain curve. After the ultimate strength value is reached (the highest value of stress achievable), the crack expands rapidly, which is reflected in the abrupt decrease in the stress values.

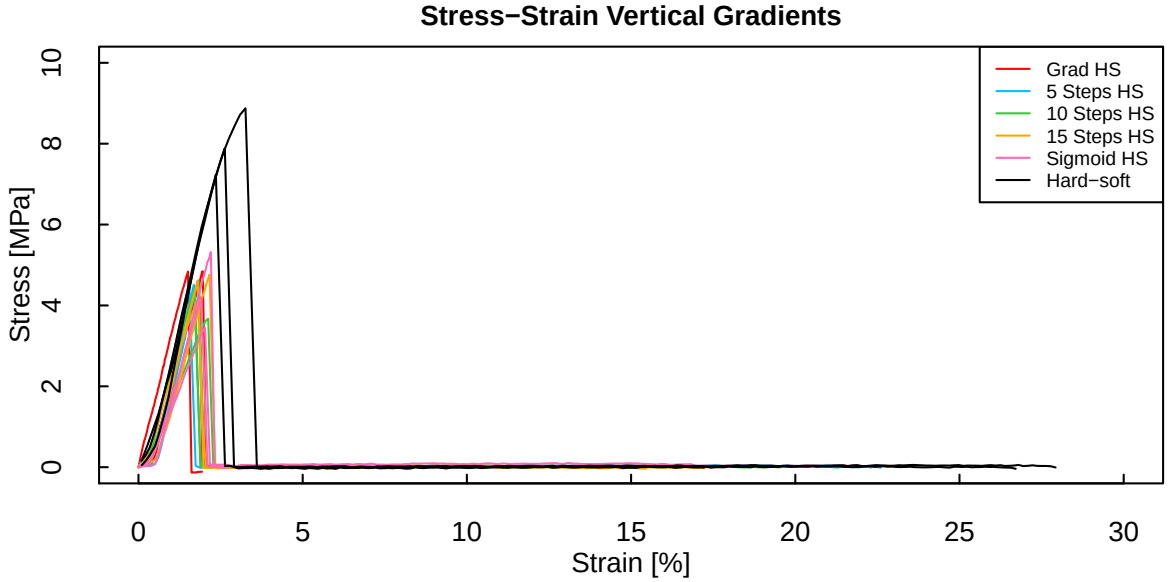

Figure 3.1: Stress-strain graph of vertical gradients. The material transition is from hard at the crack tip to soft at the lower part

The stress-strain curves of the samples with horizontal gradients are presented on Figure 3.2. The horizontal transitions are all symmetric, meaning that they vary in a hard-soft-hard manner. The crack tip is placed in the middle of the sample, surrounded by soft material. The curves presenting the lowest stress

values are those corresponding to the discrete gradients of 5 and 10 steps and the sigmoidal transition. The sample with the sharp interface between hard and soft material undergoes a larger elongation, but does not reach high values of maximal stress. The linearly graded hard-soft-hard transition and the discrete transition of 15 steps reach slightly higher values of maximal stress, compared to the other transitions from 0 to 100% hard material. However, there is still no great contribution to the fracture energy, in other words, the area below the stress-strain curve. By contrast, the samples whose transitions do not reach completely 0 or 100% hard material, but varying in a 80-20-80 or 60-40-60% ratio of hard material experience a four fold and two fold increase respectively compared to the linearly graded horizontal transition (100-0-100% hard material). They present a ductile fracture, where the crack tip was blunting while the crack was propagating. Thus, there is a significant increase in the fracture energy.

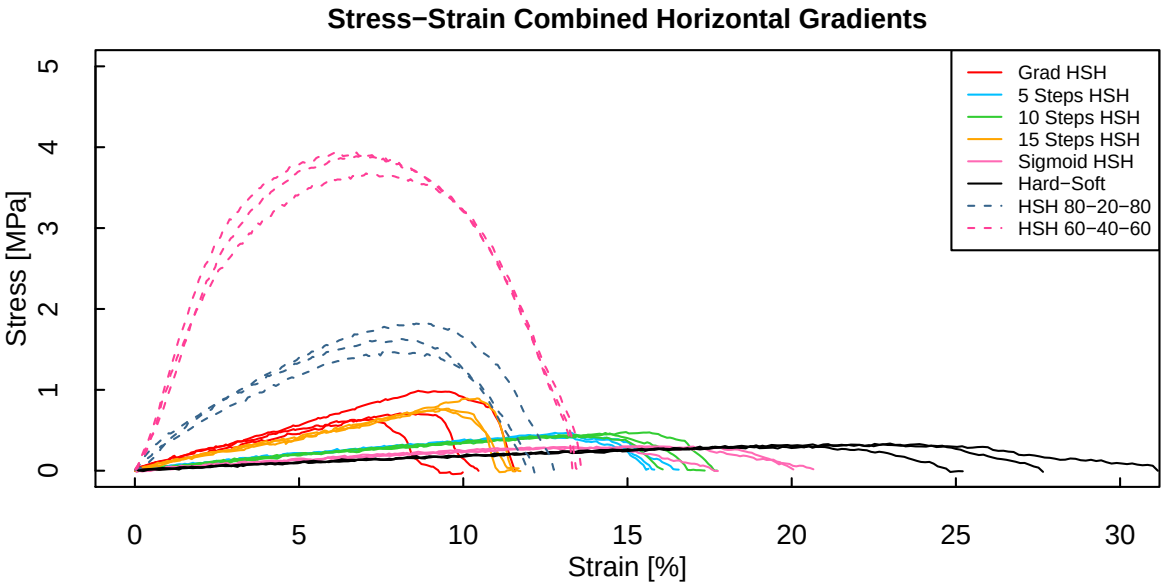

Figure 3.2: Stress-strain graph of horizontal gradients. The material transition is symmetric, being hard at the gripper's site and soft in the middle, where the crack tip is located.

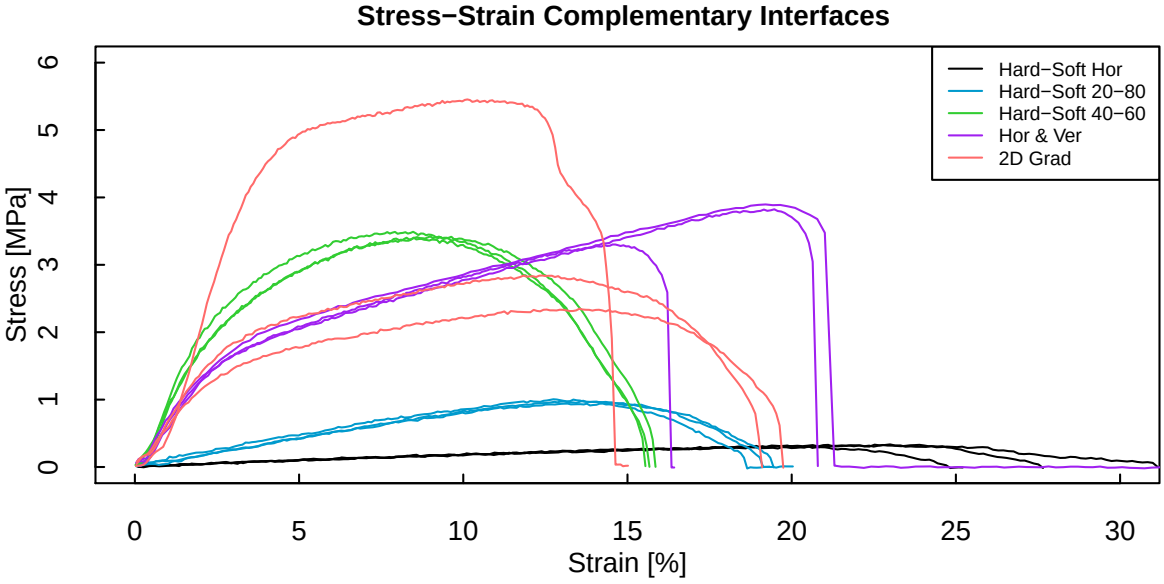

Figure 3.3: Stress-strain graph of samples presenting complementary material concentrations at both sides of the interface.

Similarly, the stress-strain graphs regarding the samples with complementary amount of hard material at both sides of the material interface are depicted in Figure 3.3. The crack tip is placed at the interface, in order to drive crack spreading through the interface, given that it is the weakest point of the structure. A sample

designed containing a sharp interface of 100-0% hard material is also displayed, showing a ductile behaviour due to the stretching of the soft material side, with large deformation and reaching little stress values. A sharp interface is also presented by two more specimens, with hard material ratio at both sides of the interface of 20-80% and 40-60% respectively. As it can be observed in Figure 3.3, the interface of the 40-60% hard material increases the amount of fracture energy released, due to a good trade-off of the increased amount of stress and strain. In addition, the subtle blunting of the crack tip triggers a ductile behaviour. An interesting behaviour is provided by the horizontally and vertically graded sample. Through its interface, the amount of material runs inversely and in a complementary manner, starting with a material difference of 100-0% hard material at the crack tip and reaching 50% hard material in the bottom part. This elaborate interface design shows an optimal combination of high stress and strain values, increasing significantly the fracture energy. The stretching occurring at a lower stress and the later breakage at a higher stress demonstrates the hardening of the sample. Thus, the material is strengthened due to plastic deformation. The last sample depicts a radial two-dimensional gradient where the crack is placed in the region with full soft material. As observed, the fracture energy released is remarkable, showing both high stress and strain values.

3.1.2. FRACTURE PROPERTIES

In the barplots below, the mean values of the fracture stress, fracture energy, elastic modulus and strain at fracture are compared simultaneously for the vertical and horizontal gradients with equivalent patterns, together with the horizontally and vertically graded pattern and the two-dimensional radial gradient. The values for the standard deviation are indicated as well in the bars.

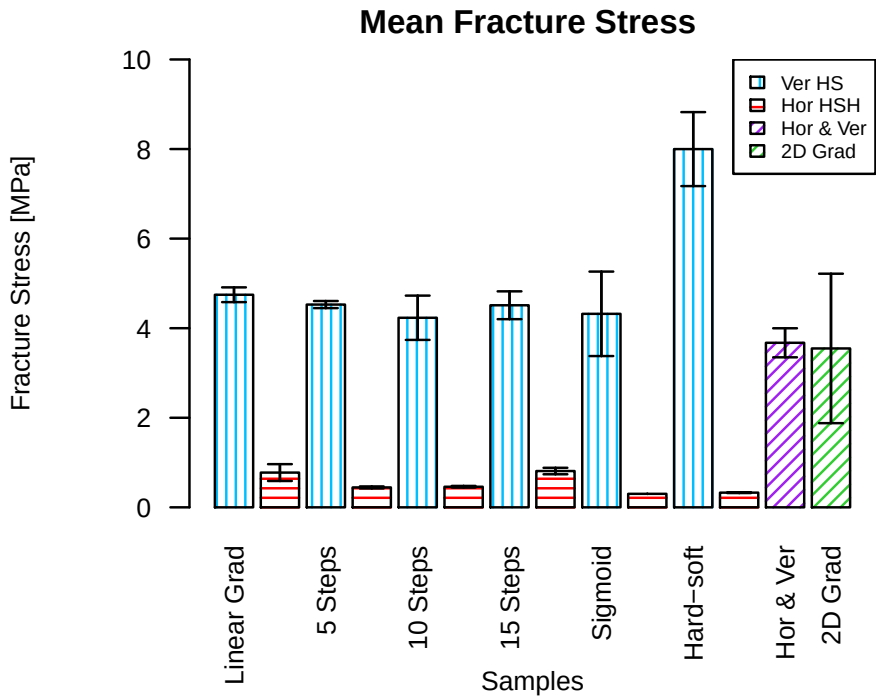

Figure 3.4: Barplot of the mean fracture stress of vertical, horizontal, horizontal and vertical and 2D gradients. The standard deviation for each sample set is represented by the lines within the barplots.

The mean fracture stress is shown in Figure 3.4. The results put into evidence the higher fracture stress experienced by the vertical gradients. This is caused because the hard material is located at the crack tip, thus inducing more stress when the load is applied. The lowest mean fracture stress is given by the sample with 10 steps, although the values do not vary much for the other samples. The wider hard material region in the hard-soft vertical transition triggers a two-fold increase in the mean fracture stress value. In contrast to the vertical gradients, the horizontal symmetric graded patterns present significantly lower mean fracture stress values, being slightly higher in the linear gradient and 15 step-wise. This is caused by the narrower region of purely soft material in the middle part. The horizontal and vertical pattern and the two dimensional gradient

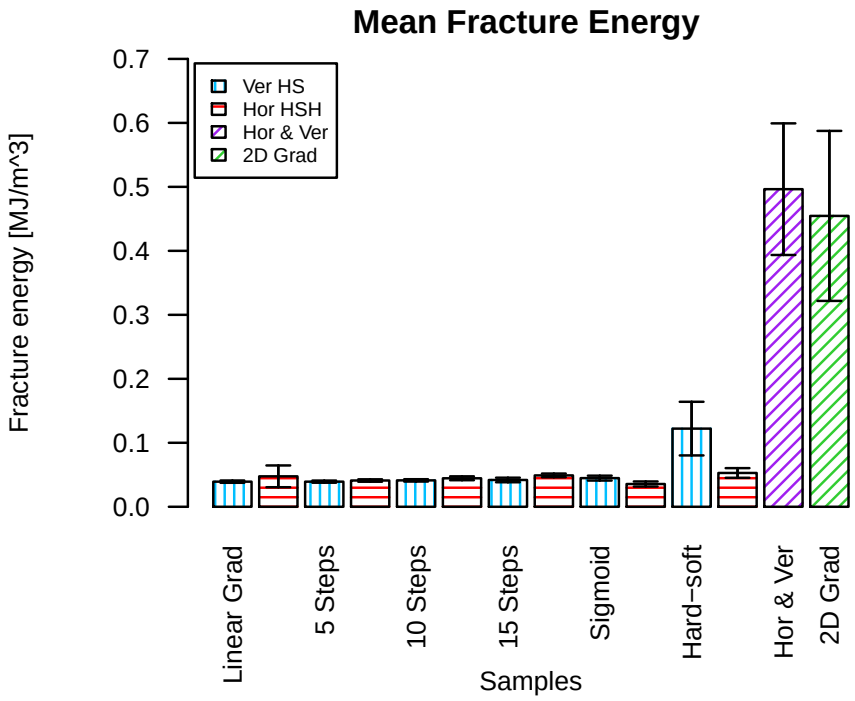

Figure 3.5: Barplot of the mean fracture energy of vertical, horizontal, horizontal and vertical and 2D gradients.

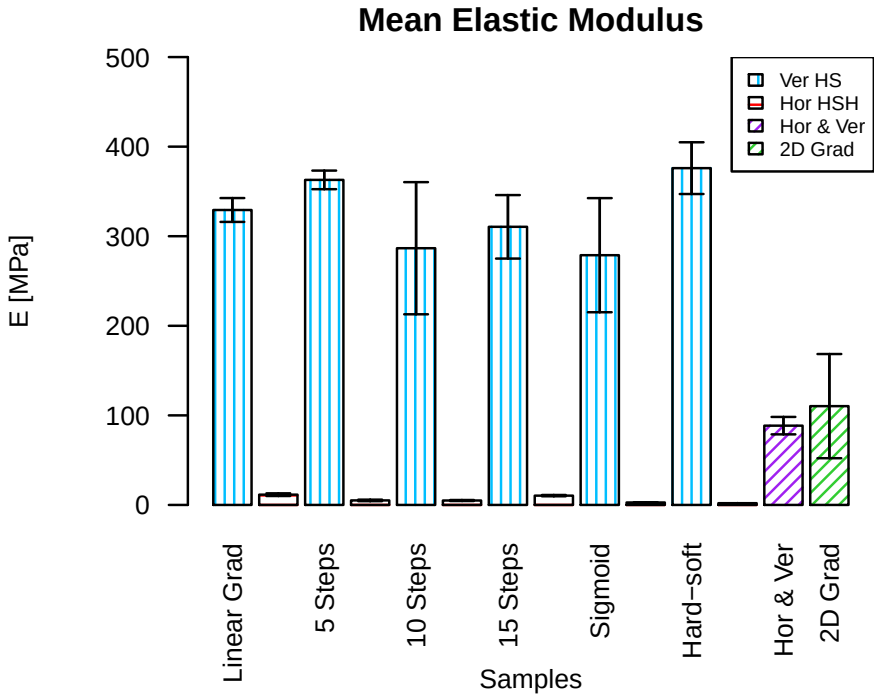

Figure 3.6: Barplot representing the mean Young's modulus of vertical, horizontal, horizontal and vertical and 2D gradients.

result in a similar behaviour in terms of fracture stress.

An overview of the mean fracture energy of the samples is shown in Figure 3.5. From the results, it is clear that none of the horizontal and vertical gradients displayed there contributes to an increase in the fracture energy, in contrast to the horizontal and vertical gradient and the two-dimensional gradient, which present the highest values. As for the stiffness of the samples, those with vertical gradients present considerably higher values for the elastic modulus than those with the horizontal gradients, as it is illustrated in Figure 3.6.

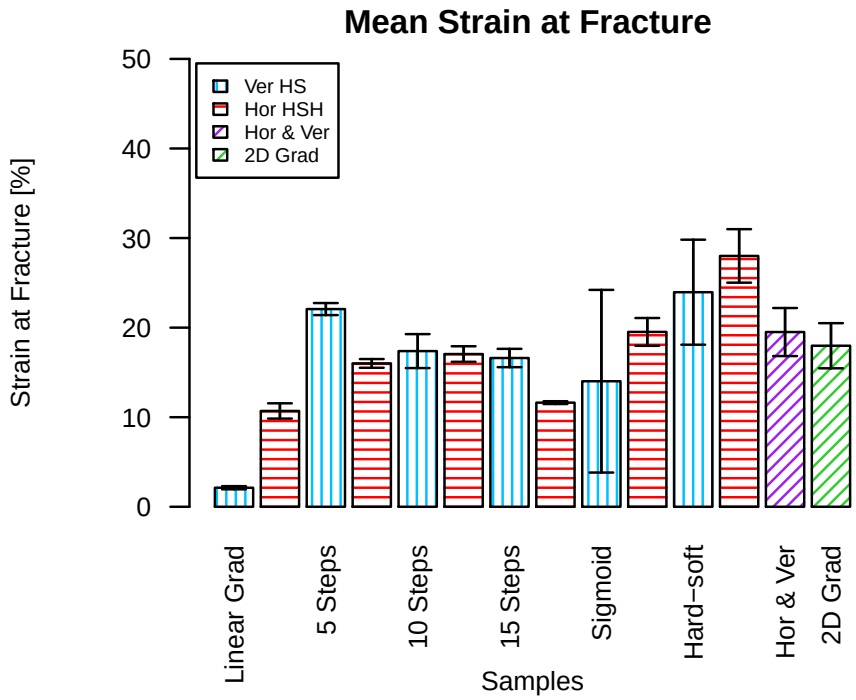

Figure 3.7: Barplot of the mean strain at fracture of vertical, horizontal, horizontal and vertical and 2D gradients.

These differences were clearly visible in the previous stress-strain graphs (Figures 3.1 and 3.2). The brittle fracture of the vertical gradients renders a steep linear slope in the curve, which is linked to the higher elastic modulus value of the vertical samples. On the other hand, the horizontal gradients present a ductile fracture behaviour and the linear slope of the curve is not so steep, meaning that the samples do not have high stiffness. The horizontal and vertical and the 2 dimensional gradient present a relatively low value for the elastic modulus compared to the vertically graded patterns, reaching values close to 100 MPa. The mean value of the strain at the moment of fracture was interesting to inspect the degree of elongation reached by the polymers. It is observed in Figure 3.7 that there is no common trend between the horizontal and vertical patterns, and that in many cases both types of patterns behave in a similar way. The sample that experiences the lowest strain at fracture is the vertical linearly graded sample. This is caused by its smaller region full of soft material at the bottom part, meaning that the area of highly stretchable material is more confined. Thus, the bigger the regions with purely hard material, the larger the degree of elongation. The sharp hard-soft material interfaces present relatively high strain due to the stretchability of the soft material. The horizontal and vertical gradient undergoes strain of almost 30%, and the 2D radial gradient reaches an strain of almost 20%.

A comparison of the elastic modulus and the fracture stress of all the graded samples and complementary interfaces is depicted in Figure 3.8. Additional samples from a previous study were considered, containing 50% hard material following a semi-random arrangement [71]. Below the graphs, two zoomed pictures provide more detailed information about the horizontal and vertical samples. As it can be observed, all the horizontally graded patterns follow the same behaviour as the samples made of pure soft material, having both low stiffness and low values of fracture stress. The vertically graded patterns present values for the elastic modulus ranging between 300 to 400 MPa. All of them follow the same trend for the fracture stress, reaching values about 5 MPa. Among the vertical patterns, the only exception lies in the sharp interface of hard and soft material, reaching a higher value of fracture stress. The pure hard material sample, as expected, is the stiffest and breaks at the highest stress values. The sample containing 50% hard material distributed through the voxels in a semi-random manner presents values of the elastic modulus and fracture stress in between those of pure hard and pure soft material, presenting lower mean elastic modulus than the vertical samples and higher values for the fracture stress. The horizontal and vertical pattern, containing a complementary and varying material interface and the two-dimensional radial gradient present a very similar behaviour in terms of elastic modulus and fracture stress values, and close to fracture stress as the vertical samples set.

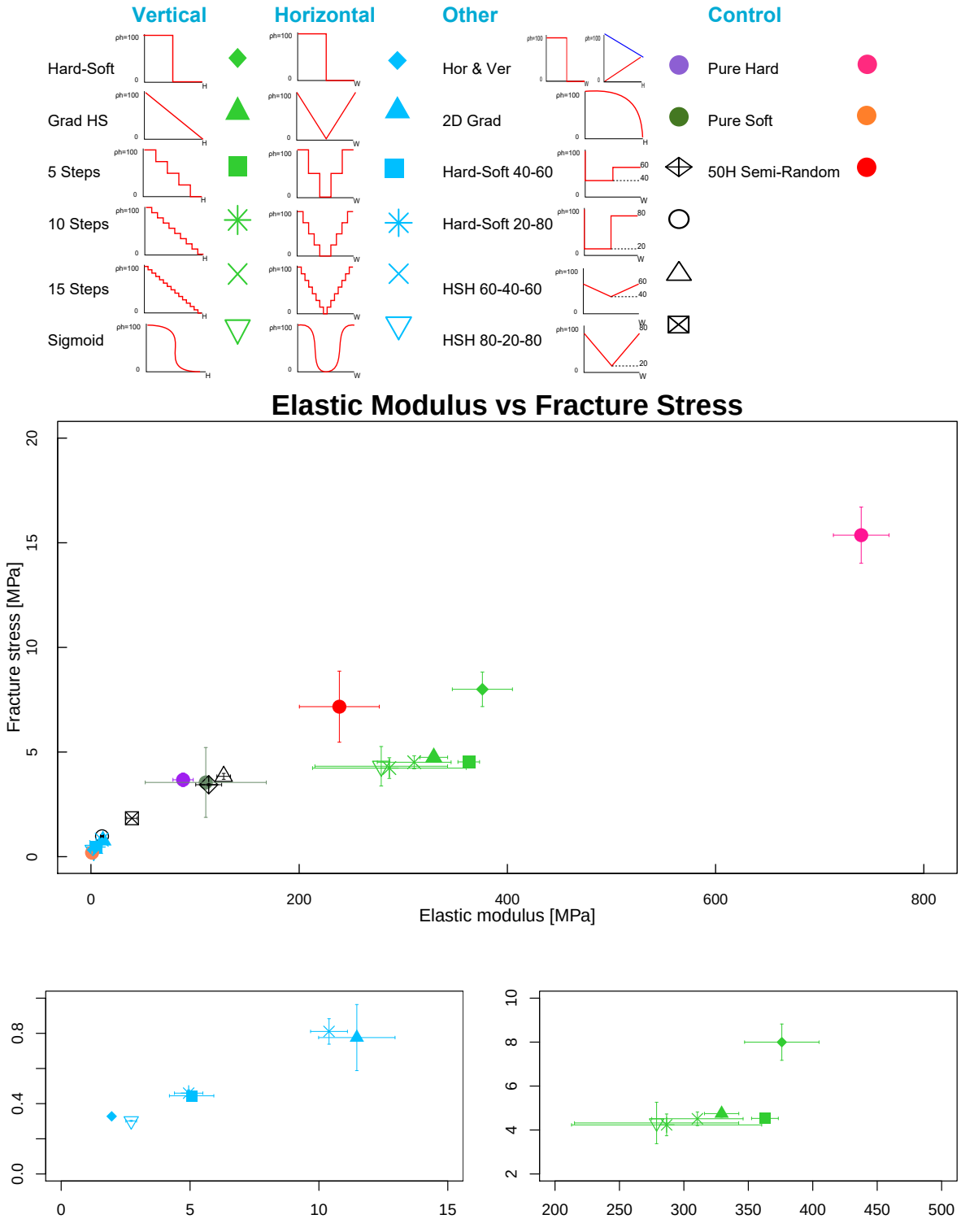

Figure 3.8: Elastic modulus vs fracture stress of graded patterns. Below a zoomed plot indicates in detail the distribution of the horizontal symmetric patterns (right) and the vertical patterns (left). The samples are compared with patterns containing 50% hard material arranged in a semi-random manner from a previous study [71].

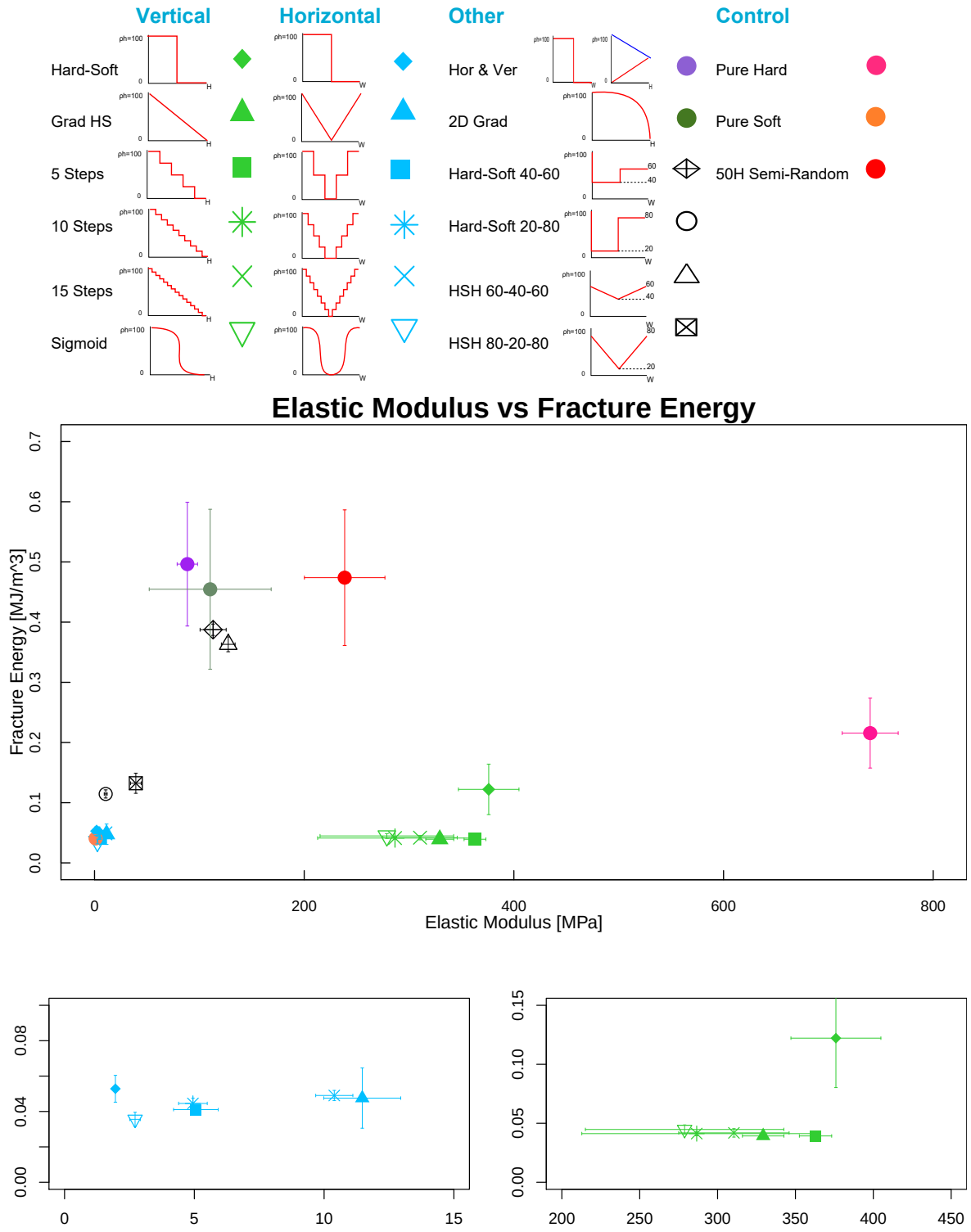

Figure 3.9: Elastic modulus vs fracture stress of graded patterns. Below a zoomed plot indicates in detail the distribution of the horizontal symmetric patterns (right) and the vertical patterns (left).

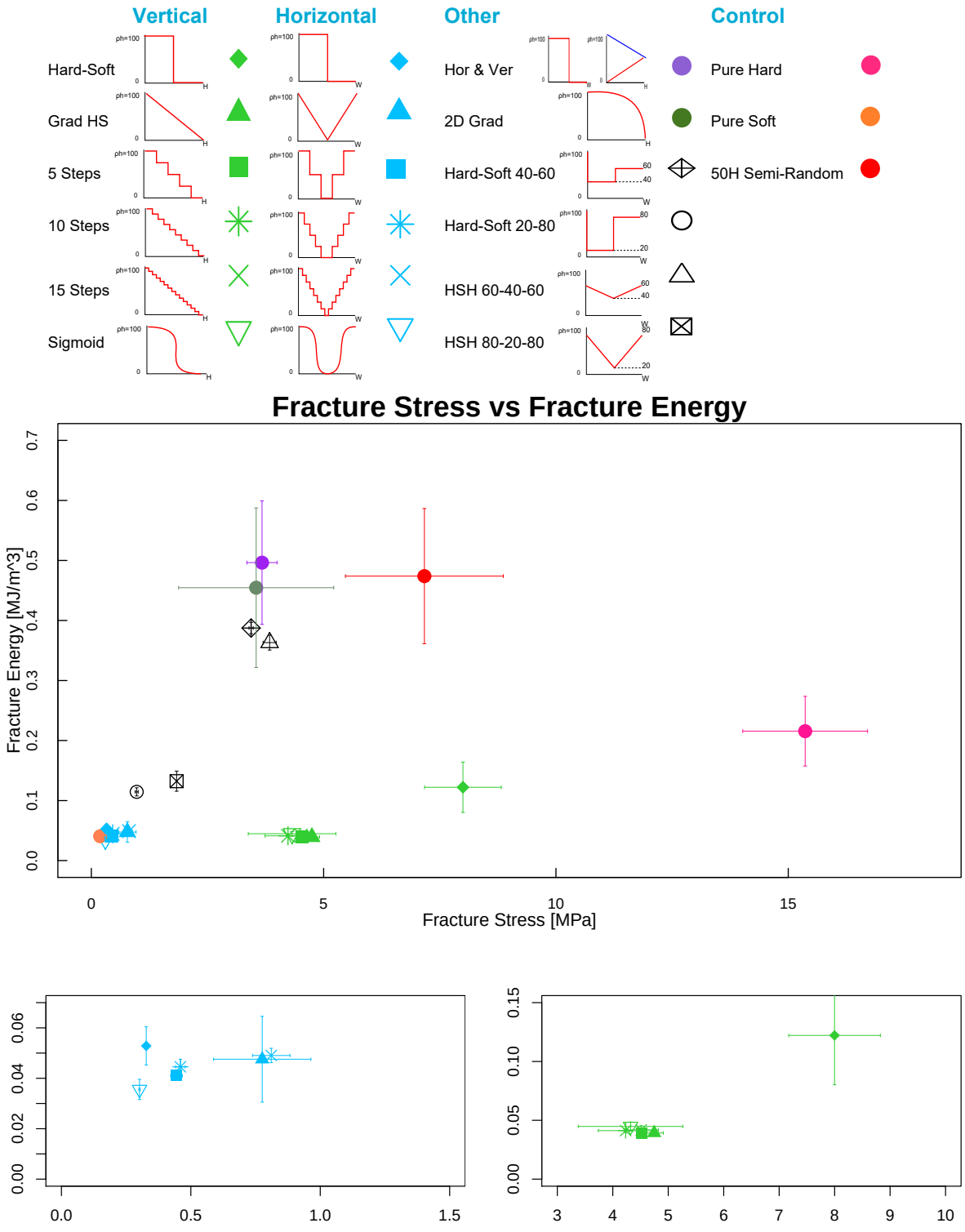

Figure 3.10: Fracture stress vs fracture energy of graded patterns. Below a zoomed plot indicates in detail the distribution of the horizontal symmetric patterns (right) and the vertical patterns (left).

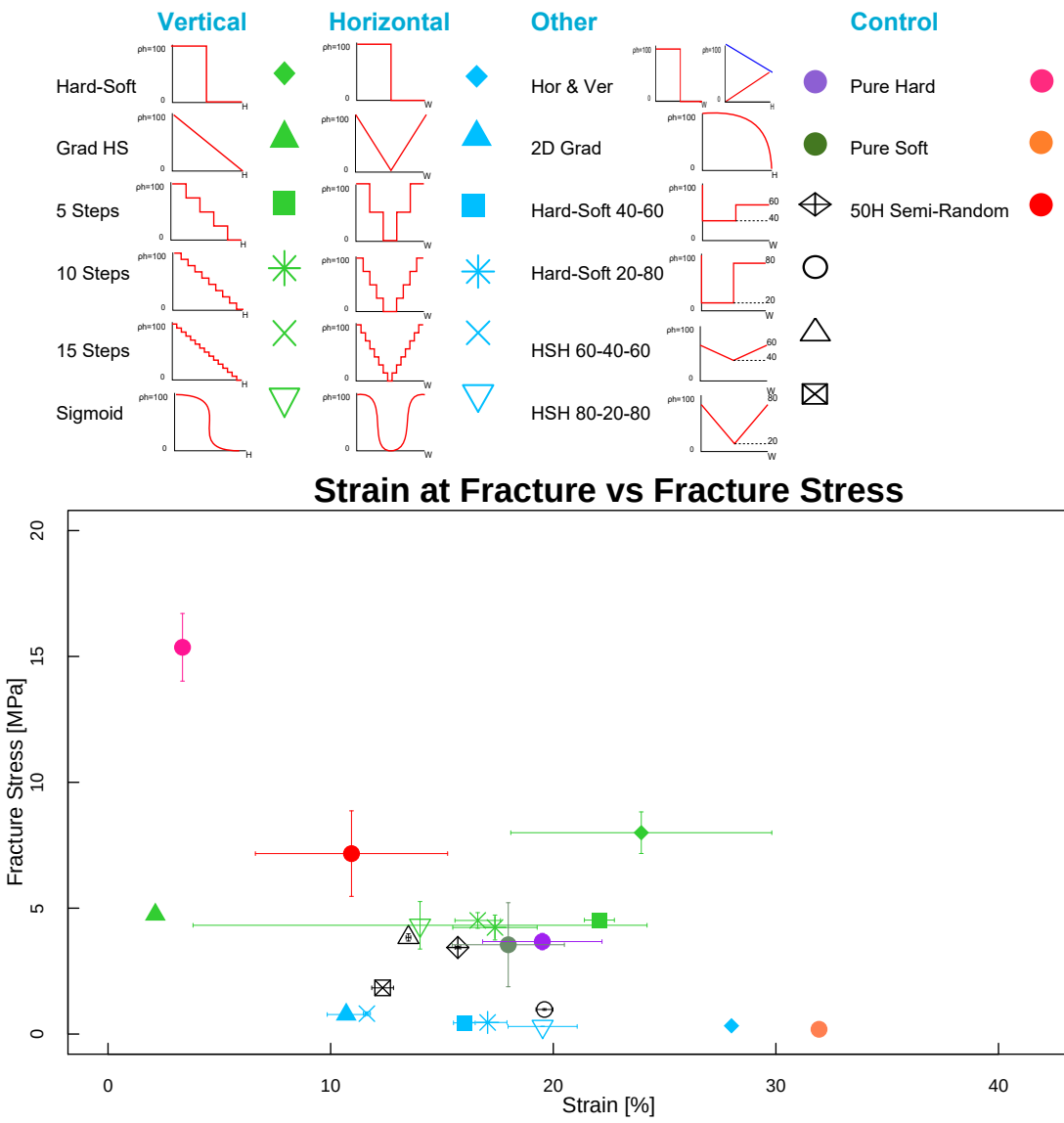

Figure 3.11: Strain at fracture vs fracture stress of graded patterns.

However, their stiffness decreases by a 2-fold compared to them. As for the samples containing a complementary interfaces of 40-60% and 20-80% hard material, there are great differences on their behaviour. The 20-80 interface follows a trend very much alike to the horizontally graded patterns, while the 40-60 interface presents the same behavior as the two-dimensional gradient. The horizontal linear gradient with ratio of hard material 60-40-60 presents a slight improvement in the values of fracture stress and elastic modulus than the 40-60 interface. Similarly, the linear gradient of 80-20-80% hard reaches higher values for both properties than the 20-80 interface, but scores below the 60-40-60.

The elastic modulus and fracture energy of the samples are juxtaposed together in Figure 3.9. As it can be observed, both the horizontal and vertical gradients do not present high fracture energy, however, the elastic modulus of the vertical gradients is higher than for the horizontal samples. The horizontal and vertical and the two dimensional sample gradients perform better in terms of reaching higher fracture energy than the other samples, even though the best trade-off between the two properties is given by the control semi-random pattern. The two samples with 40-60% hard interface and horizontal 60-40-60% hard pattern behave similarly, with fracture energy values below those of the 2D gradient and the horizontal and vertical, but slightly higher elastic modulus. By contrast, the 20-80 interface and the horizontal gradient 80-20-80 reach both little values of elastic modulus and fracture energy, only surpassing those of the horizontal graded specimens.

An analogy of the mean fracture stress and mean fracture energy values experienced by the samples is displayed in Figure 3.10. The horizontally graded patterns score the lowest for both properties, presenting the lowest values and without substantial differences among the samples of the set. The vertically graded patterns do not increase their fracture energy, however, their fracture stress increases by 8-10 fold. The sharp hard-soft vertical interface follows a different trend, with a fracture stress of 8 MPa and a fracture energy of 0.12 MJ/m^3. The 20-80 interface and the horizontal gradient with 80-20-80% hard material increase their fracture energy by a 2 fold compared to the horizontal samples, followed by a slight increase in their fracture stress. The highest value of fracture energy is given by the horizontal and vertical gradient, with 0.5 MJ/m^3, followed close by the two dimensional gradient. Still, none of them outperforms the combination of both properties provided by the semi-random pattern. The 40-60 interface and the horizontal 60-40-60 gradient reach values of fracture energy close to 0.4 MJ/m^3 and fracture stress of around 4 MPa.

Finally, an overview of the strain at fracture and the fracture stress is provided in Figure 3.11. The strain at fracture indicates the degree of elongation that the polymers experience at the moment of total breakage. The purely soft sample experiences the larger strain and the lowest fracture stress, given the ductile nature of the fracture behaviour. It is followed by the hard-soft horizontal interface. All the horizontally graded patterns experience strain percentages between 10 and 20%, with little fracture stress. The elongation is higher in the samples where the regions with higher amount of soft material are higher. Vertical gradients keep their fracture stress relatively constant in the range of 5 MPa, and with elongation values in the range of 12-22%. The exception is the linearly graded vertical sample, whose strain does not reach 5%. The horizontal and vertical gradient presents a high elongation, of about 28%, with a fracture stress of about 4 MPa. The 2D gradient presents a similar number for the fracture stress, but with a lower degree of elongation, below 20%. The 40-60 interface and the horizontal gradient of 60-40-60% hard material experience higher fracture stress than the 20-80 and the horizontal 80-20-80% hard, and their strain values range from 12 to 20%.

3.1.3. DIGITAL IMAGE CORRELATION

Digital image correlation was performed on selected samples in order to inspect the evolution of the strain distributions in x and y directions through the whole crack propagation process. The samples which were subjected to DIC are the linear and 5 steps vertically graded samples, the horizontal and vertical gradient, the linear and 5 steps horizontally graded and the hard-soft horizontal sharp interface.

Figure 3.12 explains the correspondence of the stress-strain curve of the horizontal and vertical pattern with the different frames selected for inspecting the distribution of the ϵ_{yy} component of the strain. In all of them, higher strain distributions are observed through the upper half of the sample, which contains a greater comprehensive amount of soft material. The first frame is taken at the initial time of application of the tensile load. As it can be observed, higher strains are starting to concentrate at the crack tip, where a large red area

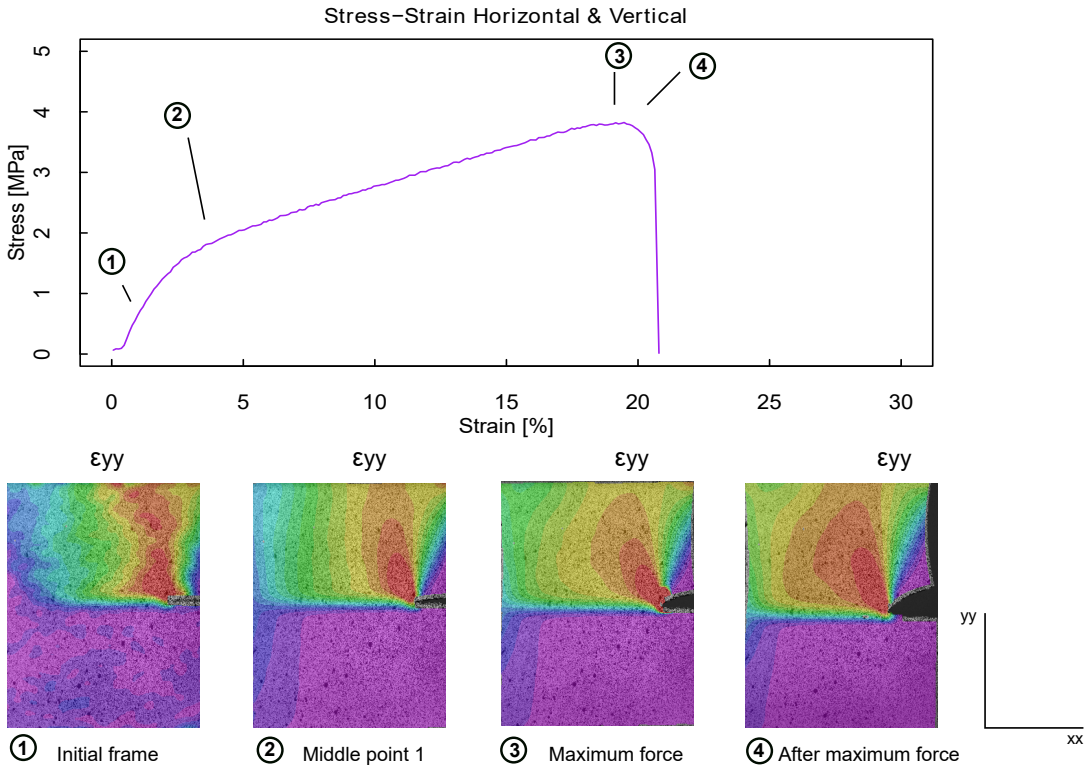

Figure 3.12: DIC results of the horizontal and vertical pattern representing the variation of the strain component ϵ_{yy} though the stress-strain curve.

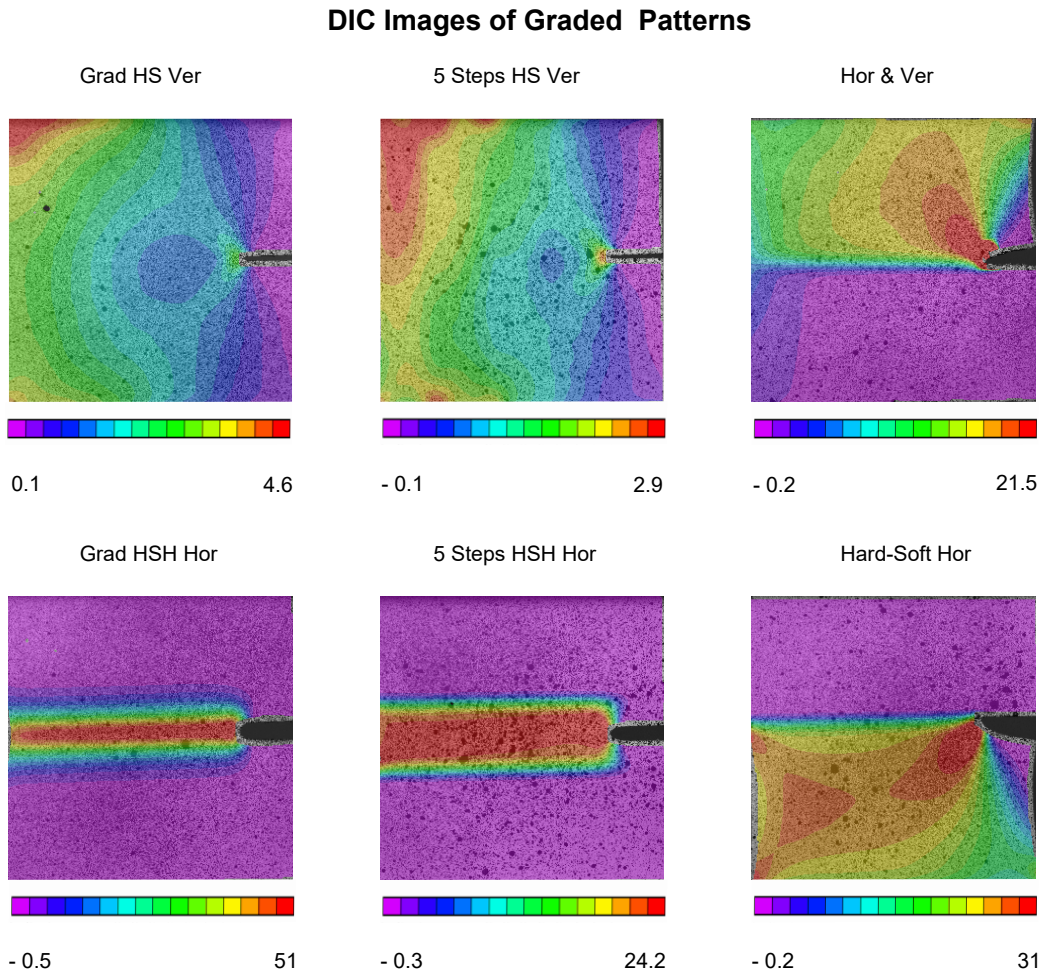

Figure 3.13: DIC results of graded patterns. The images represent the strain values of ϵ_{yy} at the maximum force. The legend bars indicate the percentages of the highest strain values in red and the lowest in purple.

spreads from the crack tip to the upper edge. However, the pattern that defines the area of higher plasticity becomes more defined in the coming frames, adopting an oval shape.

The second frame was taken before the maximum force was achieved and revealed how the strain values increase at the crack tip and form concentric shapes that decrease their strain values from the center to the outer part, indicating that the crack is starting to open. This opening is caused to the increasing load the sample is undergoing and it is more obvious in the upper part, given that the sample presents purely soft material at that site.
At the moment of maximum force (third frame), right before the crack begins to propagate, larger strains begin at the crack tip, and decrease in a radial manner the further they are from the crack tip. The lower half of the sample only experiences low values of strain, due to the higher density of hard material that is present in there. After the maximum force is reached, the strain patterns are maintained, decreasing in a radial manner, however the area of higher strain in slightly larger. When crack propagation has begun it spreads relatively fast, presenting an acute blunting at the crack tip that increases the fracture energy.

Figure 3.13 shows the DIC results for the ϵ_{yy} component of the strain at the maximum force, obtained right before the crack begins to propagate. The linear vertical gradient and the discrete vertical gradient with 5 steps reach moderate strain values at the crack tip at the point of maximal force. The highest strain values are concentrated on the upper left corner, and are 4.6 and 2.9% respectively. The lowest values of strain are located at the right most part, from the edge until the length of the crack. This strain distribution is linked to the locations of hard and soft material through the sample. In both cases, the soft material is located on

the left side, and given its elastic nature it can stretch more, in contrast to the hard material, placed on the right side and limiting the degree of elongation at that site. The design of the samples, from hard material at the crack tip to soft on the opposite edge, is responsible for the low values of maximum strain in the vertical patterns.

The horizontal and vertical gradient presents localized high strain in the crack tip (21.5 %), that is spread in a circular manner through the upper part, decreasing in a radial manner. The lower half experiences a subtle compressive strain of 0.2%. This is an interesting strain distribution, given that the sample carries a complementary interface that bears an abrupt material difference of 0 to 100 at both sides of the crack. This triggers a higher deformation of the half that contains a greater amount of soft material.
The horizontally graded patterns -linear and discrete 5 step- present a high confinement of large strains (51 and 24.2% respectively) at the crack tip and through the whole middle part. This is linked to the distribution of purely soft material, which is narrower in the linearly graded than in the 5 steps graded. In both samples, the central area is framed by two regions that undergo slight compressive strains (0.5 and 0.3%).
To complete the tests, the sharp interface of hard and soft material was assessed. The lower part contains the pure soft material, and presents high values of strain, of 31%, that start at the crack tip and distribute through the lower part until the upper and lower right corners. The upper half reaches strain values of 0.2% in compression.

3.2. TENSILE PROPERTIES OF GRADED PATTERNS

After performing the fracture mechanics tests, tensile specimens were created for certain patterns that were previously analyzed according to their fracture mechanics. The designed patterns were incorporated in dog-bone specimens, and the tensile properties and stress-strain curves were assessed. The selected patterns for this set of tests include the horizontal and symmetric linear and sigmoidal gradients, the step-wise gradients of 5, 10 and 15 steps and the hard-soft-hard sharp interfaces. The abrupt hard-soft interface was included as well to complete the test.

3.2.1. STRESS-STRAIN GRAPHS

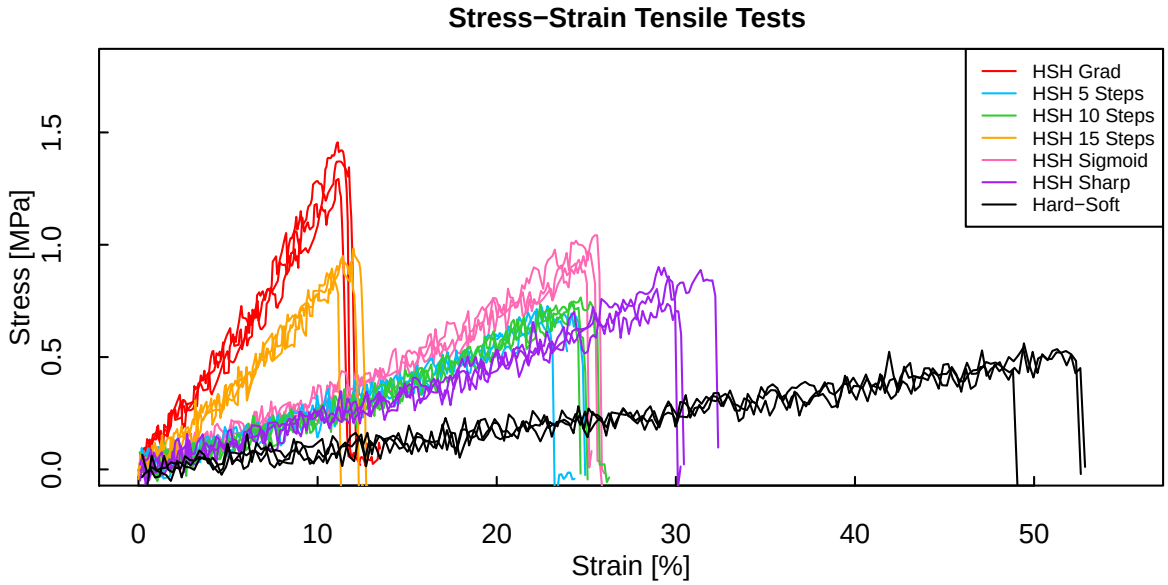

Figure 3.14: Stress-strain graphs of the patterns selected for standard tensile tests.

The stress-strain graphs of the standard tensile samples are shown in Figure 3.14. The sample containing the hard-soft sharp interface presents a high degree of elongation, reaching strain values beyond 50%. It exhibits a highly ductile behavior, due to the necking of the soft material. The patterns that present the sharp hard-soft-hard interface reach 30% strain and maximum stress values above 0.5 MPa. The graded sig-

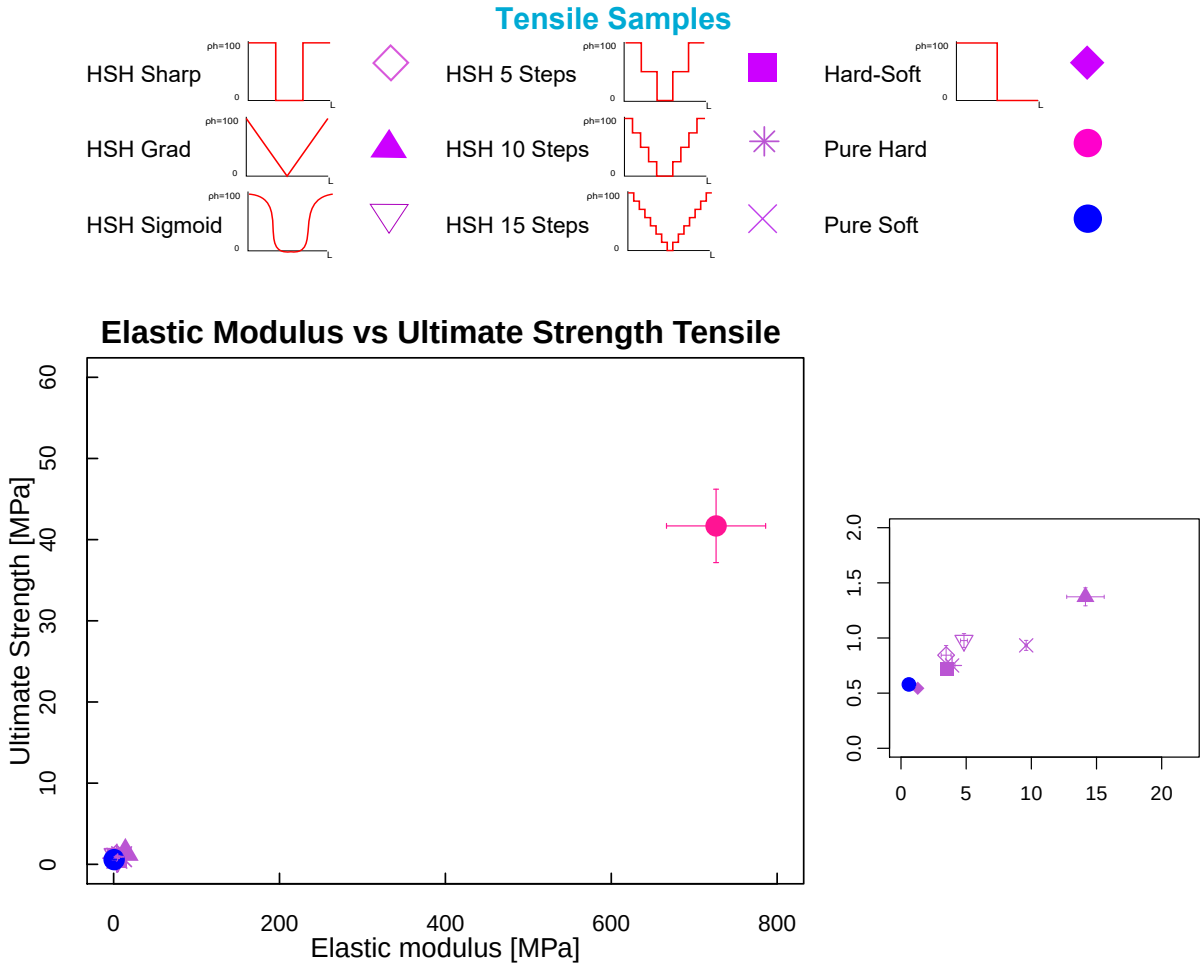

Figure 3.15: Elastic modulus vs ultimate strength of standard tensile tests samples. The augmented graph is placed on the right, providing more detailed information about the distribution of the patterns.

moid transition and 5 and 10 steps present a common behavior, reaching equivalent strain values, around 25%, and maximum stress values of about 0.5 MPa. This trend is also followed in the stress-strain curves of the single-edged notched samples (Figure 3.2). The linearly graded sample and the 15 steps reach the higher values of maximum stress, over 1 MPa, and the lowest strain, slightly above 10%. Both of them present a narrower region of soft material in the central part, which influences the degree of elongation of the samples, and the increase of the maximum stress.

3.2.2. TENSILE PROPERTIES

In this section, the tensile properties are inspected. The juxtaposed effects of the elastic modulus and the ultimate strength of the tensile samples is assessed in Figure 3.15. The majority of designs exhibit low values of both properties, and their behavior is far from the highly stiff pure hard sample, with a mean elastic modulus greater than 700 MPa. Among the patterns, the linear gradient hard-soft-hard presents the higher elastic modulus, 15 MPa, and highest ultimate strength, 1.5 MPa; followed by the 15 steps hard-soft-hard sample, with elastic modulus of 10 MPa and 1 MPa of ultimate strength. The sigmoid transition, the linear transition hard-soft-hard and the 5 and 10 steps present a similar behavior, maintaining 5 MPa for the elastic modulus and 1 MPa of ultimate strength. The hard-soft sharp interface follows the tendency of the completely soft sample.

The relation between the elastic modulus and toughness of the patterns is detailed in Figure 3.16. The pure hard sample exhibits high elastic modulus and the highest toughness of all the samples, reaching 5

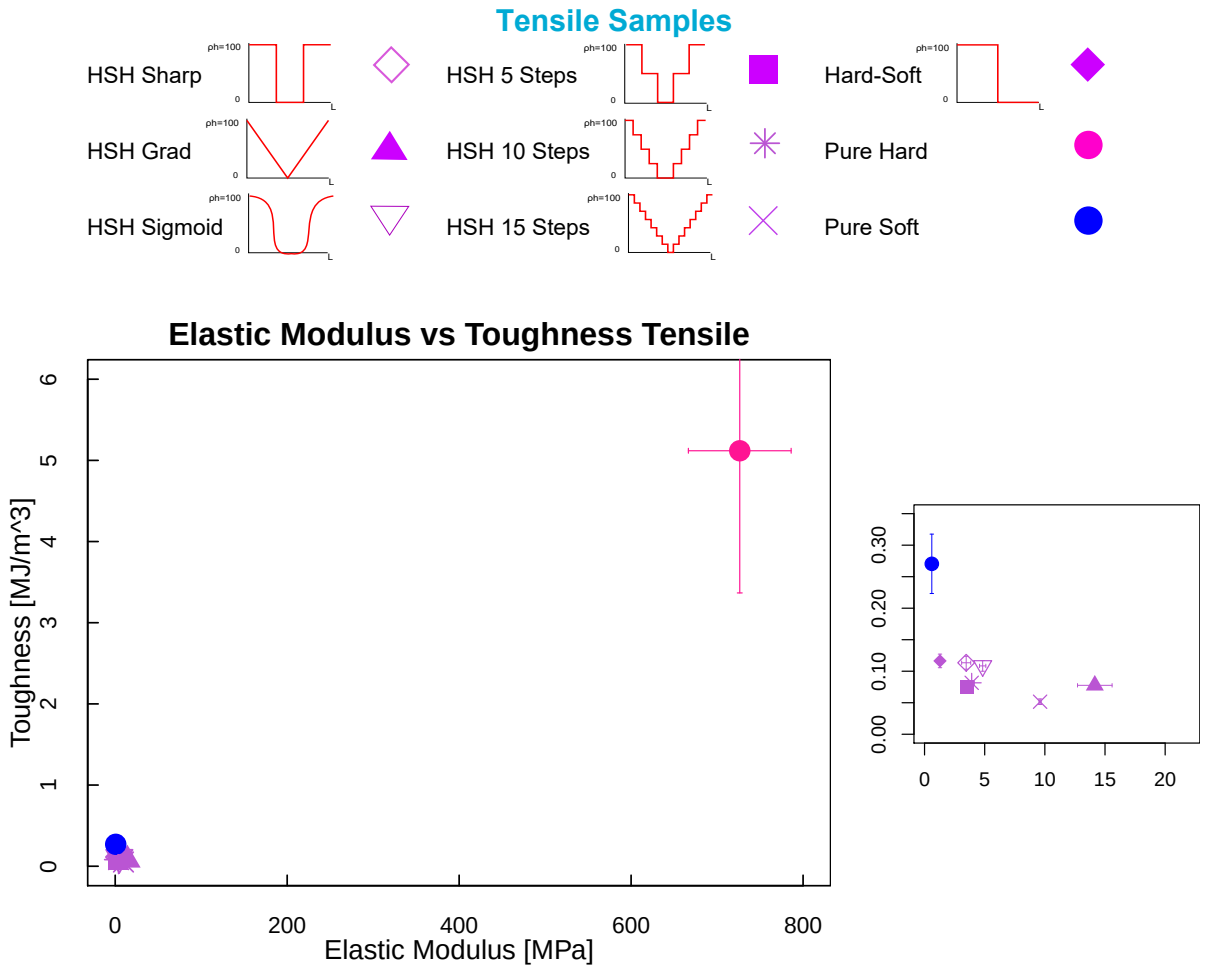

Figure 3.16: Elastic modulus vs toughness of standard tensile tests samples. Detailed information about the distribution of the patterns is provided in the augmented graph on the right.

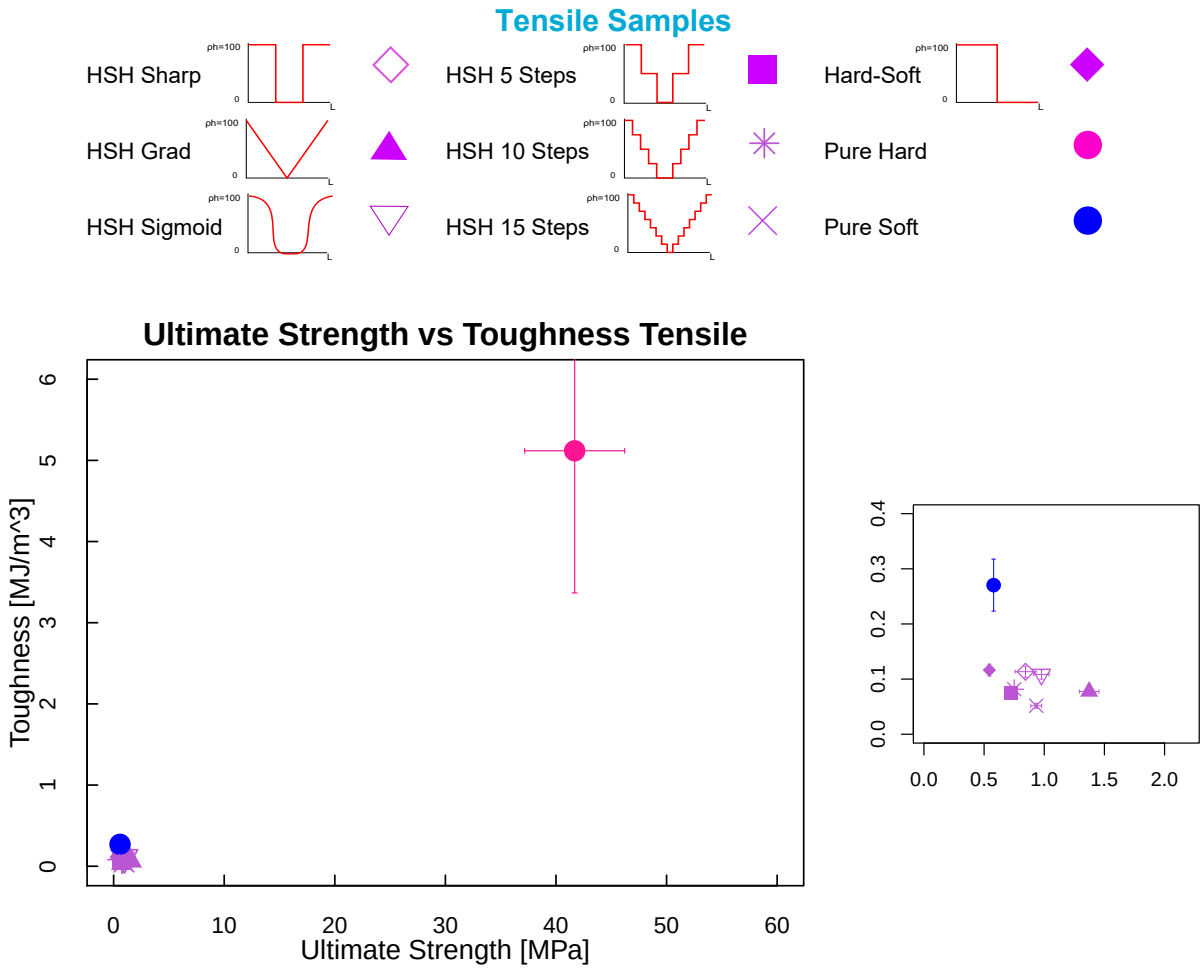

Figure 3.17: ultimate strength vs toughness of standard tensile tests samples. Detailed information about the distribution of the patterns is provided in the augmented graph on the right.

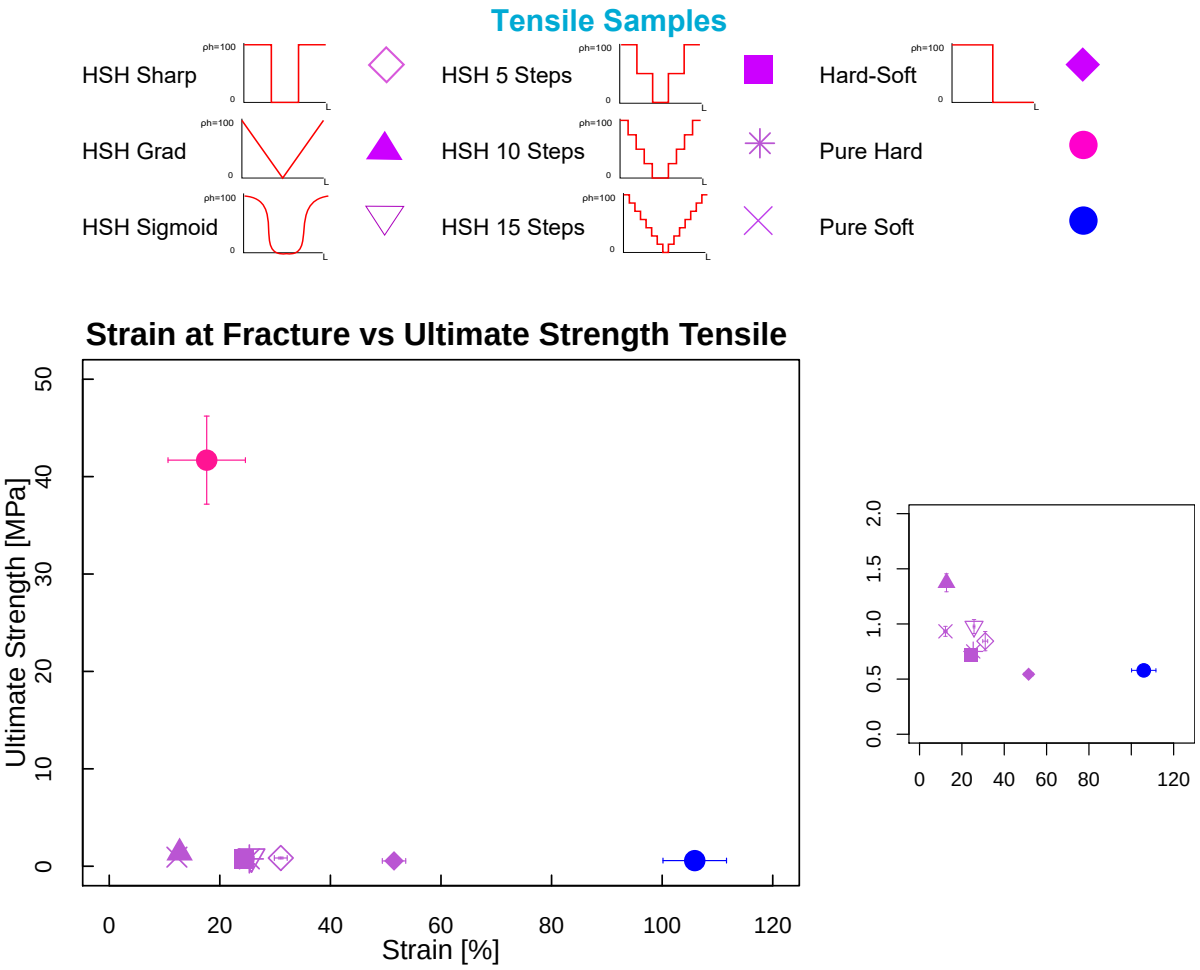

Figure 3.18: Strain at fracture vs ultimate strength of standard tensile samples. Detailed information about the distribution of the patterns is provided in the augmented graph on the right.

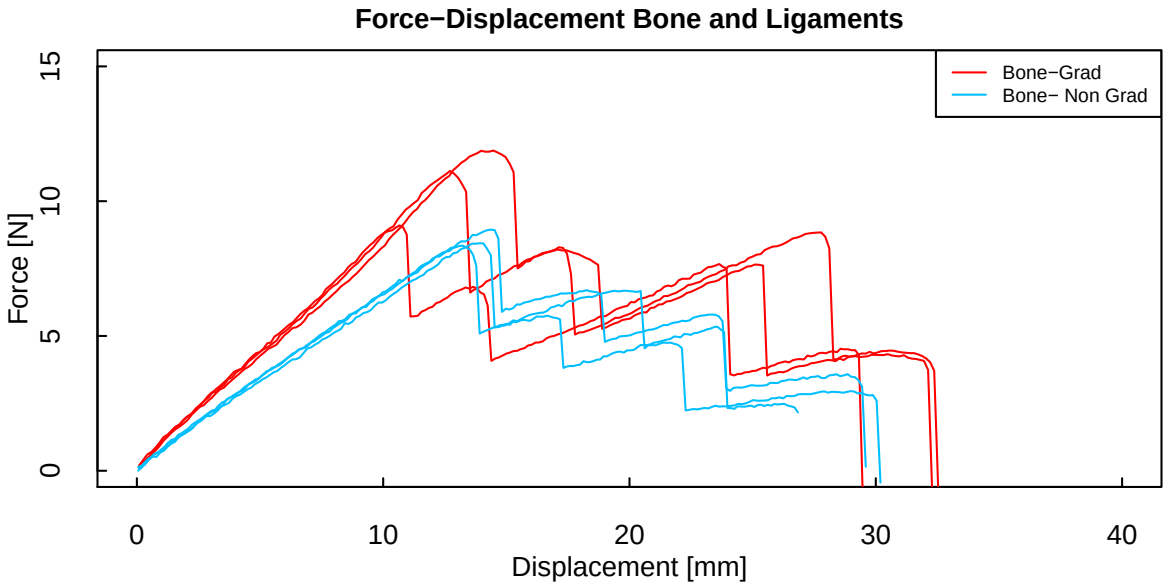

Figure 3.19: Force vs displacement of the bioinspired bone and ligaments model. The graded ligament connections are shown in red and the samples with sharp interfaces are shown in blue.

MJ/m^3. Besides the purely hard sample, none of the specimens presents a great improvement to the toughness, and the values of all of them range from 0.05 to 0.1 MJ/m^3. The linear gradient exhibits the highest elastic modulus, and the least stiff is the sharp interface.

A close comparison about the ultimate strength and toughness of the patterns demonstrates little variations between the different designs of the specimens, as it is shown in Figure 3.17. The patterns present ultimate strength values between 0.5 and 1.5 MPa, but none of them increase their toughness beyond 0.1 MJ/m^3, thus, performing below the purely soft sample.

Finally, the strain at fracture and the ultimate strength are evaluated in Figure 3.18. As it can be perceived, the purely soft sample elongates twice as much its initial length, while the purely hard presents the highest ultimate strength (40 MPa) while only bearing 20% strain. Due to its greater proportion of soft material, the sharp hard-soft interface presents the highest strain of all the designs, reaching 50%. The rest of the motifs experience strain in the range of 10 to 30%, being the lowest for the 15 steps and the linear gradient, given their narrow frame of soft material in their middle part.

3.3. BIOINSPIRED MODEL

The effectiveness of the graded connections in comparison to sharp hard-soft interfaces was assessed by mimicking a situation in nature: the bone-tendon enthesis. The 3D printed models simplified the human knee and its main ligaments, and presented two distinct features: graded and non-graded connections of the soft ligaments to the hard bones. The samples were subjected to tensile tests and the data regarding the force withstand and the displacement were analyzed for 3 samples of each model. The results are presented in Figure 3.19.

As it can be observed, the common trend for both models is that the force decreases in a peak manner. After each peak, the force experiences a slight increase. These fluctuations are caused by the successive breaking of the four rods that mimic the ligaments at distinct rates. An overview of the breaking of the ligaments is detailed in Figure 3.20. The first two peaks correspond to the rupture of the rods that mimic the cruciate ligaments, the posterior and anterior respectively. The third one breaking is the medial collateral and finally the lateral collateral. The sharp interface presents load values lower than those required for the breakage of the rods which were gradually attached to the hard material. The elongation of both models shows equivalent values, reaching a displacement of approximately 30 mm. The manner in which the ligaments break is also of

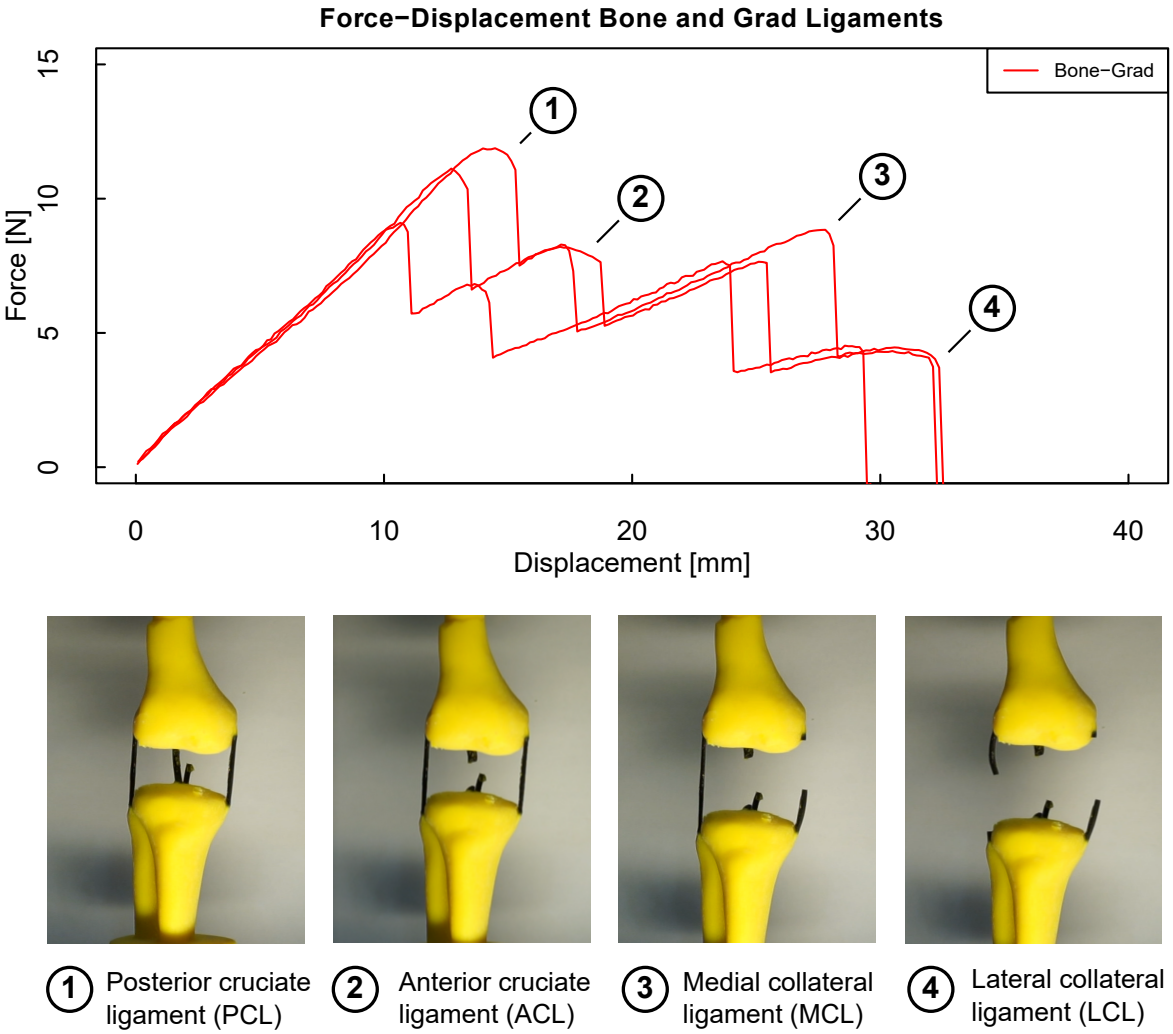

Figure 3.20: Overview of the breaking process of the ligaments in the bioinspired knee model. The force displacement graph for the graded ligaments is shown above, and each peak in the graph is linked to the breaking of an specific ligament. The breaking of the two cruciate ligaments, posterior and anterior, represent the two initial peaks in the graphs, whereas the two last peaks correspond to the breaking of the medial collateral and lateral collateral ligaments respectively.

great interest. For the ligaments with an abrupt interface, the fracture of the ligaments started clearly at the interface, whereas for the rods with a graded material variation, the breaking took place in the middle part of the ligament.

3.4. FRACTURE MECHANICS OF HIERARCHICAL AND GRADED PATTERNS

After assessing the fracture behavior and properties of patterns presenting different gradient designs and complementary interfaces, the effects of brick-and-mortar motifs and their incorporation into hierarchical arrangements was inspected. Furthermore, the combined effects of hierarchy and graded material variations through the bricks were also evaluated.

3.4.1. FRACTURE PROPERTIES

In this section, the fracture properties of three groups of samples were analyzed. The groups consist on the purely brick-and-mortar designs, those designs combined with a linear horizontal symmetric gradient with 100-40-100% hard material, and semi-random, random and ordered arrangements from previous research containing each 50 and 75% hard material [71].

A comparison of the elastic modulus and fracture stress is provided in picture 3.21. The brick-and-mortar motifs are located on the left most side of the graph, presenting a mean elastic modulus that surpasses 500 MPa. They all keep a constant fracture stress of about 10 MPa. Among them, the sample that introduces a second level of hierarchy (2L BM ratio 5.6 & 15) presents slightly lower elastic modulus than the other designs with only one level of hierarchy. The samples where a horizontal gradient of 100-40-100% hard material is incorporated through the bricks decrease both their elastic modulus and fracture stress considerably, by 2.5 and 2 fold respectively. Those numbers are way lower than the graded samples without the brick-and-mortars, which presents an elastic modulus of 320 MPa and a fracture stress of about 7 MPa. As for the groups with different material arrangements, there are clearly two different clusters following their material proportion. The semi-random, random and ordered patterns with 50% hard material present an elastic modulus in between those of the brick-and-mortar and graded designs and the linearly graded one, and reaching a slightly higher fracture stress. By contrast, the same pattern designs containing 75% hard material show lower stiffness than the brick-and-mortar and hierarchical patterns (about 400 MPa) but increase their fracture stress above 10 MPa.

The correlation between the elastic modulus and the fracture energy is depicted in Figure 3.22. As it can be observed, the brick-and-mortar motifs present a high elastic modulus, but their contribution to the fracture energy is not remarkable, reaching values of 0.15 MJ/m^3. The introduction of the gradient through the brick units does not improve those properties, and rather than increasing the elastic modulus and fracture energy, both are decreased, reaching elastic modulus values of around 200 MPa and fracture energy values ranging from 0.2 to 0.3 MJ/m^3. The highest fracture energy values are provided by the group of 50% hard material of semi-random, random and ordered patterns, whose fracture energy ranges from 0.4 to 0.5 MJ/m^3, and their stiffness varies from 200 to 300 MPa. By increasing their proportion of hard material to 75% their elastic modulus increases to the range of 400 MPa but it is linked to a 2 fold decrease in fracture energy.

The fracture stress and fracture energy are contrasted in Figure 3.23. The lowest values of fracture stress and fracture energy are reached by the brick-and-mortar pattern with 10 MPa and 0.15 MJ/m^3 respectively. The designs that combine the gradient with the brick-and-mortar pattern undergo a two fold decrease in fracture stress and a subtle increase in fracture energy, however, the values obtained by the combination are below those of the effect of the single horizontal pattern. The amount of hard material does really influence the fracture energy of the samples. Higher fracture energy is achieved by the samples with 50% hard material, whereas a decrease in fracture energy and an increase in fracture stress is accomplished by the samples with 75% hard material.

Finally, the relation of the strain at fracture and the fracture stress is expressed in Figure 3.24. The samples containing the gradient and the brick-and-mortar pattern present a strain at fracture of 10% , with a fracture stress below 5 MPa. The semi-random, random and ordered patterns with an even amount of hard and soft

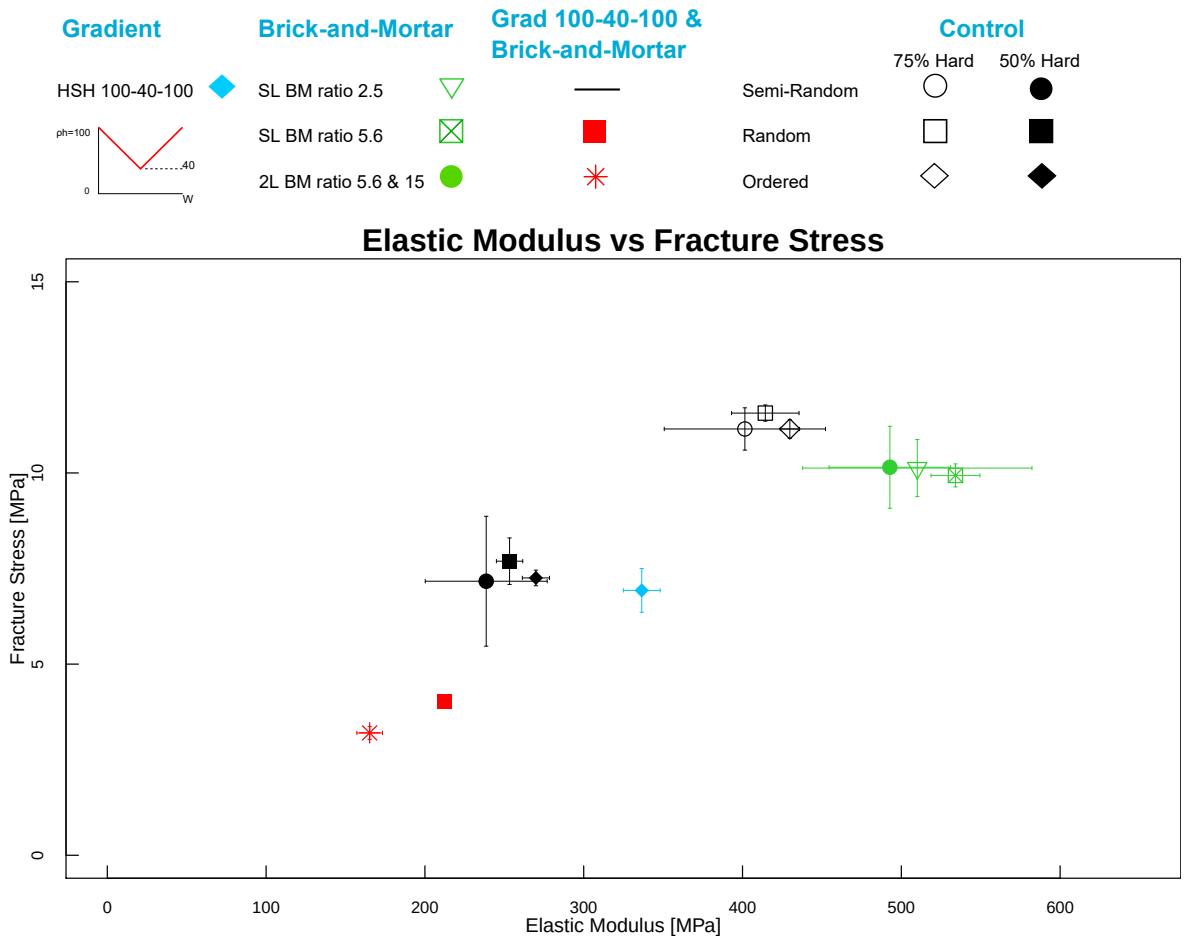

Figure 3.21: Elastic modulus vs fracture stress of hierarchical and graded structures. Samples with material ratio of 50 and 75% hard material from a previous study [71] have been introduced for a more accurate comparison

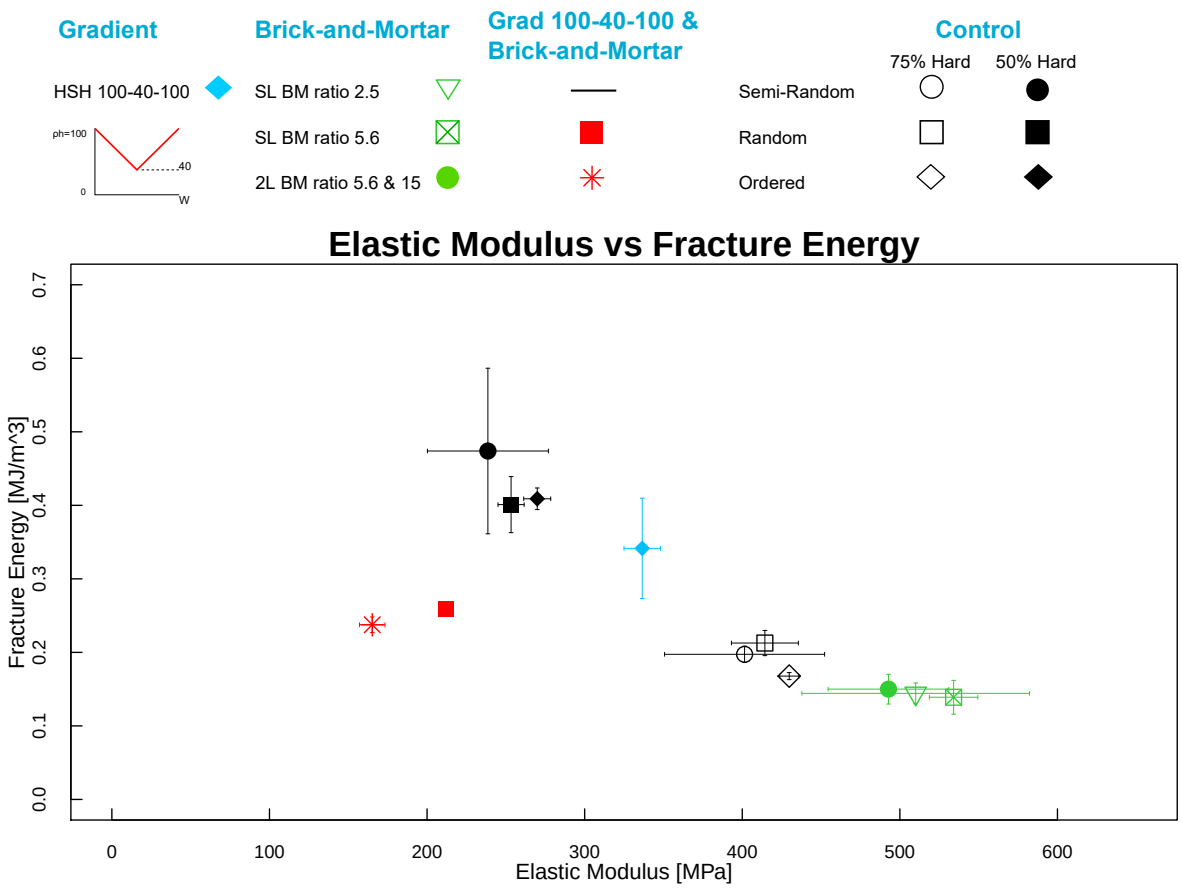

Figure 3.22: Elastic modulus vs fracture stress of hierarchical and graded structures.

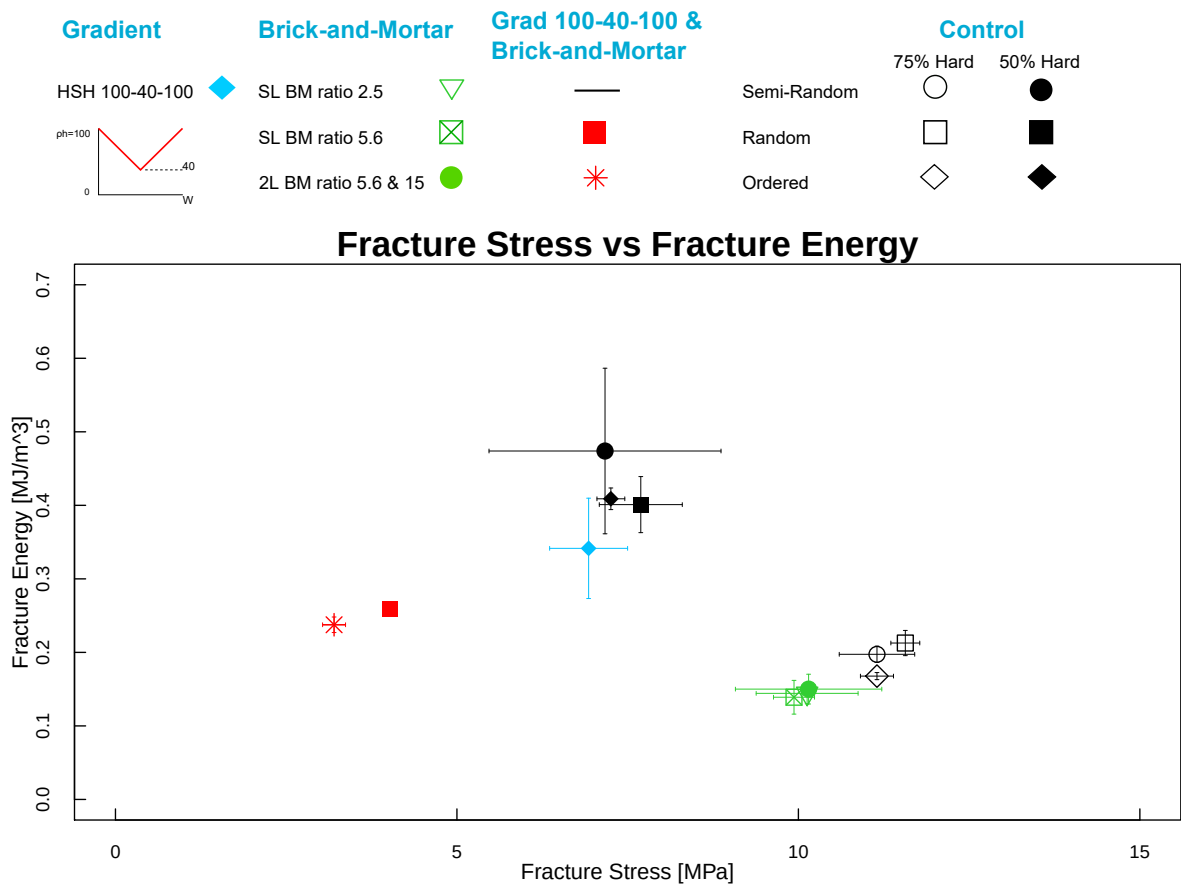

Figure 3.23: Fracture stress vs fracture energy of hierarchical and graded structures.

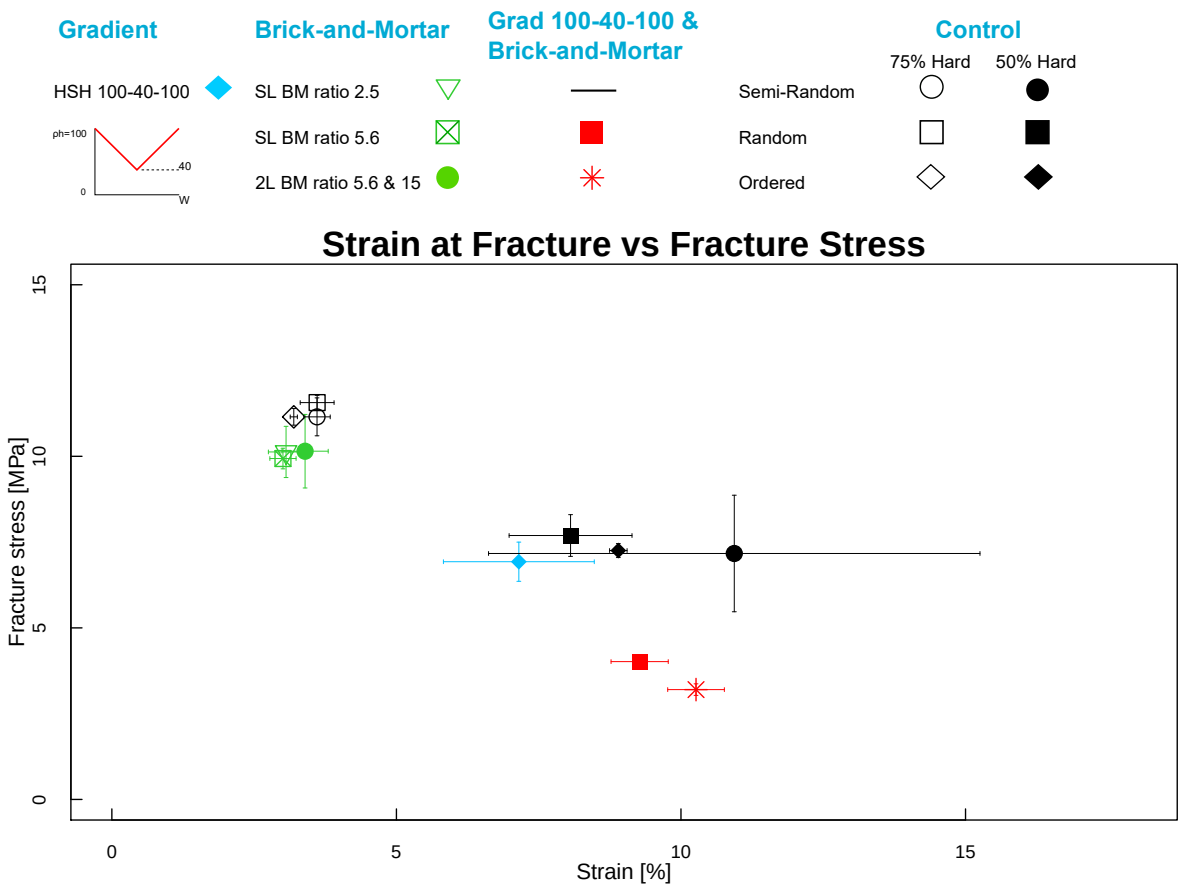

Figure 3.24: Strain at fracture vs fracture stress of hierarchical and graded structures.

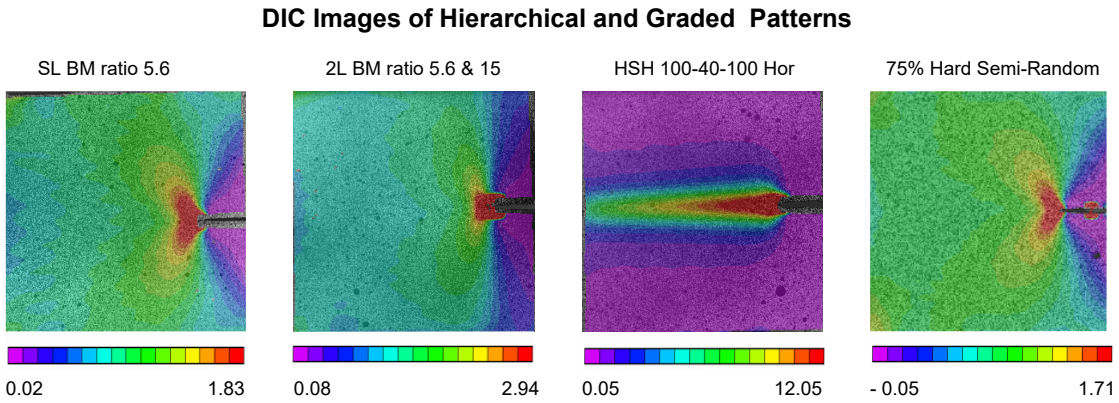

Figure 3.25: DIC results of brick-and-mortar and graded patterns. The images represent the strain values of ϵ_{yy} at the maximum force. The leyend bars indicate the percentages of the highest strain values (red) and the lowest (purple).

material present moderate strain at fracture as well, ranging from 8 to 12%, but increasing the fracture stress to about 10 MPa. The samples containing a higher amount of hard material, that is, the brick-and-mortar patterns and the ordered, semi-random and random designs with 75% hard material experience high stress at fracture, above 10 MPa. Given the brittle nature of those designs, the strain at fracture is, as expected, lower than with the other arrangements, below 5%.

3.4.2. DIGITAL IMAGE CORRELATION

Some designs were selected for further analysis by DIC imaging. Those samples were the single level brick-and-mortar pattern, the two level hierarchical brick-and-mortar with ratios 5.6 and 15 and the linear horizontal gradient with 100-40-100% hard material. The DIC results from the semi-random sample of 75% hard material were added to the analysis. The ϵ_{yy} component of the strain at the time of maximum force is analyzed in Figure 3.25.

The single level sample with brick-and-mortar pattern of ratio 5.6 presents a higher strain concentration at the crack tip, of 1.83%, in a butterfly wing shape. The overall high percentage of hard material limits the degree of strain in this case. The lowest values of strain are perceived at both sides of the crack, since they are not affected by the tensile load applied to the specimen. As a higher level of hierarchy is introduced in the two level brick-and-mortar sample, presenting ratios of 5.6 and 15, the maximum value of strain increases slightly to 2.94%. In addition, the region with higher strain is located at the crack tip as well, but more concentrated on a smaller area. The region with the lowest strain value (0.08%) spans the whole area of the crack and is perpendicular to it. The horizontally graded sample with variation of hard material of 100-40-100% presents a sharp confinement of higher strain in the middle part, of 12.05%, which decreases to moderate levels of strain as it approaches the left edge. Following the trend observed in previous horizontal samples (Figure 3.13), the upper and lower half, with higher amount of hard material, present lower values of strain, of 0.05%, distributed uniformly. Finally, the DIC image of the 75% hard material semi-random sample were compared. As with the single level brick-and-mortar sample, the higher strain values (of 1.71%) are located at the crack tip, and again they present the butterfly wing shape. The rest of the sample presents moderate uniform strain values except for the regions located where the crack is and ahead of its tip, which present the lowest strain (0.05% in compression).

4

DISCUSSION

4.1. GRADED PATTERNS

In this project, the effects of functionally graded material transitions on the mechanical properties of structures have been assessed. Even though the design of functionally graded structures has drawn much interest in recent years, not much research has been done into the mechanical properties of graded patterns created by voxel-based 3D printing and material jetting technology. Consequently, many questions arise regarding the mechanical properties of these materials, and how different functional graded transitions influence them.

4.1.1. FRACTURE MECHANICS OF GRADED PATTERNS

Even though the overall composition of hard and soft material are 50% for each sample, the results outlined a completely different behavior for the distinct design sets. Former studies had outlined the influence of the voxel length-scale in the fracture properties of the samples, and determined that the native resolution of the printer (40 μm) presented the highest values for fracture toughness and the wider range of stiffness values [71]. In this project, the native voxel resolution was kept and the influence of the graded pattern for material rate change was evaluated.

Vertical gradients resulted in brittle fracture, presenting high values of elastic modulus and fracture stress, and low fracture toughness (Figures 3.8 3.10). The strain at fracture was higher in the patterns that presented a wider region of pure soft material at the lower part, meaning a higher ability to elongate (Figure 3.11). Thus, the 5 steps pattern, with the greater amount of soft material on the bottom, presents the highest strain at fracture.
On the other hand, horizontal symmetric patterns reached low values of fracture stress and elastic modulus. Those samples varied their hard material composition from 100% hard in both edges to 0% hard in the middle part, were the crack tip is located. The fracture energy did not improve in those patterns. Nonetheless, the mean strain at fracture varied from pattern to pattern and was affected by the orientation of the gradient. It appeared to be tightly related to the width of the regions of the sample with pure soft material concentration. The linearly graded sample or the horizontal sample of 15 steps present narrower confinement of soft material than other samples with higher strain at fracture.

The results of the vertical and horizontal designs outlined the little contribution of the function that determines the material graded transition to a considerable improvement on material properties. Therefore, it was necessary to assess whether the fracture energy and stiffness of the designs could be enhanced by modifying the material distribution while keeping a constant 50-50 ratio over the whole structure. In addition, and given the important role that material interfaces play in the mechanical performance of a structure, new designs were taken into consideration. The designs evaluated sharp interfaces: with pure hard and pure soft material, and with complementary ratios of hard material of 20-80% and 40-60%. The pure sharp interfaces were created for both horizontal and vertical patterns, and the complementary sharp interfaces were horizontally oriented. The crack tip was strategically placed at the interface, which is the weakest point of the structure. It was demonstrated that the effect of the interface reached higher values in terms of stiffness and

fracture toughness in the complementary interfaces than in the abrupt interfaces with purely hard and soft material (Figure 3.9). In particular, the 40-60% interface increases both the stiffness and fracture energy of the assembly the most, presenting the largest area under the stress-strain curve than the more abrupt interface. Furthermore, those complementary material ratios were incorporated in horizontally graded patterns with transitions of 60-40-60% hard material and 80-20-80% hard. Similarly, the horizontal gradient with 60-40-60% hard material outperforms the elastic modulus, fracture stress and fracture energy of the gradient with 80-20-80% hard material (Figures 3.8, 3.9, 3.10), meaning that the material ratio distribution of 40-60% hard material reaches the most optimal values compared to other horizontal graded transitions or sharp interfaces.

Finally, the horizontal and vertical gradient and the two dimensional radial gradient were analyzed. The horizontal and vertical gradient presented the highest amount of fracture energy, while having a relatively low elastic modulus (Figure 3.9). The most characteristic fact about the horizontal and vertical pattern is that it undergoes strain hardening, which significantly increases the fracture energy of the structure [78]. The soft material of the designs has a rubber-like structure, which allows for stretchability and recovering of the original shape after the load is removed. The polymeric chains of the soft material have an amorphous arrangement. When combined with the rigid material in the patterned design and subjected to tensile loading, the structure undergoes a progressive strengthening after being stretched beyond the yield stress. This is due to the alignment of the polymeric chains. The distribution of the materials increases the blunting of the crack tip, generating a ductile fracture behavior. This phenomenon is also observed in the two dimensional radial sample, although to a lower extend, with slightly higher stiffness and lower fracture stress.

Even though the results provide some insights on how different gradient functions and graded material distributions behave, still it was not possible to increment both the elastic modulus and fracture energy of the materials at the same time, or to increase the elastic modulus without a simultaneous increase of the fracture stress, and so far it was not possible to improve the performance presented by the semi-random distribution of hard and soft material though the voxels.

4.1.2. DIGITAL IMAGE CORRELATION

The DIC results highlight the differences in strain distributions of selected characteristic patterns. It is particularly interesting to understand the strain concentration since it gives valuable insight into the fracture mechanisms.

In Figure 3.13, the linear graded and 5 steps vertical gradients present moderate strain concentration at the tip of the pre-formed crack at the moment of maximum force, that is, right before crack extension. The highest amount of hard material is located at the crack site, and that prevents the area from experiencing large elongation without breaking. The low fracture energy dissipated and the brittle fracture of the samples is reflected in the moderate to low values of strain in the crack tip. However, larger strain concentrations are found on the upper right corner, in the connection to the hard grippers. That is indeed a vulnerable site, given that there is a higher stiffness mismatch between the soft material in the pattern and the hard material of the grippers. These areas of high strain far from the crack tip do not augment the fracture toughness since they could contribute to crack growth and therefore reduce the energy required to propagate the crack.

The equivalent horizontally graded samples pose, by contrast, high concentrations of strain that begin at the crack tip and extend to the opposite edge. Ideally, a high plasticity region in front of the crack tip dissipates energy and increases the fracture toughness of the sample. However, in the case of the horizontal patterns the fracture energy dissipated is not high. Those large strain regions do not contribute to an increase of the energy dissipated because they span the whole area, from the crack tip to the edge of the sample, and the high amount amount of flexible material present there only facilitates a weaker pathway for crack propagation.

The sharp hard-soft horizontal interface bears high concentration of strains, but they spread from the lower half to the upper and lower right corner. As a consequence, the amount of fracture energy only experiences a subtle increase. Finally, the higher fracture toughness of the horizontal and vertical pattern is justified by the high plasticity zone at the crack tip and its confinement to a small area of the sample right in front of the crack tip. Thus, it is demonstrated that the strategic placement of gradients can tune the failure mechanisms of the sample and its confinement to a certain area [68].

4.2. TENSILE SAMPLES

The effect of graded patterns was further assessed on specimens with dimensions that followed the standard size for tensile tests. This was meant for being sure about the trend that these patterns follow, and to validate the former fracture tests.

The results highlighted a correlation in the performance of the single-edge notched samples and the standard tensile models, following a common trend. The linear symmetric gradient presents a slightly higher Young's modulus, followed by the 15 steps gradient. The rest of the samples present equivalent stiffness, with values of around 5 MPa. Moreover, it was observed that an increase in the elastic modulus values is followed by an increase of the ultimate strength of the sample (Figure 3.15). It was also confirmed that none of the samples inspected contributed significantly to the increase of the toughness of the structure, and they do not outperform the behaviour of the purely soft sample. As for the strain experienced at fracture, higher elongation was experienced by the patterns with higher areas of purely soft material.

4.3. BIOINSPIRED MODEL

The bioinspired model mimicking the ligaments in the human knee revealed interesting results. For both samples, the same final displacement was reached and the rupture of the rods followed the same trend and order, starting by the cruciate ligaments and followed by the medial and lateral ligaments. Several studies have been carried out about tearing of the knee ligaments, particularly the ACL [43, 79]. The reported ultimate tensile force for the ACL ligament on cadaveric samples ranges from 600 to 2300 N, which is far from the values reached on our study [80, 81]. These discrepancies are due to the differences in dimensions, material and contact area with the original tissue. However, the reported elongation values at the breakage point of the ACL ligament under tensile loading are 15 mm, thus being consistent with the values of the model which ranged from 15 to 18 mm [82]. This highlights the influence on the gradient over the strain the rod can exhibit, limiting excessive elongation. Nonetheless, the amount of force required to break the rods with graded ligaments was on average 35% larger than the amount of force that the ligaments with sharp connections experienced to break. This clearly shows the improved resistance to fracture that was conferred to the assembly by adjusting the connections to the hard material in a graded manner.

Moreover, the breakage of the graded rods did not occur at the interface, but upstream the gradual change. In the samples with sharp interface, the crack started to propagate at the material interface. This fact correlates to the manner of how ligaments injury occurs in nature, taking place in the middle part rather than at the interface [43, 79]. Thus, the graded connection provided by the varying density of mineral content and the untangling of collagen fibers in the bone-ligament enthesis is an impressive optimization provided by nature that was successfully replicated [36].

4.4. BRICK-AND-MORTAR AND GRADED PATTERNS

Brick-and-mortar patterns are inspired by nacre's high mechanical performance, and throughout scientific literature, several attempts have been performed in order to replicate it [57–59, 66]. However, none of those studies performs a tight control over the design of the pattern, taking into account the length scale of the bricks and the introduction of an extra level of hierarchy in the structure. The designs analyzed here determined the specific position of each material, and distinct sizes of the bricks and hierarchy were inspected. Furthermore, the joint contribution of a brick-and-mortar pattern and a gradient that varies the amount of hard material through the bricks has not been determined. In order to choose the most appropriate graded transition, the profiles that describe the amount of hard material through the width of the pattern were obtained for the two main architectures: the single level brick-and-mortar pattern with platelet aspect ratio 5.6 and the two level brick-and-mortar pattern with ratios 5.6 and 15. The results outlined that through the width, the patterns present proportions of hard material that range from 38 to 75% for the single level and 32 to 68% for the two hierarchical level samples. Therefore, the horizontal gradient containing a 100-40-100% variation of hard material reaches at its lowest hard material concentration point, 40%, the closest percentage

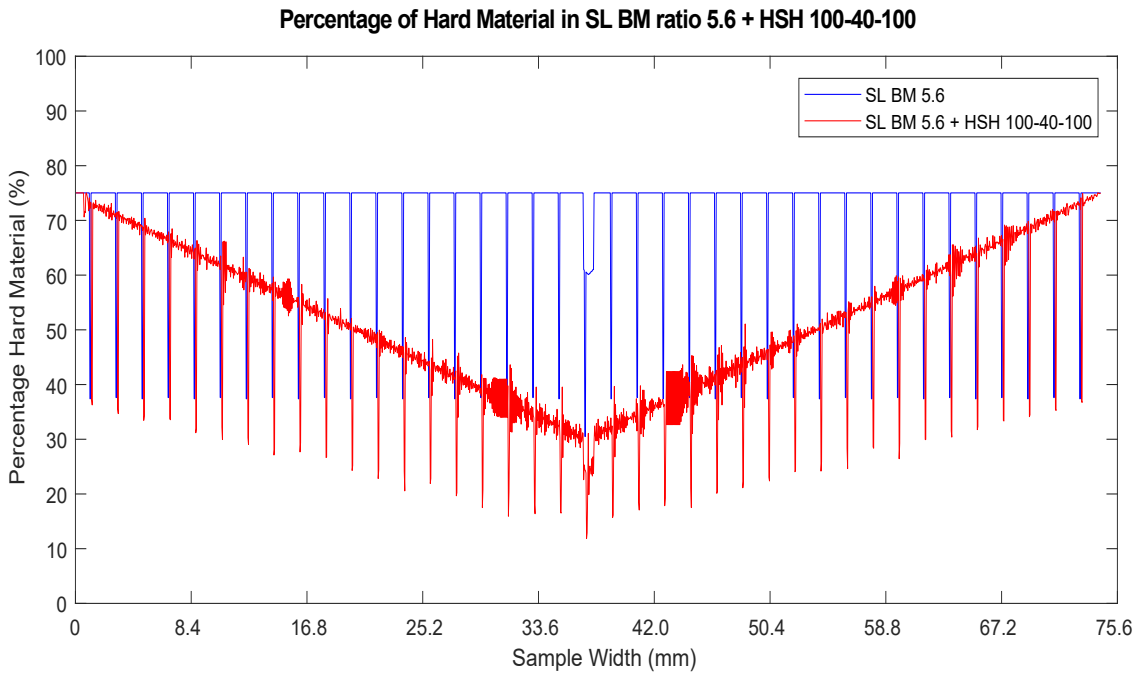

Figure 4.1: Profile of hard material through the width of the pattern. In blue the single level brick-and-mortar pattern with platelet is displayed, depicting values from 75 to 38% hard material. The profile of hard material of the pattern combined with a 100-40-100% hard gradient is indicated in red

.

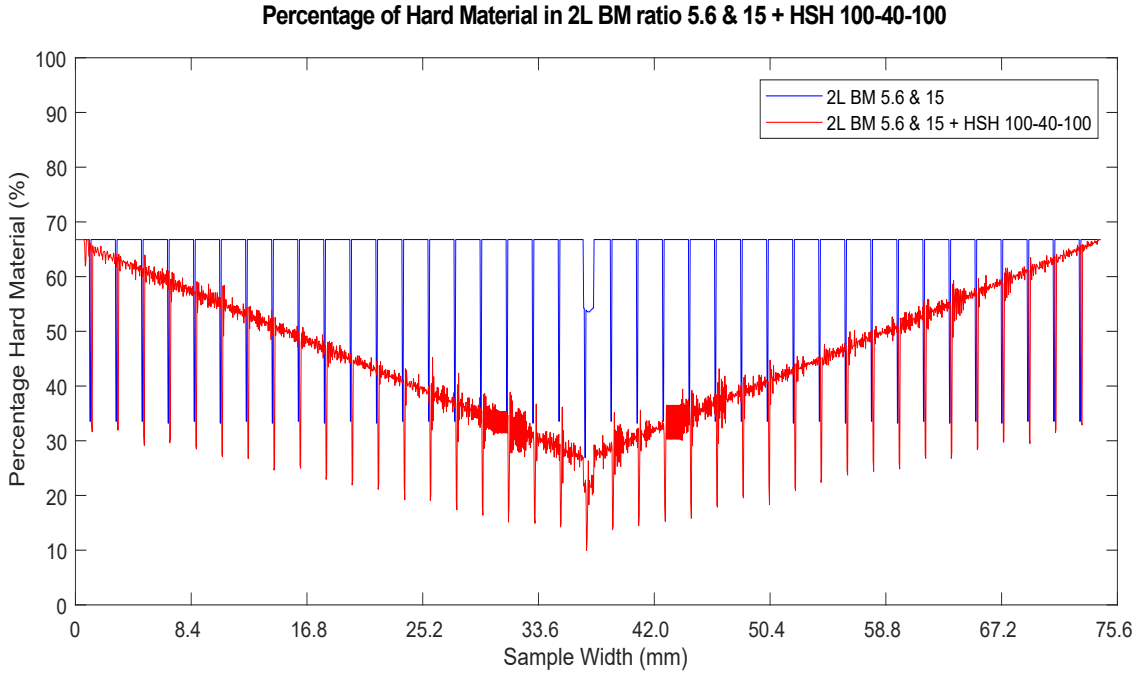

Figure 4.2: Profile of hard material through the width of the pattern. In blue the two level brick-and-mortar pattern with platelet ratio 5.6 and 15 is shown, presenting values from 68 to 32% hard material. The profile of hard material of the pattern together with a 100-40-100% hard gradient is indicated in red

.

of material as the brick-and-mortar pattern. This can be clearly seen in Figures 4.1 and 4.2, where the profile of hard material is displayed together with the profile of the same pattern with the addition of the gradient.

Furthermore, the hard material ratio of the single level and two level brick-and-mortar motifs is about 70%, as well as for the 100-40-100% gradient alone. The resulting combined patterns approximate the 50% hard material ratio. To broaden the effects of hard material ratio and distribution of materials through the pattern, two sets of semi-random, random and ordered patterns were introduced; one with 50% hard material and the other with 75% hard material [71].

4.4.1. FRACTURE MECHANICS OF HIERARCHICAL AND GRADED PATTERNS

The fracture mechanics of brick-and-mortar and graded patterns were obtained after the samples underwent tensile tests. It is important to note that the pre-formed crack was intentionally and strategically placed at the weakest point of the structure, in order to make the crack tip prone to stress concentrations. All the brick-and-mortar samples present a high elastic modulus, and presenting stiffness values are comparable to other studies of the same pattern at a similar composition of 70% hard material [8]. However, the samples did not reach high values for the fracture energy. It was expected that an optimized pattern such as brick-and-mortar would increase the fracture energy values through crack deflection mechanisms, but that is not found in this case. The size of the bricks in the samples are 10 times smaller than in previous research where crack deflection and bridging were the main contributions to a simultaneous increase in strength and toughness [8]. The length scale of the brick-and-mortar pattern can be the cause of the drop in toughness. It had been shown in previous research that when the total amount of hard material is about 75%, the contributions of soft material have little effect in increasing the fracture toughness at the native resolution of the printer [71]. The small size also leads to a block-wise fracture pattern, rather than promoting crack deflection and bridging.

When the patterns are combined with the horizontal gradient, their elastic modulus experiences a 2.5 fold decrease, but it is not followed by an increase in the fracture energy. Given that the simply graded pattern performs optimally in both properties, it would have been expected that the combined result of both designs would surpass those properties. The highest fracture energy values are achieved by the set of semi-random, random and ordered motifs with 50% hard material, even though the same motifs with 75% hard material increase their elastic modulus values. Previous research have shown that at an even 50% concentration of hard and soft material was the most appropriate ratio to reach the highest values of fracture toughness [71]. Here, the composition of hard material of the graded and brick and mortar samples is 50% (Table A.1), and the architecture has contributed to a slight increase of the fracture toughness of the sample.

As for the fracture stress values, there is a tight relation with the elastic modulus; the higher the stiffness, the greater the fracture stress. Finally, the samples with higher amount of hard material; brick-and-mortar and 75% semi-random, random and ordered, experience the smaller strain at fracture, surpassed by the samples containing a more even ratio between the two materials.

4.4.2. DIGITAL IMAGE CORRELATION

The digital image correlation results showed that all of the samples presented higher strain concentrations at the crack tip, following a butterfly shape. An increase of plasticity at the crack tip at the moment of maximum stress triggers fracture energy dissipation and an increase of the toughness of the material. The modest values of fracture toughness of the single and two-level brick-and-mortar and the 75% hard semi-random sample are related to the low values of the strain that the DIC unravelled. The horizontal pattern presents 6 times higher strain values confined at the crack tip, which triggers a boost in the amount of energy dissipation.

4.5. LIMITATIONS

In this section, several limitations concerning the design and arrangement of the samples will be inspected, as well as some considerations that should be taken into account for further research.

The novelty of this project uncovered many limitations regarding the design of these samples. In order to avoid material failure at sharp interfaces, it is necessary to avoid the designs where regions with materials with high mismatch in stiffness come together. Thus, the patterns where soft material is located next to the grippers site create high instability and concentrate stresses that could result in fracture at the hard-soft in-

terface rather than at the crack tip. Thus, the samples would not provide accurate information in the fracture mechanics tests.

The manner in which the material is distributed, in other words, the orientation of the gradient, influences greatly the mechanical behaviour of the sample. If the pattern has been inverted, meaning that the transition would be from purely soft material at the crack tip to purely hard material at the bottom part, the breakage would not had taken place at the crack tip either. Given that the crack tip would be surrounded by highly elastic material, there would be blunting at the crack tip, which would initially stretch rather than break, while the purely hard region at the opposite site would concentrate stresses before experiencing a sudden and detrimental breakage. This breakage would take place preferably at sites vulnerable to experience high concentration of stresses, such as the holes designed for the pinned attachment to the grippers, and which require from less energy input to break.

Therefore, and to assess the potential solutions for avoiding sudden breakage at the attachment site, it was attempted to determine the maximum amount of hard material at the opposite side of the crack tip. Thus, distinct percentages for hard material at the lowest part of the sample were assessed: 90, 80, 70, 50 and 25%. All of the samples presented a linear gradient and started with fully soft material at the crack. The samples with the highest amount of hard material at the bottom part -90, 80 and 70%- still broke at the attachment holes, but the samples containing 50 and 25% hard material on the bottom base followed crack propagation starting at the crack tip. Therefore, demonstrating that the overall ratio of material highly influences the way breakage occurs.

Considering the vulnerability of interfaces with a high mismatch in material stiffness, some changes were accommodated in the design of the horizontal complementary interfaces of 40-60 and 20-80% of hard material. The half with lowest concentration of hard material is more prone to experience the breakage at the interface with the hard material of the grippers. Thus, a graded transition through a few voxels connects the purely hard material of the grippers to the sample in its most vulnerable site. This implementation has greatly contributed to the success of the crack propagation through the interface.

The brick-and-mortar patterns were expected to present high stiffness and toughness. However, the results showed that the toughness was not enhanced considerably, while the high stiffness of all patterns was maintained. In the single edge notched samples, the crack was placed in the weakest location of the pattern. For the brick-and-mortar, the weakest points are the mortars, which are made of soft material, and the crack tip is linked to the connection of several bricks by soft material. However, the properties might be different if the crack tip would strategically be placed at a mortar, thus requiring higher amount of energy to break and extend. The location of the crack tip does influence the fracture behavior of the structure.

4.6. FUTURE RESEARCH DIRECTIONS

A better understanding of the advantages of functionally graded materials created by voxel-based 3D printing could have an enormous impact on many industrial applications. Nevertheless, the mechanical properties could be enhanced by improving the design of the patterns and adding several levels of hierarchy.

In order to gain a better insight into how the positioning of the crack tip affects the behavior in the brick-and-mortar and hierarchical patterns, further research could be performed by promoting the crack tip to be placed at a hard brick. Therefore, the fracture toughness of the samples could be increased, and thus obtaining an optimized performance in terms of strength and toughness, which is conventionally not reached in synthetic materials. Furthermore, more designs could be inspected and analyzed. For instance, the effects of introducing the gradient through the mortars instead of through the bricks, or the effect of two simultaneous gradients that run in a complementary manner, presenting hard bricks at places with soft mortars and hard mortars with soft bricks. The region where the gradient is applied can be narrowed by keeping more hard material on both edges, close to the grippers.

Once a greater insight of the behavior of these synthetic composite and graded structures is characterized, the guidelines for their design and manufacturing could be used broadly in many industries, such as medical

devices and biomaterials.

The biomedical industry could truly benefit from the development of functionally graded materials which can adapt their stiffness to the specific needs of the structure. In particular, the design cues presented in this project could be extremely beneficial in the design of orthopedic implants or scaffolds for tissue engineering. Stiffness incompatibility is one of the major causes of implant failure together with wear phenomena, and requires the patient to undergo revision surgeries [83]. Bone is a dynamic material that can adapt to the loading conditions to which it is subjected. Therefore, if the implant is stiffer than the bone, stress shielding will occur followed by bone resorption. By contrast, if the implant is too flexible, it will compromise the instability of the interface [84, 85]. Graded transitions in implants would help in linking the implant to the tissue in an appropriate manner and avoiding mismatches in stiffness [86].

Graded synthetic grafts could also bring considerable improvements to the current surgical techniques for ligament reconstruction after injuries. Ligament tearing is a common problem among athletes, specially in the case of knee ligaments like the ACL. Besides the reconstruction surgery and the treatment, the patient must undergo many months of rehabilitation and rest [43]. In addition, there is an increased risk on developing osteoarthritis 10-20 years after the intervention and loss of the biomechanical properties of the knee [87, 88]. The current reconstruction techniques use grafts from the patellar tendon or hamstring grafts, whose attachment implies drilling and fixing the graft through holes in the tibia and femur and can lead to grow disturbances [43, 89, 90]. After the surgery, there is an increased donor site morbidity and higher loads during walking, resulting in more risk of degenerative arthritis [90]. The design cues presented here could improve the fabrication of surgical grafts with better tolerance to gait loads, and thus reduce the risk of damage in the joint.

Finally, the results of this project could contribute to the production of functionally graded scaffolds for tissue engineering, and help in the regeneration of tissues with little ability to repair, such as articular cartilage [91]. By the use of hydrogels with graded properties, a more effective level of differentiation of cells and development of cartilage or cartilage-bone interfaces could be reached [92].

5

CONCLUSION

Throughout this project, the design of graded patterns and their effect on the mechanical properties of the materials have been assessed. The gradients were first defined on gray-scaled motifs and material distribution through the pattern was determined at voxel level. Additionally, more elaborate patterns were created and tested, in which brick-and-mortar designs were combined with a graded pattern and hierarchy. The values of stress, strain, fracture energy, fracture stress, elastic modulus and strain at fracture were obtained for all the samples to gain a better insight into their mechanical behaviour. The validation of the properties was performed by standard tensile tests. Furthermore, a model was created incorporating graded interfaces, mimicking the performance of the ligaments in a human knee. The results were compared to the same model which lacked the graded connections to the interface.
Below the main conclusions to the research questions are drawn:

Question 1: How does the gradient pattern in material variation affect the fracture and tensile properties of the specimens?
The results outlined the little variation in mechanical properties between samples containing vertically or horizontally graded structures. When regions with pure hard or pure soft material are desired, the function that determines material rate change does not contribute to an improvement of the composite mechanical properties. The combination of hard and soft material in a graded manner ranging from regions with pure material has little influence of the pattern, and the overall mechanical properties do not outperform the properties of pure material.

Question 2: How does the different material ratio distribution influence the mechanical properties of graded patterns?
Keeping an overall ratio of 50% hard and soft material in the sample, the distribution of material ratio through the sample does influence the mechanical properties. The fracture toughness of the specimen can be increased by keeping complementary material ratios at both sides of an interface, as well as by the development of graded transitions that do not reach points of purely hard or soft material. However, these modifications do not contribute much to an increase of the stiffness of the assembly.

Question 3: Would the functionally graded transitions outperform sharp material interfaces in a situation that mimics a real scenario?
Approach: A biomimetic model based on a human knee was successfully created and replicated to create multiple samples. The rods mimicking the knee ligaments presented graded and non-graded connections to the hard material. The samples presenting graded connections required a 35% increment of force to break with respect to the non-graded samples. In addition, the order in which the ligaments break follows the trend observed in nature, and the breakage of the graded samples occurred in the middle part, rather than at the interface. Thus, the application of gradients did outperform the behavior of connections made by sharp interfaces in an scenario that replicated a model in nature.

Question 4: How would be the effect of combining gradients with brick-and-mortar patterns? How do additional levels of hierarchy affect the mechanical behaviour?

The brick-and-mortar designs did not increase the overall fracture energy of the structure, compared to other non-optimized material arrangements with equivalent hard material ratio. The addition of a higher level of hierarchy neither did it influence significantly any of the fracture properties analyzed, and presents a similar trend to the brick-and-mortar patterns in a single level. The small length scale of the pattern does not contribute to crack deflection through the soft material, and therefore it does not contribute to the an increase in the fracture toughness. The introduction of a gradient through the bricks of the brick-and-mortar pattern renders a decrease of stiffness and a higher fracture energy release with respect to the brick-and-mortar pattern, but it does not outperform the fracture energy of the simply graded pattern. Further research regarding the strategic placement of the crack tip needs to be performed to assess whether it affects the mechanical properties and can improve the toughening mechanisms.

BIBLIOGRAPHY

[1] A. R. Studart, *Biological and bioinspired composites with spatially tunable heterogeneous architectures,* Advanced Functional Materials **23**, 4423 (2013).

[2] Z. Liu, M. A. Meyers, Z. Zhang, and R. O. Ritchie, *Functional gradients and heterogeneities in biological materials: Design principles, functions, and bioinspired applications,* Progress in Materials Science **88**, 467 (2017).

[3] U. G. Wegst, H. Bai, E. Saiz, A. P. Tomsia, and R. O. Ritchie, *Bioinspired structural materials,* Nature materials **14**, 23 (2015).

[4] H. D. Espinosa, J. E. Rim, F. Barthelat, and M. J. Buehler, *Merger of structure and material in nacre and bone–perspectives on de novo biomimetic materials,* Progress in Materials Science **54**, 1059 (2009).

[5] A. R. Studart, *Towards high-performance bioinspired composites,* Advanced Materials **24**, 5024 (2012).

[6] M. J. Buehler, *Tu (r) ning weakness to strength,* Nano Today **5**, 379 (2010).

[7] F. Libonati and M. J. Buehler, *Advanced structural materials by bioinspiration,* Advanced Engineering Materials **19**, 1600787 (2017).

[8] G. X. Gu, F. Libonati, S. D. Wettermark, and M. J. Buehler, *Printing nature: Unraveling the role of nacre's mineral bridges,* Journal of the mechanical behavior of biomedical materials **76**, 135 (2017).

[9] R. O. Ritchie, *The conflicts between strength and toughness,* Nature materials **10**, 817 (2011).

[10] M. E. Launey and R. O. Ritchie, *On the fracture toughness of advanced materials,* Advanced Materials **21**, 2103 (2009).

[11] J. W. Dunlop, R. Weinkamer, and P. Fratzl, *Artful interfaces within biological materials,* Materials Today **14**, 70 (2011).

[12] F. Barthelat, Z. Yin, and M. J. Buehler, *Structure and mechanics of interfaces in biological materials,* Nature Reviews Materials **1**, 16007 (2016).

[13] M. E. Launey, M. J. Buehler, and R. O. Ritchie, *On the mechanistic origins of toughness in bone,* Annual review of materials research **40**, 25 (2010).

[14] F. Marin, N. Le Roy, and B. Marie, *The formation and mineralization of mollusk shell,* Front Biosci **4**, 125 (2012).

[15] F. Barthelat, A. K. Dastjerdi, and R. Rabiei, *An improved failure criterion for biological and engineered staggered composites,* Journal of The Royal Society Interface **10**, 20120849 (2013).

[16] M. I. Lopez, P. E. M. Martinez, and M. A. Meyers, *Organic interlamellar layers, mesolayers and mineral nanobridges: contribution to strength in abalone (haliotis rufescence) nacre,* Acta biomaterialia **10**, 2056 (2014).

[17] Z. Huang and X. Li, *Nanoscale structural and mechanical characterization of heat treated nacre,* Materials Science & Engineering C **6**, 1803 (2009).

[18] F. Barthelat, H. Tang, P. Zavattieri, C.-M. Li, and H. Espinosa, *On the mechanics of mother-of-pearl: a key feature in the material hierarchical structure,* Journal of the Mechanics and Physics of Solids **55**, 306 (2007).

[19] R. Wang, Z. Suo, A. Evans, N. Yao, and I. Aksay, *Deformation mechanisms in nacre,* Journal of Materials Research **16**, 2485 (2001).

[20] A. Ural and D. Vashishth, *Hierarchical perspective of bone toughness–from molecules to fracture,* International Materials Reviews **59**, 245 (2014).

[21] S. Suresh, *Graded materials for resistance to contact deformation and damage,* Science **292**, 2447 (2001).

[22] P.-Y. Chen, J. McKittrick, and M. A. Meyers, *Biological materials: functional adaptations and bioinspired designs,* Progress in Materials Science **57**, 1492 (2012).

[23] J. C. Weaver, Q. Wang, A. Miserez, A. Tantuccio, R. Stromberg, K. N. Bozhilov, P. Maxwell, R. Nay, S. T. Heier, E. DiMasi, *et al.*, *Analysis of an ultra hard magnetic biomineral in chiton radular teeth,* Materials Today **13**, 42 (2010).

[24] J. H. Waite, H. C. Lichtenegger, G. D. Stucky, and P. Hansma, *Exploring molecular and mechanical gradients in structural bioscaffolds,* Biochemistry **43**, 7653 (2004).

[25] A. Miserez, T. Schneberk, C. Sun, F. W. Zok, and J. H. Waite, *The transition from stiff to compliant materials in squid beaks,* Science **319**, 1816 (2008).

[26] I. H. Chen, W. Yang, and M. A. Meyers, *Alligator osteoderms: Mechanical behavior and hierarchical structure,* Materials Science and Engineering: C **35**, 441 (2014).

[27] C.-Y. Sun and P.-Y. Chen, *Structural design and mechanical behavior of alligator (alligator mississippiensis) osteoderms,* Acta biomaterialia **9**, 9049 (2013).

[28] P.-Y. Chen, A. Lin, Y.-S. Lin, Y. Seki, A. Stokes, J. Peyras, E. Olevsky, M. Meyers, and J. McKittrick, *Structure and mechanical properties of selected biological materials,* Journal of the Mechanical Behavior of Biomedical Materials **1**, 208 (2008).

[29] L. J. Gibson, *The hierarchical structure and mechanics of plant materials,* Journal of the Royal Society Interface , rsif20120341 (2012).

[30] M. Eder, K. Jungnikl, and I. Burgert, *A close-up view of wood structure and properties across a growth ring of norway spruce (picea abies [l] karst.),* Trees **23**, 79 (2009).

[31] D. Raabe, C. Sachs, and P. Romano, *The crustacean exoskeleton as an example of a structurally and mechanically graded biological nanocomposite material,* Acta Materialia **53**, 4281 (2005).

[32] J. Färber, H. Lichtenegger, A. Reiterer, S. Stanzl-Tschegg, and P. Fratzl, *Cellulose microfibril angles in a spruce branch and mechanical implications,* Journal of Materials Science **36**, 5087 (2001).

[33] S. J. Marshall, M. Balooch, S. Habelitz, G. Balooch, R. Gallagher, and G. W. Marshall, *The dentin–enamel junction—a natural, multilevel interface,* Journal of the European Ceramic Society **23**, 2897 (2003).

[34] Y. Chan, A. Ngan, and N. King, *Nano-scale structure and mechanical properties of the human dentine–enamel junction,* Journal of the mechanical behavior of biomedical materials **4**, 785 (2011).

[35] C. P. Lin, W. H. Douglas, and S. L. Erlandsen, *Scanning electron microscopy of type i collagen at the dentin-enamel junction of human teeth.* Journal of Histochemistry & Cytochemistry **41**, 381 (1993).

[36] G. M. Genin, A. Kent, V. Birman, B. Wopenka, J. D. Pasteris, P. J. Marquez, and S. Thomopoulos, *Functional grading of mineral and collagen in the attachment of tendon to bone,* Biophysical journal **97**, 976 (2009).

[37] S. Thomopoulos, G. R. Williams, J. A. Gimbel, M. Favata, and L. J. Soslowsky, *Variation of biomechanical, structural, and compositional properties along the tendon to bone insertion site,* Journal of orthopaedic research **21**, 413 (2003).

[38] L. Rossetti, L. Kuntz, E. Kunold, J. Schock, K. Müller, H. Grabmayr, J. Stolberg-Stolberg, F. Pfeiffer, S. Sieber, R. Burgkart, *et al.*, *The microstructure and micromechanics of the tendon–bone insertion,* Nature materials **16**, 664 (2017).

[39] S. Thomopoulos, J. P. Marquez, B. Weinberger, V. Birman, and G. M. Genin, *Collagen fiber orientation at the tendon to bone insertion and its influence on stress concentrations,* Journal of biomechanics **39**, 1842 (2006).

[40] Y. Hu, V. Birman, A. Deymier-Black, A. G. Schwartz, S. Thomopoulos, and G. M. Genin, *Stochastic interdigitation as a toughening mechanism at the interface between tendon and bone,* Biophysical journal **108**, 431 (2015).

[41] G. M. Genin and S. Thomopoulos, *The tendon-to-bone attachment: Unification through disarray,* Nature materials **16**, 607 (2017).

[42] B. Wopenka, A. Kent, J. D. Pasteris, Y. Yoon, and S. Thomopoulos, *The tendon-to-bone transition of the rotator cuff: a preliminary raman spectroscopic study documenting the gradual mineralization across the insertion in rat tissue samples,* Applied spectroscopy **62**, 1285 (2008).

[43] C. R. LaBella, W. Hennrikus, T. E. Hewett, *et al.*, *Anterior cruciate ligament injuries: diagnosis, treatment, and prevention,* Pediatrics , peds (2014).

[44] Y. Liu, S. Thomopoulos, V. Birman, J.-S. Li, and G. M. Genin, *Bi-material attachment through a compliant interfacial system at the tendon-to-bone insertion site,* Mechanics of Materials **44**, 83 (2012).

[45] S. Deville, E. Saiz, R. K. Nalla, and A. P. Tomsia, *Freezing as a path to build complex composites,* Science **311**, 515 (2006).

[46] E. Munch, M. E. Launey, D. H. Alsem, E. Saiz, A. P. Tomsia, and R. O. Ritchie, *Tough, bio-inspired hybrid materials,* Science **322**, 1516 (2008).

[47] R. P. Wilkerson, B. Gludovatz, J. Watts, A. P. Tomsia, G. E. Hilmas, and R. O. Ritchie, *A novel approach to developing biomimetic ("nacre-like") metal-compliant-phase (nickel–alumina) ceramics through coextrusion,* Advanced Materials **28**, 10061 (2016).

[48] F. Libonati, C. Colombo, and L. Vergani, *Design and characterization of a biomimetic composite inspired to human bone,* Fatigue & Fracture of Engineering Materials & Structures **37**, 772 (2014).

[49] F. Libonati, L. Vergani, *et al.*, *Cortical bone as a biomimetic model for the design of new composites,* Procedia Structural Integrity , 1319 (2016).

[50] F. Libonati *et al.*, *Bio-inspired composites: Using nature to tackle composite limitations,* Advanced Engineering Materials and Modeling , 165 (2016).

[51] M. Mirkhalaf, A. K. Dastjerdi, and F. Barthelat, *Overcoming the brittleness of glass through bio-inspiration and micro-architecture,* Nature communications **5**, 3166 (2014).

[52] M. J. Mirzaali, V. Mussi, P. Vena, F. Libonati, L. Vergani, and M. Strano, *Mimicking the loading adaptation of bone microstructure with aluminum foams,* Materials & Design **126**, 207 (2017).

[53] T. Guillén, Q.-H. Zhang, G. Tozzi, A. Ohrndorf, H.-J. Christ, and J. Tong, *Compressive behaviour of bovine cancellous bone and bone analogous materials, microct characterisation and fe analysis,* Journal of the mechanical behavior of biomedical materials **4**, 1452 (2011).

[54] G. X. Gu, I. Su, S. Sharma, J. L. Voros, Z. Qin, and M. J. Buehler, *Three-dimensional-printing of bio-inspired composites,* Journal of biomechanical engineering **138**, 021006 (2016).

[55] A. Doraiswamy, T. M. Dunaway, J. J. Wilker, and R. J. Narayan, *Inkjet printing of bioadhesives,* Journal of Biomedical Materials Research Part B: Applied Biomaterials: An Official Journal of The Society for Biomaterials, The Japanese Society for Biomaterials, and The Australian Society for Biomaterials and the Korean Society for Biomaterials **89**, 28 (2009).

[56] E. Doubrovski, E. Y. Tsai, D. Dikovsky, J. M. Geraedts, H. Herr, and N. Oxman, *Voxel-based fabrication through material property mapping: A design method for bitmap printing,* Computer-Aided Design **60**, 3 (2015).

[57] L. S. Dimas, G. H. Bratzel, I. Eylon, and M. J. Buehler, *Tough composites inspired by mineralized natural materials: computation, 3d printing, and testing,* Advanced Functional Materials **23**, 4629 (2013).

[58] L. S. Dimas and M. J. Buehler, *Modeling and additive manufacturing of bio-inspired composites with tunable fracture mechanical properties,* Soft Matter **10**, 4436 (2014).

[59] R. Mirzaeifar, L. S. Dimas, Z. Qin, and M. J. Buehler, *Defect-tolerant bioinspired hierarchical composites: simulation and experiment,* ACS Biomaterials Science & Engineering **1**, 295 (2015).

[60] F. Libonati, G. X. Gu, Z. Qin, L. Vergani, and M. J. Buehler, *Bone-inspired materials by design: Toughness amplification observed using 3d printing and testing,* Advanced Engineering Materials **18**, 1354 (2016).

[61] T. Swetly, J. Stampfl, G. Kempf, R.-M. Hucke, M. Willing, and M. Warkentin, *Bioinspired engineering polymers by voxel-based 3d-printing,* BioNanoMaterials **17**, 145 (2016).

[62] L. Djumas, A. Molotnikov, G. P. Simon, and Y. Estrin, *Enhanced mechanical performance of bio-inspired hybrid structures utilising topological interlocking geometry,* Scientific reports **6**, 26706 (2016).

[63] G. X. Gu, F. Libonati, S. D. Wettermark, and M. J. Buehler, *Printing nature: Unraveling the role of nacre's mineral bridges,* Journal of the mechanical behavior of biomedical materials **76**, 135 (2017).

[64] L. Djumas, G. P. Simon, Y. Estrin, and A. Molotnikov, *Deformation mechanics of non-planar topologically interlocked assemblies with structural hierarchy and varying geometry,* Scientific reports **7**, 11844 (2017).

[65] D. Kokkinis, M. Schaffner, and A. R. Studart, *Multimaterial magnetically assisted 3d printing of composite materials,* Nature communications **6**, 8643 (2015).

[66] J. J. Martin, B. E. Fiore, and R. M. Erb, *Designing bioinspired composite reinforcement architectures via 3d magnetic printing,* Nature communications **6**, 8641 (2015).

[67] K. Kumar, J. Liu, C. Christianson, M. Ali, M. T. Tolley, J. Aizenberg, D. E. Ingber, J. C. Weaver, and K. Bertoldi, *A biologically inspired, functionally graded end effector for soft robotics applications,* Soft robotics **4**, 317 (2017).

[68] D. Kokkinis, F. Bouville, and A. R. Studart, *3d printing of materials with tunable failure via bioinspired mechanical gradients,* Advanced Materials **30**, 1705808 (2018).

[69] J. Mueller, K. Shea, and C. Daraio, *Mechanical properties of parts fabricated with inkjet 3d printing through efficient experimental design,* Materials & Design **86**, 902 (2015).

[70] I. Vu, L. Bass, N. Meisel, B. Orler, C. B. Williams, and D. A. Dillard, *Characterization of mutli-material interfaces in polyjet additive manufacturing,* in *Solid Freeform Fabrication Symposium* (2014) pp. 959–982.

[71] M. Mirzaali, M. Edens, A. H. de la Nava, S. Janbaz, P. Vena, E. Doubrovski, and A. Zadpoor, *Length-scale dependency of biomimetic hard-soft composites,* Scientific Reports **8**, 12052 (2018).

[72] M. Mese and P. Vaidyanathan, *Recent advances in digital halftoning and inverse halftoning methods,* IEEE Transactions on Circuits and Systems I: Fundamental Theory and Applications **49**, 790 (2002).

[73] R. W. Floyd, *An adaptive algorithm for spatial gray-scale,* in *Proc. Soc. Inf. Disp.*, Vol. 17 (1976) pp. 75–77.

[74] A. Standard *et al.*, *Standard test methods for plane-strain fracture toughness and strain energy release rate of plastic materials,* D5045-96 (1996).

[75] L. S. Dimas and M. J. Buehler, *Modeling and additive manufacturing of bio-inspired composites with tunable fracture mechanical properties,* Soft Matter **10**, 4436 (2014).

[76] G. X. Gu, S. Wettermark, and M. J. Buehler, *Algorithm-driven design of fracture resistant composite materials realized through additive manufacturing,* Additive Manufacturing **17**, 47 (2017).

[77] *Skeleton,* https://www.thingiverse.com/thing:660681/attribution_card, accessed: 2018-10-08.

[78] H. Van Melick, L. Govaert, and H. Meijer, *On the origin of strain hardening in glassy polymers,* Polymer **44**, 2493 (2003).

[79] M. Marieswaran, I. Jain, B. Garg, V. Sharma, and D. Kalyanasundaram, *A review on biomechanics of anterior cruciate ligament and materials for reconstruction,* Applied bionics and biomechanics **2018** (2018).

[80] J. Kennedy, R. Hawkins, R. Willis, and K. Danylchuck, *Tension studies of human knee ligaments. yield point, ultimate failure, and disruption of the cruciate and tibial collateral ligaments.* The Journal of bone and joint surgery. American volume **58**, 350 (1976).

[81] F. R. Noyes and E. S. Grood, *The strength of the anterior cruciate ligament in humans and rhesus monkeys.* The Journal of bone and joint surgery. American volume **58**, 1074 (1976).

[82] F. Noyes, D. Butler, E. Grood, R. Zernicke, and M. Hefzy, *Biomechanical analysis of human ligament grafts used in knee-ligament,* J. Bone Joint Surg. Am **66**, 344 (1984).

[83] P. Kowalczyk, *Design optimization of cementless femoral hip prostheses using finite element analysis,* Journal of Biomechanical Engineering **123**, 396 (2001).

[84] R. Huiskes, H. Weinans, and B. Van Rietbergen, *The relationship between stress shielding and bone resorption around total hip stems and the effects of flexible materials,* Clinical orthopaedics and related research , 124 (1992).

[85] R. Huiskes, *Stress shielding and bone resorption in tha: clinical versus computer-simulation studies,* Acta Orthop Belg **59**, 118 (1993).

[86] A. Sola, D. Bellucci, and V. Cannillo, *Functionally graded materials for orthopedic applications–an update on design and manufacturing,* Biotechnology advances **34**, 504 (2016).

[87] B. Barenius, S. Ponzer, A. Shalabi, R. Bujak, L. Norlén, and K. Eriksson, *Increased risk of osteoarthritis after anterior cruciate ligament reconstruction: a 14-year follow-up study of a randomized controlled trial,* The American journal of sports medicine **42**, 1049 (2014).

[88] N. Pujol, P. Boisrenoult, and P. Beaufils, *Post-traumatic knee stiffness: surgical techniques,* Orthopaedics & Traumatology: Surgery & Research **101**, S179 (2015).

[89] G. Vinagre, N. I. Kennedy, J. Chahla, M. E. Cinque, Z. B. Hussain, M. L. Olesen, and R. F. LaPrade, *Hamstring graft preparation techniques for anterior cruciate ligament reconstruction,* Arthroscopy techniques **6**, e2079 (2017).

[90] C. D. Johnston, J. S. Goodwin, J. T. Spang, B. Pietrosimone, and J. T. Blackburn, *Gait biomechanics in individuals with patellar tendon and hamstring tendon anterior cruciate ligament reconstruction grafts,* Journal of Biomechanics (2018).

[91] R. Karuppal, *Current concepts in the articular cartilage repair and regeneration,* Journal of orthopaedics **14**, A1 (2017).

[92] H. Kang, Y. Zeng, and S. Varghese, *Functionally graded multilayer scaffolds for in vivo osteochondral tissue engineering,* Acta biomaterialia **78**, 365 (2018).

A

List of samples and percentage of hard and soft material

Table A.1: Overview of samples and their proportion of hard and soft material

Sample	Hard material (%)	Soft Material (%)
Vertical Gradients		
Grad HS	50.058	49.942
5 Steps HS	50.160	94.840
10 Steps HS	49.890	50.110
15 Steps HS	50.400	49.600
Sigmoid HS	50.020	49.980
Hard- Soft	50.000	50.000
2D Gradient	50.000	50.000
Horizontal Gradients		
Grad HSH	50.000	50.000
5 Steps HSH	60.000	40.000
10 Steps HSH	50.020	49.980
15 Steps HSH	53.500	46.500
Sigmoid HSH	49.530	50.470
Hard- Soft	50.000	50.000
Hor & Ver	50.030	49.970
HSH 100- 40 -100	70.000	30.000
HSH 80- 20- 80	50.000	50.000
HSH 60- 40- 60	50.010	49.990
Hard- Soft 20-80 (Smooth)	50.151	49.849
Hard- Soft 40-60 (Smooth)	50.079	49.921
Brick- and- Mortar Patterns		
Single Level BM ratio 2.5	71.216	28.784
Single Level BM ratio 5.6	73.360	26.640
Two Level BM ratio 5.6 and 15	65.246	34.754
Brick- and- Mortar Patterns and Gradients		
Single Level BM ratio 5.6 + HSH 100- 40- 100	51.380	48.620
Two Level BM ratio 5.6 and 15 + HSH 100- 40- 100	45.733	54.267
Tensile Specimens		
HSH Sharp	66.700	33.300
HSH Grad	50.000	50.000
HSH 5 Steps	60.000	40.000
HSH 10 Steps	50.200	49.800
HSH 15 Steps	53.400	46.600
HSH Sigmoid	50.000	50.000
Hard- Soft	50.000	50.000

B

FORCE-DISPLACEMENT GRAPHS

B.1. FORCE-DISPLACEMENT GRAPHS OF GRADED SAMPLES

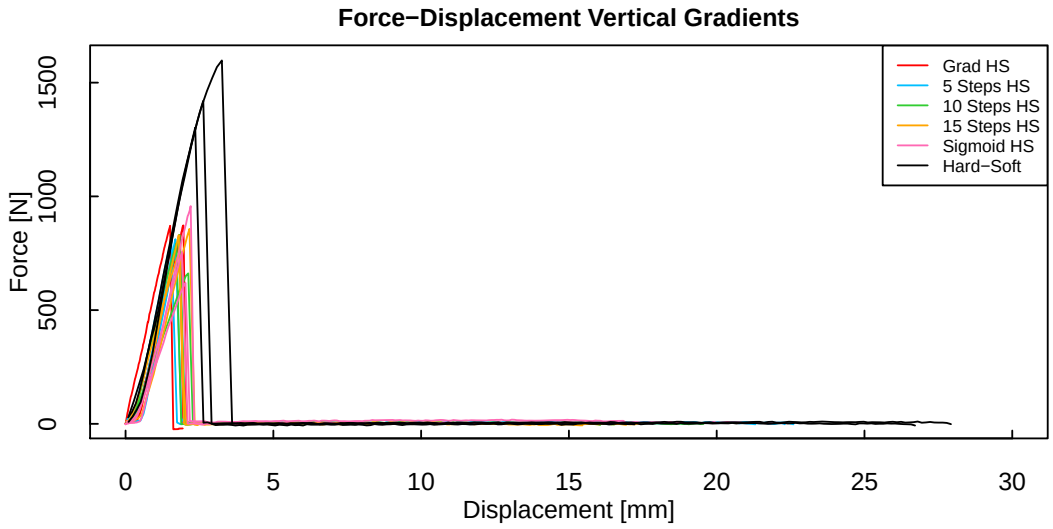

Figure B.1: Force-Displacement graphs of vertical gradients

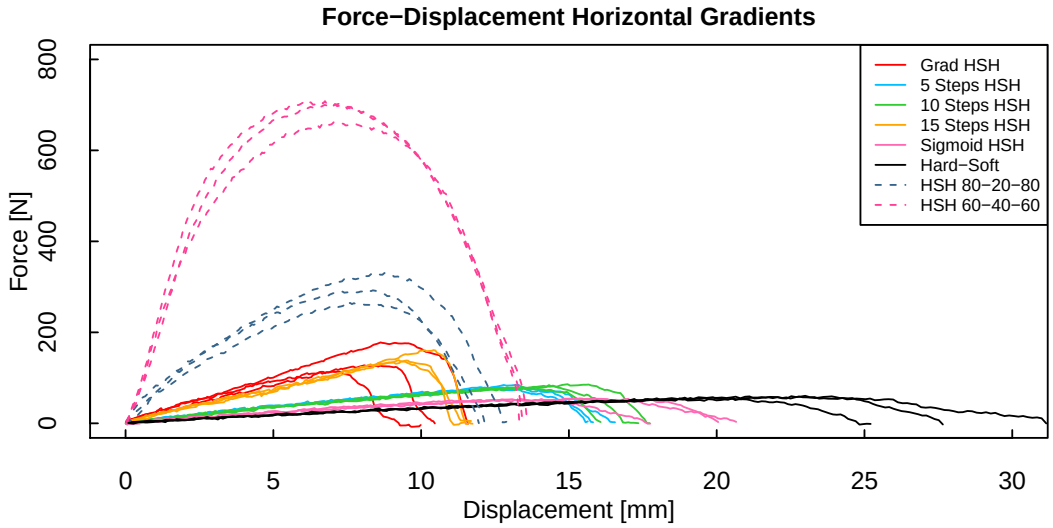

Figure B.2: Force-Displacement graphs of horizontal gradients

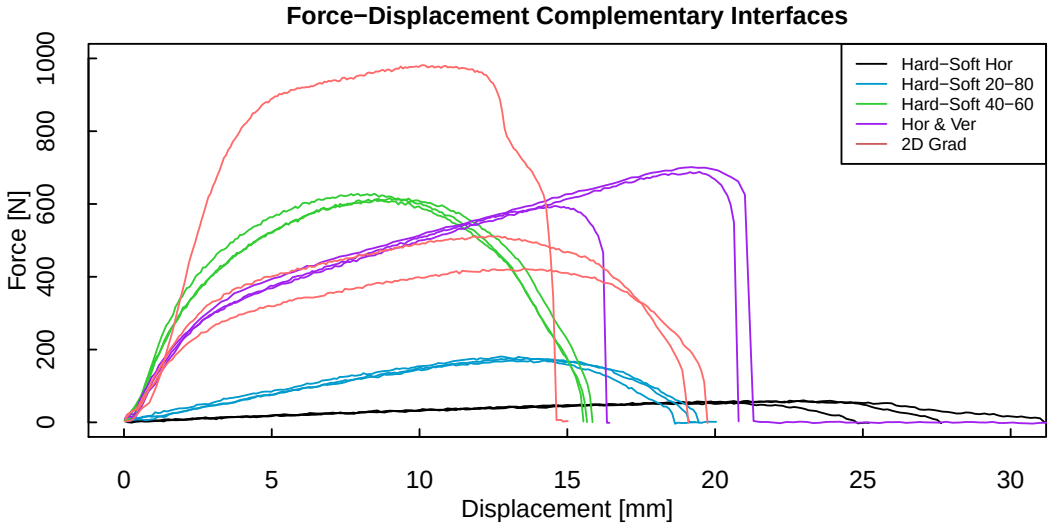

Figure B.3: Force-Displacement graphs of complementary interfaces

B.2. FORCE-DISPLACEMENT GRAPHS OF TENSILE SAMPLES

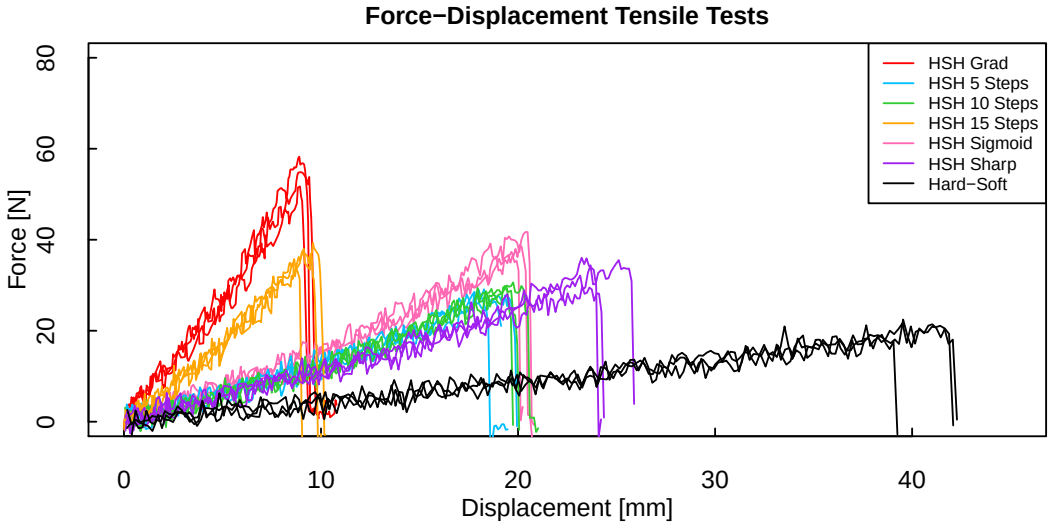

Figure B.4: Force-Displacement graphs of tensile samples

B.3. FORCE-DISPLACEMENT GRAPHS OF HIERARCHICAL AND GRADED SAMPLES

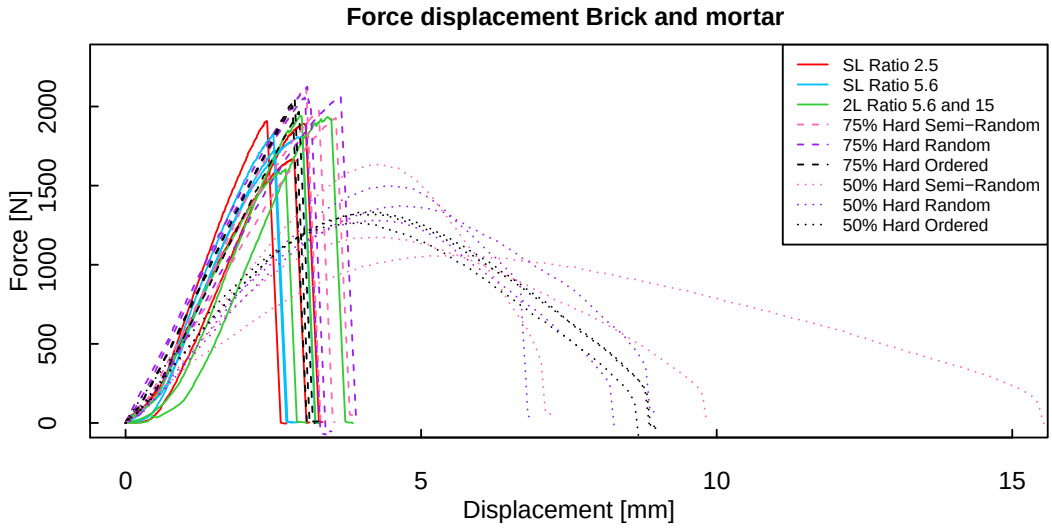

Figure B.5: Force-Displacement graphs of Brick-and-Mortar and Hierarchical samples. The samples are compared with other designs containing 75% hard and 50% hard material in different assemblies: Semi-Random, Random and Ordered.

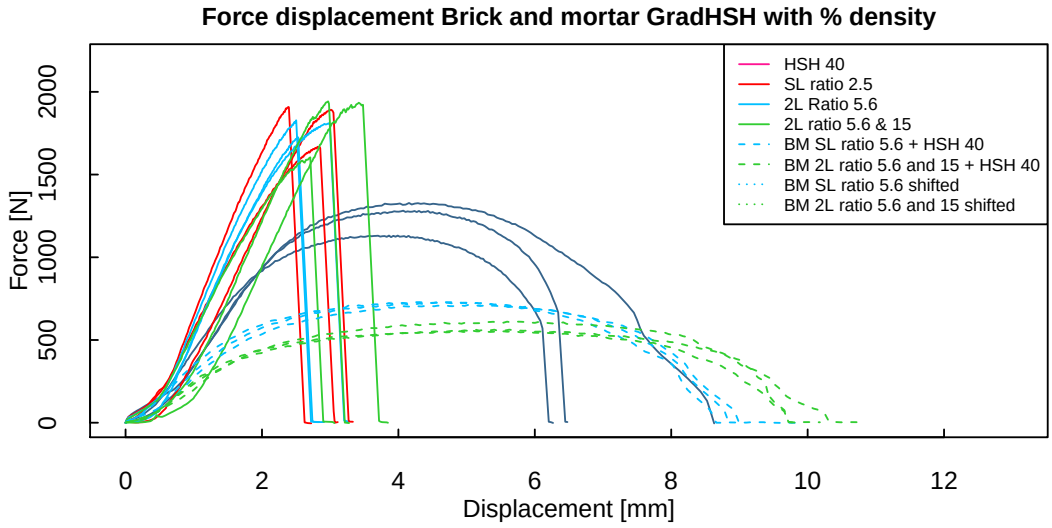

Figure B.6: Force-Displacement graphs of Brick-and-Mortar and graded samples

C

STRESS-STRAIN GRAPHS OF BRICK-AND-MORTAR SAMPLES

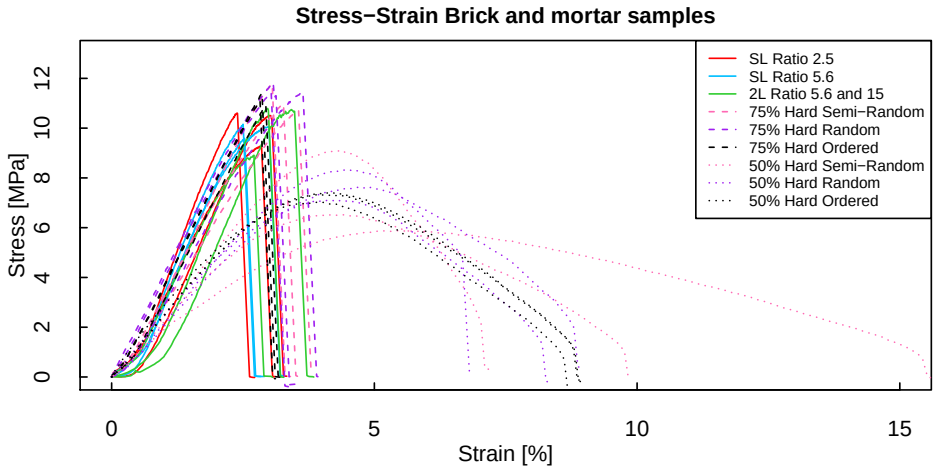

Figure C.1: Stress-Strain graphs of Brick-and-Mortar and Hierarchical samples. The samples are compared with other designs containing 75% hard and 50% hard material in different assemblies: Semi-Random, Random and Ordered.

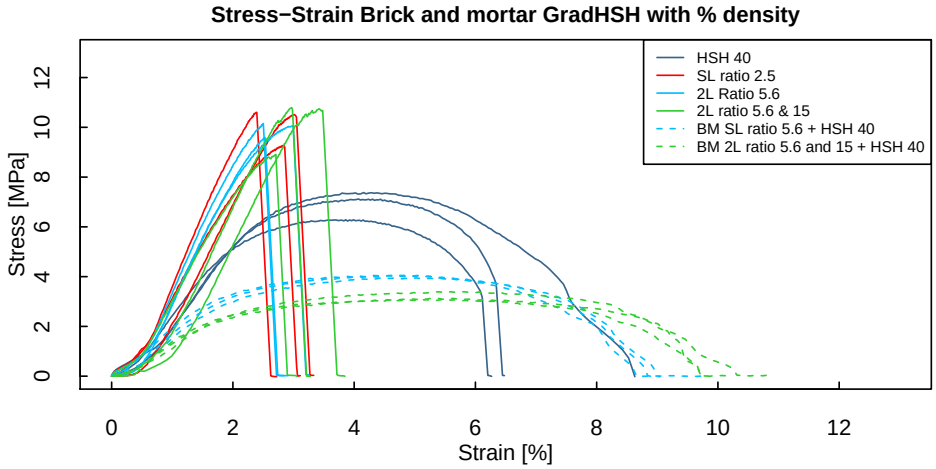

Figure C.2: Stress-Strain of Brick-and-Mortar and graded samples